THE EFFECTS OF ADSORPTION ON INJECTION INTO AND PRODUCTION FROM VAPOR DOMINATED GEOTHERMAL RESERVOIRS

A DISSERTATION
SUBMITTED TO THE DEPARTMENT OF PETROLEUM ENGINEERING
AND THE COMMITTEE ON GRADUATE STUDIES
OF STANFORD UNIVERSITY
IN PARTIAL FULFILLMENT OF THE REQUIREMENTS
FOR THE DEGREE OF
DOCTOR OF PHILOSOPHY

By
John Wirt Hornbrook
January, 1994

I certify that I have read this thesis and that in my opinion it is fully adequate, in scope and in quality, as a dissertation for the degree of Doctor of Philosophy.

Dr. Roland N. Horne
(Principal Adviser)

I certify that I have read this thesis and that in my opinion it is fully adequate, in scope and in quality, as a dissertation for the degree of Doctor of Philosophy.

Dr. Paul Kruger

I certify that I have read this thesis and that in my opinion it is fully adequate, in scope and in quality, as a dissertation for the degree of Doctor of Philosophy.

Dr. Martin J. Blunt

Approved for the University Committee on Graduate Studies:

Abstract

An analysis was undertaken on the effects of adsorption on geothermal reservoir injection performance. Thermodynamic properties of adsorbate were determined so pressure depletion in reservoirs affected by adsorption could be modeled accurately. A semi-analytical solution was constructed for isothermal vapor flow with a sorbing phase present. Similarity analysis was used to isolate the effects of adsorbed mass and the rate of change of adsorbed mass. Vapor flow in a porous medium in the presence of a sorbing phase was solved numerically to determine the validity of the isothermal assumption made in the analytical derivation and to study other thermal effects of adsorption. An analysis of the heat balance for fluids flowing in geothermal systems was used to determine the heat effects of adsorption at a boiling front and for single phase vapor flow.

Production characteristics of an injected tritiated water tracer were studied for the Geysers geothermal reservoir. Effects of tracer sorption, diffusion, and partitioning were included to determine the relative importance of each effect and to explain field tracer production characteristics.

Semi-analytical results indicate that effects of adsorption on pressure are significant for a wide range of adsorption isotherms. The slope of the adsorption isotherm is shown to be much more significant than the magnitude of adsorbed mass.

Numerical results indicate that the isothermal assumption is valid for vapor dominated flow in geothermal reservoirs. The numerical scheme is also shown to agree well with analytical results for a wide range of conditions.

The effects of adsorption on the propagation of injected tracer are shown to be insignificant for a linear system. By use of stream tube modeling of a long-term tracer

test at the Geysers geothermal reservoir, adsorption effects are shown not to be the likely explanation for the observed spread in tracer production data.

Acknowledgements

I gratefully acknowledge the guidance I received from my advisor, Dr. Roland N. Horne. He provided much valuable insight and helped to steer my research in the right direction.

I thank my dissertation defense committee comprised of Dr. Paul Kruger, Dr. Martin J. Blunt, Dr. Paul Roberts, and Dr. William E. Brigham. Special thanks go to Dr. Kruger and Dr. Blunt for serving as readers. I also thank Dr. Brigham for providing career and academic advice throughout my stay at Stanford.

It was an honor and a great pleasure to have worked with Dr. Henry J. Ramey, Jr. He was a brilliant engineer and teacher and one of the nicest people I have ever met.

My office mates, Rafael E. Guzman and Marco R. Thiele, were always available to help me work through difficult problems, give advice, or just shoot the breeze when I needed a break. They helped make my stay at Stanford memorable and enjoyable.

Funding for this project was provided, in part, by the Department of Energy, Geothermal Division, under contract number DEFG0790ID12934. I gratefully acknowledge their financial support.

Finally, I thank my parents, Charles and Marilyn Hornbrook, and my brother and sister-in-law, Marc and Rosemary Hornbrook. When the research seemed like a little too much or my finances began to run low they were always there to help. I appreciate their support very much.

Contents

List of Tables

List of Figures

Chapter 1

Introduction

In the current era of environmental awareness, geothermal energy represents an excellent and significant alternative to conventional energy resources. With increasingly strict clean air standards and concern over the long term effects of pollution from fossil fuels, geothermal exploration and development has been increasing. Reed and McLarty [48] estimated that, as of 1992, geothermal resources accounted for about 1 billion dollars of annual revenue and displaced over 30 million barrels of imported oil. They also estimated that about 7 % of the electrical energy needs in California were met by geothermal sources.

In addition to the United States, significant geothermal development has taken place in the Philippines, Mexico, Italy, New Zealand, and Japan. Most U.S. development has taken place in the western states with 18 resource sites currently operating in California, Nevada, and Utah, accounting for over 2700 MW of electrical generation capacity.

Geothermal reservoirs may be described as vapor-dominated, liquid-dominated, or hot dry rock reservoirs. Vapor-dominated geothermal reservoirs are characterized by low pressures and high temperatures which requires that all or most of the resident fluid is in the form of superheated or saturated steam. Electrical generation from the reservoirs is accomplished by simply producing steam into conventional turbines to drive electrical generators.

At somewhat lower temperatures are liquid-dominated geothermal reservoirs. In

these systems most of the resident fluid is in the form of liquid. Electrical generation is accomplished either by partially flashing the produced water to steam for subsequent flow through turbines, or by using heat from the produced water to vaporize a more volatile liquid and using the generated vapor to power turbines.

Hot dry rock geothermal reservoirs consist of high temperature rock bodies with insufficient liquid flow to carry the heat to the surface. Injection of water into artificially induced fractures to produce steam for electrical generation is the method of heat extraction in these systems.

This research focuses on vapor-dominated reservoirs. Specifically, the Geysers geothermal reservoir, the largest developed geothermal steam resource in the world, was studied to determine the effects of adsorption on injection into this type of geothermal reservoir. Methods generally applied to oil and gas reservoirs were used to determine the characteristics of geothermal reservoirs when an adsorbed phase is present.

As in oil and gas reservoirs, the fluids in geothermal reservoirs are depletable. The difference between depletion of petroleum and geothermal reservoirs is that the energy usually is not depleted from geothermal reservoirs even when all the fluid has been produced. The energy stored in geothermal reservoirs is in the form of heat, and, due to the high heat capacity and total mass of the formation itself, most of the heat stored in geothermal reservoirs cannot be removed under primary production. It is common, therefore, to inject produced water back into the reservoir to maximize the energy extraction.

To design effective injection and production programs for geothermal reservoirs, the physics of the flow in the reservoirs must be understood. However, understanding this flow is not an easy task. Geothermal reservoirs are, in general, highly fractured and heterogeneous, and the transport of fluids is influenced strongly by heat diffusion and by the presence of liquid retained in the porous matrix which acts as a mass source for the produced fluids. This retained liquid may be in the form of capillary condensed water or liquid adsorbed onto the rock grains.

The first stage in understanding the physics of flow in geothermal reservoirs is to understand the isothermal flow of fluids in porous and fractured media. The

petroleum engineering literature is replete with analyses of this subject.

The second stage in understanding flow in geothermal systems is to understand the simultaneous transport of fluid and heat in porous media. Beginning with the work of Whiting and Ramey [71], numerous researchers have studied transport and storage in geothermal reservoirs. Crank [17] presented a mathematical analysis of the simultaneous diffusion of pressure and heat. Brigham and Morrow [12] applied gas reservoir volumetric analysis to geothermal reservoirs with excellent results. Herkelrath, et. al. [34] and Moench and Atkinson [49] presented models for the simultaneous diffusion of fluid and heat in one dimensional systems and matched experimental data. Pruess, et. al. [56] presented an analytical solution for heat transfer at a boiling front, while Fitzgerald and Woods [24], Fitzgerald and Woods [25], Woods and Fitzgerald [73], and Doughty and Pruess [20] presented similarity solutions describing the flow of water, vapor, and heat in geothermal reservoirs. Pruess [55] studied heat transfer at the boiling front and Pruess and Narasimhan [57] considered flow in fractured vapor-dominated reservoirs. All of the research described above assumed no retained liquid phase. Thus, in much research carried out on fluid and mass transfer, an important element is missing.

The third stage in understanding flow in geothermal systems is to understand the effects of retained liquid on the flow of fluids and heat in porous media. Retained liquid (adsorption) effects have been studied for a number of vapor storage systems. Lin and Ma [42], Bojan, et. al. [10], and Pogorelov and Churmayev [54] provided theoretical analyses of adsorption in an array of porous media. Blazek, et. al. [9] studied the effects of adsorption in methane storage tanks. Morrow [50], Schettler, et. al. [63], Lane, et. al. [39], and Calson and Mercer [14] studied the effects of gas adsorption in low permeability gas reservoirs. Hawkins, et. al. [33], Anbarci and Ertekin [4], Nguyen [53], Matranga, et. al. [43], Matranga, et. al. [44], Bhatia [8], and McElhiney, et. al. [47] studied the effects of adsorption in coal-bed methane reservoirs. The research listed above shows that in methane storage systems, coal-bed methane reservoirs, and low permeability gas reservoirs, adsorption of vapor can play a major role on the storage and pressure depletion characteristics in these systems. For geothermal reservoirs, the same systematic analysis of adsorption effects is not

yet complete.

Research by Calhoun, et. al. [13], Udell [66], Hsieh and Ramey [36], and Economides and Miller [21], indicates that adsorption and/or capillary condensation may play a significant role in determining the flow and storage characteristics in geothermal reservoirs as well. The third stage, then, in understanding fluid flow in geothermal reservoirs is to incorporate retained liquid (adsorption) effects into geothermal flow models. The initial steps in understanding adsorption effects in geothermal reservoirs have been taken by Pruess and O'Sullivan [58] who presented an overview of the effects of adsorption on depletion of a geothermal reservoir and Phu and Ramey [52] who presented a numerical model of a geothermal reservoir which included mass balance effects of adsorption.

1.1 Fundamentals of Storage and Flow in Geothermal Reservoirs

In a geothermal reservoir, water may exist in four phases. These phases are: mobile liquid water, capillary condensed liquid water, adsorbed water, and vapor. The existence of water in the liquid and vapor phases may be observed directly from injection and production experience. In many geothermal reservoirs, liquid water at a temperature much lower than the reservoir temperature is injected into one portion of the reservoir and predominantly vapor is produced from another area. Clearly, liquid water flows to a certain extent in these reservoirs as does water vapor. The existence of capillary condensed water and adsorbed water may only be inferred by more indirect means. Specifically, there are three processes which may be used to determine the magnitude of liquid storage due to adsorbed and capillary condensed water. The first is mass balance calculations for a given producing reservoir. Knowledge of the extent of a reservoir coupled with analysis of the production history can give an engineer a gross estimate for the amount of fluid stored in a given phase in a geothermal reservoir. Second, experiments on core from a given reservoir can

yield actual measurements of the adsorbed and capillary condensed phases. The relative amounts of adsorbate and capillary condensed phase may also be deduced from experimental results as will be discussed in Chapter 2. Third, an application of the physics of capillary behavior may be used to determine whether a capillary condensed phase or an adsorbed phase is present for a given range of pore sizes. When used together, the three processes described above can provide a better understanding of the distributions, thermodynamics, and relative amounts of the adsorbed and capillary condensed phases present.

Accurate determination of the characteristics and relative amounts of each of the phases present in geothermal reservoirs is of paramount importance to understand flow in these reservoirs.

Despite the extensive research directed at flow in geothermal reservoirs, no generally applicable determination of adsorptive effects has yet been presented. Most of the previous work has focused on specific reservoirs or has been carried out by numerical means under very specific conditions. There is a need, therefore, to determine, in a general way, the effects of a retained liquid phase on the pressure response and flow characteristics in geothermal reservoirs. This research develops that general approach and applies it to flow in the Geysers geothermal reservoir.

1.2 Outline of Research

To meet the overall objectives, the research was performed in several sections:

1. **Thermodynamics of Geothermal Fluids.** Thermodynamic properties of adsorbed and capillary condensed liquid were studied in detail to determine their properties for subsequent modeling. At present, there is some confusion as to the differences, if any, between adsorbed and condensed phases. In this section, differences between the two phases were explained. Quantitative conclusions were drawn as to the relative volumes of adsorbed and capillary condensed fluids at the Geysers and the implications for fluid thermodynamics were examined.

2. **Analysis of the Energy Balance.** One method of extending the producing life of a geothermal reservoir is to inject surface water into the reservoir to replace produced mass. It is unclear whether a retained liquid phase plays a significant role in the propagation of the boiling liquid front or if it affects the heat transfer in the reservoir. In this section, a dimensional analysis of heat effects was carried out to determine heat effects of a retained liquid phase.

3. **Semi-Analytical Model.** Adsorbed liquid mass as a function of pressure is available in the form of adsorption isotherms. A straightforward method of determining the effects of this adsorbed mass on pressure would allow simple determination of adsorption effects. An analytical solution was derived for single-phase vapor flow in the presence of a retained liquid phase.

4. **Numerical Model.** To model tracer production characteristics and to check thermal assumptions not easily modeled analytically, a numerical solution is needed. A one-dimensional implicit pressure, explicit saturation and temperature finite difference model was developed to model vapor flow in the presence of an adsorbed phase.

5. **The Geysers Geothermal Reservoir.** In an attempt to track injected fluids and to infer reservoir characteristics, tracer is often injected into geothermal reservoirs along with recharge fluids. Unfortunately, due to the complicated nature of the tracer production histories, interpretation is often difficult. The purpose of this section was to determine the role of retained liquids on the production history of injected tracer. Tracer histories from the Geysers geothermal reservoir were modeled and conclusions were reached about the importance of several factors in the propagation of tracer.

Chapter 2

Thermodynamics of Geothermal Fluids

Before flow in geothermal reservoirs can be comprehensively analyzed, the different fluid phases must be defined and their thermodynamics understood. The fluids studied are free liquid, free vapor, capillary condensed liquid, and adsorbed liquid. When all four fluid phases are present in a geothermal reservoir, fluid distributions are as shown schematically in Figure 2.1.

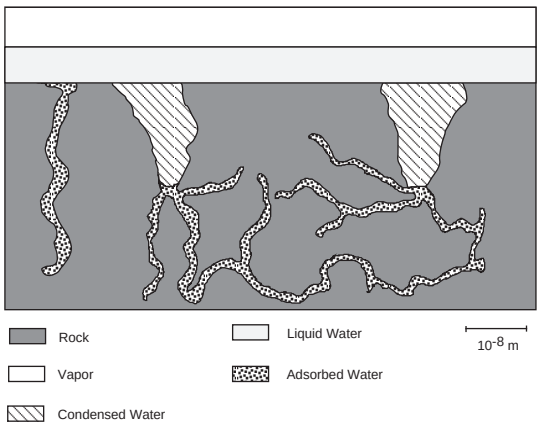

Figure 2.1: Fluid distributions in a geothermal porous medium

Vapor and liquid water occupy the largest pores and fractures. As pores decrease in size, capillary condensation occurs in accordance with the Kelvin equation:

$$RT \ln \frac{p_v}{p_0} = -\frac{2\gamma v_l}{r} \tag{2.1}$$

The Kelvin equation accounts for vapor pressure lowering over a curved interface. In Eqn. 2.1, p_v is the curved interface vapor pressure for the liquid, and p_0 is the saturation vapor pressure for the liquid. Liquid properties are designated by γ, the liquid interfacial tension and v_l, the specific volume of the liquid while r denotes the radius of curvature of the meniscus. In large pores, vapor pressure lowering is insignificant, but for very small pores, curvature effects can become large and vapor pressure may significantly deviate from saturation values. The Kelvin equation shows that in pores, where liquid interfaces are curved, the pressure at which capillary condensation occurs is lower than saturation values at a given temperature. These pressure effects may be used to determine transitions from capillary condensation, which generally occurs in large pores, to pore-filling adsorption, which is a small pore phenomenon.

For the remainder of this research, the following phase definitions will be assumed:

1. **Vapor phase.** The free vapor phase may occur in equilibrium with liquid water, condensed water, or adsorbed water phases. When determining the thermodynamics of the vapor phase, no assumptions about the curvature of the vapor-liquid interface were made.

2. **Liquid water phase.** The liquid water phase consists of water that would exist in thermodynamic equilibrium in the absence of a porous medium.

3. **Condensed water phase.** The condensed water phase consists of water that is in thermodynamic equilibrium in a porous medium due to capillary effects.

4. **Adsorbed water phase.** The adsorbed water phase consists of water adhered to the solid surface by intermolecular forces.

A description of the thermodynamics of each phase and the transition between phases is given below.

2.1 The Vapor Phase

When liquid water is present in a geothermal reservoir, all small pores are occupied by either adsorbed or condensed phases which leaves only the largest pores, those unaffected by capillary effects, to be filled with liquid water and vapor. Thus, when liquid water is present, flat surface thermodynamics are valid for the vapor phase. When liquid water is not present and the vapor phase interfaces directly with either the condensed or adsorbed phase, thermodynamics of the vapor phase are altered somewhat from standard flat-surface values. Udell [66] showed that for a given temperature, the effective pressure lowering in the liquid and vapor phases may be calculated.

The pressure difference between liquid and vapor phases across a curved interface is given by:

$$p_v \; - \; p_l \; = \; \frac{2\gamma}{r_e} \tag{2.2}$$

where the effective pore radius is given by:

$$r_e \; = \; \frac{r}{\cos\theta} \tag{2.3}$$

Udell [66] showed that, in a porous medium, both the vapor and the liquid exist in a superheated state. Therefore, in a porous medium, the physical and thermodynamic properties of both vapor and liquid differ from their properties in the absence of a porous medium. By equating the chemical potentials of the two phases (which is necessary for thermodynamic equilibrium) it is possible to derive an expression for vapor pressure lowering in the system. The chemical potential, μ for vapor phase may be written as:

$$\mu_v \; = \; \mu_0 \; - \; \int_{p_v}^{p_0} v_v dp \tag{2.4}$$

and, assuming the vapor specific volume, v_v may be written in terms of the ideal gas law, Eqn. 2.4 may be written as,

$$\mu_v \; = \; \mu_0 \; - \; RT \ln \frac{p_0}{p_v} \tag{2.5}$$

Analogous to the chemical potential balance for the vapor phase, the liquid phase potential balance is written:

$$\mu_l \;=\; \mu_0 \;-\; \int_{p_l}^{p_0} v_l dp \tag{2.6}$$

and, if the liquid phase is assumed incompressible, Eqn. 2.6 may be rewritten as,

$$\mu_l \;=\; \mu_0 \;-\; (p_0 - p_l)v_l \tag{2.7}$$

For thermodynamic equilibrium, the chemical potentials in the liquid and vapor phases must be equal. Thus, by equating the expressions obtained in Eqns. 2.5 and 2.7 and substituting Eqn. 2.2, the following expression for the vapor pressure lowering is obtained:

$$\frac{2\gamma}{r_e} \;=\; RT\rho_l \ln\frac{p_o}{p_v} \;-\; (p_o - p_v) \tag{2.8}$$

Eqn. 2.8 is analogous to the Kelvin equation and is equivalent when the saturation pressure, p_o, is equal to the pressure in the vapor phase, p_v. As will be shown, this assumption is usually a good one. It is noted that the Kelvin equation in its common form, Eqn. 2.1 makes the assumption that pressure lowering in the vapor phase is small. Eqn. 2.8 does not make that assumption *a priori*. Thus, it is possible to investigate the effects of the presence of a porous medium on the properties of the vapor phase.

For the range of pore sizes in which vapor is likely to occur, vapor pressure lowering is quite small. Udell [66] reported that, for radii greater than 0.1 μm, vapor pressure lowering is less than 0.1 percent. Figure 2.2 shows pressure lowering in the vapor phase for a range of temperatures and pore sizes. The ordinate in Figure 2.2 is written as the deviation from saturation pressure. Each curve endpoint corresponds to the point at which Eqn. 2.8 predicts a liquid pressure of 0 (this result will be explained in detail later). Based on results shown in Figure 2.2, vapor thermodynamics may be assumed to be flat surface thermodynamics regardless of fluid saturation with very little loss of accuracy.

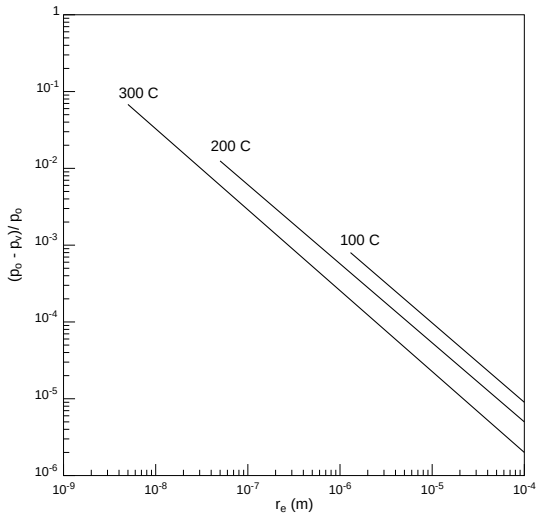

Figure 2.2: Vapor phase pressure lowering (after Udell [66])

Steam properties tabulated by the National Institute of Standards and Technology (NIST) [26] were used in this research for vapor properties.

2.2 The Liquid Water Phase

By definition, the liquid water phase is the water phase which is unaffected by capillary curvature. Thus, if a flowing liquid phase is present, the thermodynamics of that phase may be determined from standard thermodynamic tables. In all the calculations made here, it was assumed that the liquid water phase was pure water with no dissolved salts.

2.3 The Retained Liquid Phases

To model the flow of fluids in the presence of a condensed or adsorbed phase (retained liquid phase), a minimum of two characteristics of the adsorbed fluids must be known. First, a relationship between system pressure and mass of adsorbate must be known. This information is determined by adsorption isotherms and by estimates of

the adsorbate density. Second, knowledge of the internal energy and heat of adsorption (condensation) is necessary to accurately model heat effects of fluid flow in the presence of an adsorbing (condensing) phase.

No thermodynamic tables of retained water phase exist, and it is unlikely that any tables will ever be compiled since liquid retention characteristics are matrix dependent. Thus, to determine thermodynamics of the adsorbed phase, it is necessary to make inferences from measurable quantities in a given porous medium.

2.3.1 Adsorbed and Capillary Retained Liquid

In 1968, Ramey [59] showed that, in the Geysers geothermal reservoir, the volume of the reservoir was too small to store all of its mass as water vapor. In other words, even though all production from the Geysers had been vapor, the fluid must be stored as water in the reservoir. This conclusion led to the paradox that liquid water must exist in the Geysers reservoir at a pressure and temperature at which liquid water can not exist under normal conditions. The "paradox of the Geysers" led numerous authors, among them White [70] to speculate that either a separate liquid water source, external to the vapor dominated reservoir, is responsible for recharge in the Geysers, or storage in the Geysers is accomplished by capillary retained or adsorbed water which, due to vapor-pressure lowering may exist as a liquid under conditions which would normally specify vapor. Subsequent research has failed to find any evidence of a hidden water source recharging the Geysers while a number of investigations have shown retention of water within the reservoir itself to be the most plausible mass storage source. It is, however, the way that this fluid is stored and the effects of the the storage that have yet to be fully characterized.

In 1941, Leverett [41] discussed the principles of capillarity and defined the term "capillary pressure" as the difference in pressure between the wetting and non-wetting phases in a porous medium. During the following years, several authors presented experimental and theoretical analyses of capillary pressure effects under a number of conditions. It was the desire of Calhoun [13], et. al. [13] in 1949 to "amplify" existing capillary pressure correlations by extending measurements to systems with very low

liquid saturations and by expanding the range of liquids studied. Calhoun [13] presented a series of measurements of vapor pressure lowering and capillary pressure as a function of water saturation and showed that vapor pressure lowering may be very significant in small pores. Since Calhoun's [13] measurements extend to extremely low water saturations, they seem to indicate that capillary condensation is the sole mechanism for vapor pressure lowering in porous media. However, Hsieh and Ramey [35] pointed out in 1978 that at low liquid saturations, the vapor pressure lowering reported by Calhoun [13] was actually due to adsorption rather than to capillary effects. Hsieh and Ramey [35] defined a theoretical limit to vapor condensation to correspond to a pore of radius equal to the radius of a water molecule. This minimum pore radius as defined by Hsieh and Ramey [35] is 2 $\mathring{A}$. By calculating the vapor pressure lowering expected in a pore of this size, they defined a maximum vapor pressure lowering due to capillary retention. Many of Calhoun's [13] reported values of vapor pressure lowering were actually greater than the maximum possible reported by Hsieh and Ramey [35], thus leading to the conclusion that, for a given porous medium, saturation below a certain point is controlled by adsorption rather than capillary condensation.

Subsequent work has focused on accurate determination of the pore size at which adsorption becomes the dominant process in pore filling. In 1982, Ramsay and Booth [60] measured pore sizes in oxide sols and gels by neutron scattering and nitrogen adsorption. By comparing measured fluid volumes and pore sizes, they concluded that the transition radius at which adsorption pore filling begins is 1.4 nm (14 $\mathring{A}$). In 1986, Evans et. al. [23] showed that the transition from adsorption to capillary condensation is not accurately modeled by the Kelvin equation. They showed that the influence of the solid surface and the small confining volume on fluid properties may strongly affect the accuracy of the Kelvin equation below 2 nm (20 $\mathring{A}$). In 1990, Ramsay and Wing [61] measured water vapor sorption in porous silica and ceria gels by both a mass approach, and by neutron scattering methods. They were able to show that in microporous solids, pore filling adsorption of water vapor commences at pore radii of about 3.5 nm (35 $\mathring{A}$). The experiments were carried out at 150 °C so they are directly applicable to geothermal systems. Experiments in mesoporous solids

indicated that single and multi-layer adsorption are important in pores of radius as large as 12 nm (120 $\mathring{A}$).

So, measurement of fluid distributions of adsorbed and capillary condensed fluids are available in a variety of porous materials. These measurements may be used as an aid in determining the likely fluid distributions in geothermal reservoirs. However, direct measurement of fluid saturations and pore size distributions in geothermal reservoirs are necessary to accurately determine the relative amounts of adsorbed and capillary condensed liquids in these reservoirs.

In 1981, in an early attempt to determine the amount of adsorbed liquid in geothermal reservoirs, Hsieh and Ramey [36] showed that in many dry steam geothermal reservoirs, surface adsorption may be the most important mechanism in vapor pressure lowering and mass storage. They also found adsorption to be a significant storage mechanism in geothermal reservoirs and, under certain conditions, in natural gas reservoirs. Their work was carried out in consolidated and unconsolidated sandstone so it was not directly applicable to geothermal reservoirs.

Direct measurement of adsorption/capillary retention in the Geysers reservoir has been carried out by Shang and Horne [64] and Micromeritics Instrument Corporation [37]. In a series of experiments designed to measure the mass storage effects of adsorption and the effects of temperature on adsorption, Shang and Horne [64] have presented a number of measurements of liquid retention in Geysers geothermal core material. In consideration of reported adsorption isotherms, simple reasoning leads to the conclusions that at a zero pressure, liquid retention is at a minimum for a given porous medium and is often zero. At a pressure just greater than the saturation pressure, the sample must be at 100 % liquid saturation. Finally, at the saturation pressure, the saturations of liquid and vapor are determined by flat surface thermodynamics. Since it is known that both adsorption and capillary condensation occur in a porous medium, the "adsorption" isotherm must contain information on both the adsorbed amount and the capillary condensed amount between relative pressures of zero and one. (Adsorption isotherms are commonly reported in terms of "relative pressure" which is the system pressure divided by the saturation pressure). In fact, Correa [64] showed that an "adsorption" isotherm may be created by combining the

theoretical saturation vs. pressure data of adsorbed and capillary condensed liquid. Thus, from a saturation standpoint, an adsorption isotherm may be considered as an adsorbate/condensate isotherm containing information about both an adsorbed phase and a condensed phase.

By applying the radius for pore filling adsorption, as proposed by Ramsay and Wing [61], to Geysers pore size distribution data (Figure 2.3) as determined by Micromeritics [37] on a sample taken from well NEGU-17 at the Geysers, the percentage of Geysers volume that is 100% adsorbed liquid was obtained. By use of a radius cut-off of 35 $\mathring{A}$ for pore-filling adsorption, it was found that approximately 2.75 % of the volume of retained liquid at the Geysers geothermal field is likely to consist of pore-filling adsorbed liquid. This is by no means all of the adsorbed liquid in the reservoir, it is simply an estimate of that adsorbed liquid which solely occupies an individual pore and does not include an estimate of the mono- and multi-layer adsorption that occurs in larger pores. The significance of the distinction between pore-filling and mono- and multi-layer adsorption will be discussed more fully later in this section.

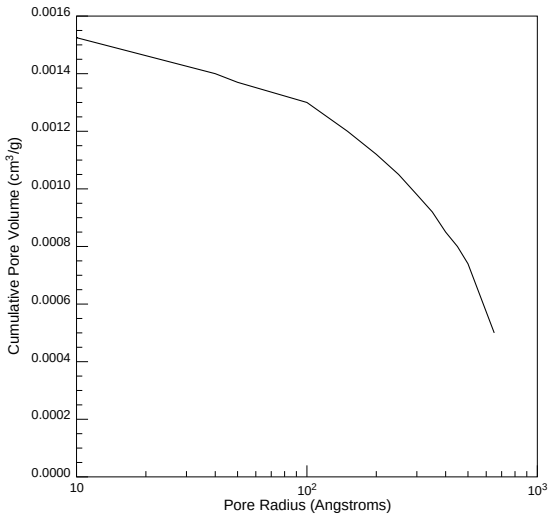

Figure 2.3: Geysers pore cumulative volume vs. pore radius (from Micromeritics [37])

For pores larger than 35 $\mathring{A}$ both adsorption and capillary condensed water are responsible for pore filling and it is difficult to determine the exact percentages of adsorbed and condensed liquid present. However, it is possible to determine an upper

limit on pore size for which adsorption is likely to occur.

Udell [66] pointed out that when capillary condensation occurs in a porous medium, both liquid and vapor exist in a superheated state which changes the shape of the two phase region and results in the existence of both the liquid and vapor phases at pressures lower than predicted by flat surface thermodynamics. The combination of Eqns. 2.8 and 2.2 yields an expression for the liquid phase pressure in terms of saturation pressure, liquid properties, and pore size at a given temperature.

$$p_0 \; - \; p_l \; = \; RT\rho_l \ln \frac{p_0}{p_l + \frac{2\gamma}{r_e}} \tag{2.9}$$

Eqn. 2.9 allows calculation of the liquid pressure as a function of pore size. In general, the liquid pressure decreases with a decrease in the pore radius. In the limit, as pore size decreases and capillary pressure increases, pressure in the liquid phase eventually is reduced to zero. The point at which liquid phase pressure is reduced to zero is assumed to correspond to a transition in which retained liquid changes from capillary retention dominated to adsorption dominated. This assumption is made for three reasons. First, as shown by Hsieh and Ramey [35], the theoretical critical radius below which capillary condensation cannot occur (pore radius equivalent to that of a water molecule) yields negative pressures when used in Eqn. 2.9. Second, the pore sizes at which pore filling adsorption occurs as measured by Ramsay and Wing [61] also yield negative liquid pressures when used in Eqn. 2.9. Third, the largest pore size shown to have a significant amount of adsorbed phase present as shown by Ramsay and Wing [61] yields a negative pressure when used in Eqn. 2.9. This mesoporous radius (120 $\mathring{A}$) is near the transition pore radius described above. Therefore, both theoretical and experimental results confirm the assumption that below a pore radius which would result in a negative liquid pressure, adsorption effects are large.

For the range of pore sizes shown, pressure lowering in the vapor phase is insignificant while the pressure lowering in the liquid phase is quite large. Figure 2.4 shows liquid-phase pressure lowering for a range of pore sizes and temperatures. Significant liquid pressure lowering occurs and liquid pressure is shown to go to zero at radii which depend upon the system temperature. Hsieh and Ramey [35] showed that, in very small pores, vapor pressure lowering as measured by Calhoun, et. al. [13] was

greater than the computed maximum for a pore of the same dimension as a water molecule. Udell [66] showed that for the large vapor pressure lowering effects computed by Hsieh and Ramey [35], corresponding liquid phase pressures calculated by Eqn. 2.9 were negative. These two results taken together led Udell [66] to conclude that the radius at which liquid pressure is calculated to be zero corresponds to the point at which some other mechanism besides capillary condensation occurs in the pore (i.e. the onset of adsorption). Thus, for pores larger than those at which liquid pressure is driven to zero (critical capillary radius), it may be assumed that retained liquid is 100% capillary condensed water. Additionally, it is assumed in this research that for pores of radius less than the critical capillary radius, adsorption is a significant pore filling mechanism. These assumptions are supported by the results of Ramsay and Wing [61], cited above, that, in mesoporous solids, adsorption may be a significant pore filling mechanism in pores as large as 120 $\mathring{A}$ which is very near to the critical capillary radius computed by Eqn. 2.9.

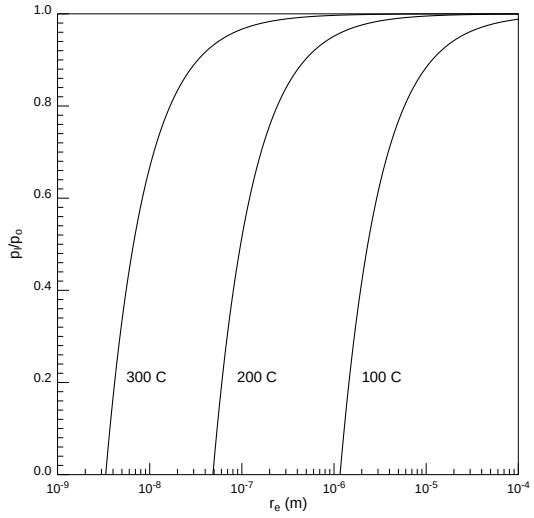

Figure 2.4: Liquid phase pressure lowering (after Udell [66])

Using an average reservoir temperature for the Geysers of 230 °C, the critical capillary radius is 200 $\mathring{A}$. By use of pore size distribution data from the Geysers, the percentage of retained liquid which may be described as capillary condensed liquid is approximately 75% by volume.

Shang, et. al. [65] presented adsorption isotherm data for the Geysers geothermal reservoir for a range of conditions. At 100 °C, the measured isotherm is shown in Figure 2.5. While the isotherm is not measured at actual reservoir temperature, it is felt that the variations with temperature are small so the illustrated isotherm may be considered typical of Geysers matrix.

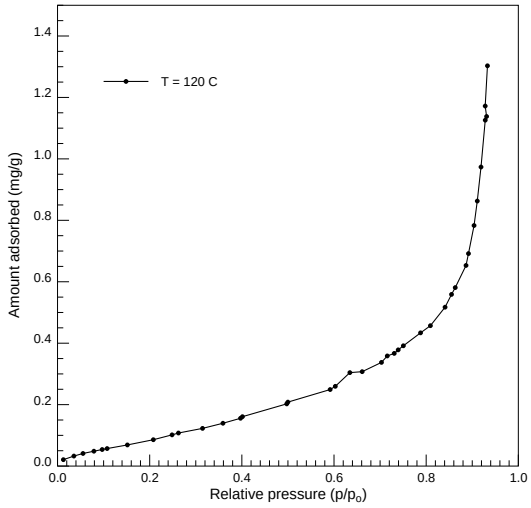

Figure 2.5: Geysers adsorption isotherm at 120 °C (after Shang [65])

From the following relationship, water saturation may be computed as a function of relative pressure based on amount adsorbed shown in Figure 2.5.

$$S_w = \frac{1-\phi}{\phi}\frac{\rho_r}{\rho_w}X \tag{2.10}$$

Gunderson [32] showed that matrix porosity values range from 0.2 % to 8.1 % for Geysers reservoir material and Micromeritics [37] show a sample from well NEGU-17 to have a matrix porosity of 0.6 %. Data on pore size distribution were computed from the NEGU-17 sample used by Micromeritics [37], therefore, a value of 0.6% was used to compute water saturation from Eqn. 2.10. Figure 2.6 shows computed water saturation as a function of relative pressure for Geysers matrix material. Based on the pore size constraints on capillary condensation and pore-filling adsorption discussed previously, a breakdown of the type of fluid saturating the matrix is included in Figure

2.6. Adsorbate density used to calculate water saturation for Figure 2.6 was assumed to be saturated water density at 230 °C.

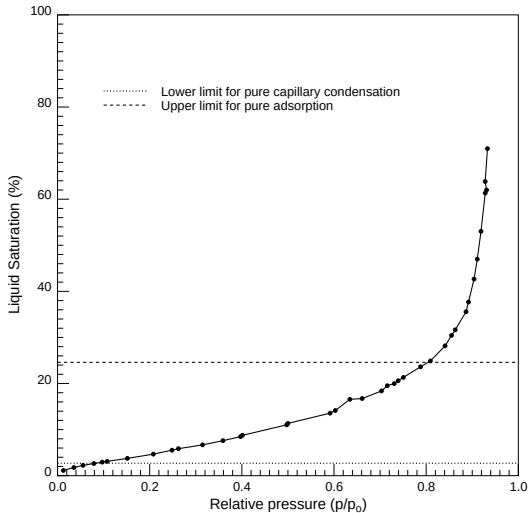

Figure 2.6: Geysers liquid saturation with constant liquid density.

Figure 2.6 shows three distinct liquid phase saturation regions for the Geysers geothermal reservoir. From relative pressures of 1.0 to 0.8, essentially all retained liquid is capillary condensate. This phase represents about 75 % of the liquid volume at the Geysers. While some surface adsorption occurs even in large pores, the overwhelming majority of liquid in pores filled at relative pressures of 0.8 to 1.0 is made up of capillary condensed liquid. From relative pressures of 0.8 to 0.01, a transition from capillary condensation to pore-filling adsorbate occurs. This phase accounts for about 22 % of the total liquid volume at the Geysers. Finally, from relative pressures of 0.01 to 0.0, the retained liquid consists of pore-filling adsorbate. This phase accounts for only about 3 % of the retained liquid volume at the Geysers. Since relative pressures must be extremely low to reach the pure adsorbed phase, it is unlikely that the pure adsorbed phase will ever be produced from the Geysers geothermal reservoir.

The above analysis answers many questions about the relative amounts of capillary condensed and adsorbed fluids in the Geysers geothermal reservoir. Questions still remain, however, as to the thermodynamics of the condensed and adsorbed phases. In other words, use of a general liquid saturation isotherm including both adsorbed

and condensed liquid is not possible until the properties (density, internal energy, latent heat) of the adsorbate and condensate are understood.

2.3.2 Density of the Retained Liquid Phases

To accurately determine the pressure effects of a retained liquid phase, the density of the retained liquid must be modeled accurately. For modeling of fluid flow in specific geothermal reservoirs, information on the relative amounts of retained liquid must be combined with information on liquid properties to determine the best way of modeling retained liquid properties.

Density of the Capillary Condensed Liquid

Extrapolation of the liquid specific volume curve provides information on the density of capillary condensed liquid. Condensed liquid phase specific volumes are shown as a function of pressure in Figure 2.7.

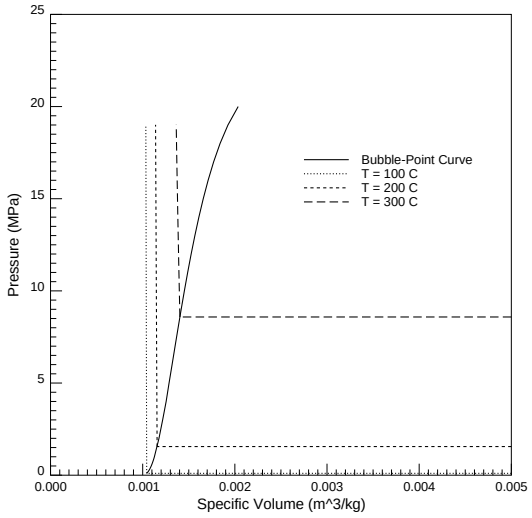

Figure 2.7: Specific volume of saturated water

Due to the low compressibility of liquid water, at a given temperature, density changes very little from liquid at saturated conditions to superheated conditions which exist in capillary condensed liquids.

Table 2.1 compares water density at saturated conditions for a range of temperatures with extrapolated values of density at superheated conditions corresponding to the critical pore radius when adsorption effects become large (i.e. $p_l \leq 0$).

Table 2.1: Density Variation Between Condensed and Saturated Liquid Phases

Temperature (°C)	Saturated water density (kg/m^3)	Adsorbate density (kg/m^3)	Percent difference (%)
100	958.393	958.350	0.0045
200	864.743	863.65	0.126
300	712.409	696.32	2.26

The above analysis indicates that the density of condensed liquid is very near to the density of liquid at saturated conditions. Since it was shown above that approximately 75 % of the stored liquid mass at the Geysers is condensed liquid water, it may be concluded that 75 % of the stored liquid as described by Geysers adsorption isotherms, i.e. liquid stored from relative pressures of about 1.0 to 0.8, has a density nearly identical to that of saturated water at a given temperature.

Density of the Adsorbed Phase

Density of the adsorbed liquid phase is difficult to determine and very few measurements have been attempted. Ramsay and Wing [61] showed that adsorbed liquid density at a given temperature is approximately 70 % of the density of liquid water at the same temperature. Their measurements were made by neutron scattering techniques and indicated that the ordering of adsorbed liquid molecules changes from that in the bulk liquid phase.

At the Geysers, as shown above, less than 3% of the retained liquid phase is likely due to pore-filling adsorbed liquid. The range in relative pressures at which this phase is dominant (0.0 to 0.01) is also quite low and it is unlikely that production of this low density fluid will ever take place. Therefore, the liquid mass stored as low density adsorbate can be ignored in most geothermal modeling efforts at the Geysers.

Density in the Capillary/Adsorbed Phase Transition

In the previous two sections, the density of the pure capillary condensed liquid and the pure adsorbed phases have been established. It has also been shown that, at the Geysers geothermal reservoir, these two phases, in essentially pure form, account for about 78% of the stored liquid mass. The remaining liquid, accounting for 22% of the liquid mass, is made up of both adsorbed vapor and condensed liquid. Assuming a linear transition from condensed liquid to adsorbed liquid, it is possible to determine the density of liquid consisting of both condensate and adsorbate. Figure 2.8 shows density of the retained liquid phase as a function of pressure for the Geysers geothermal reservoir. A similar analysis may be applied to other geothermal reservoirs. Effects of density assumptions for the retained liquid phase are discussed in Chapter 4.

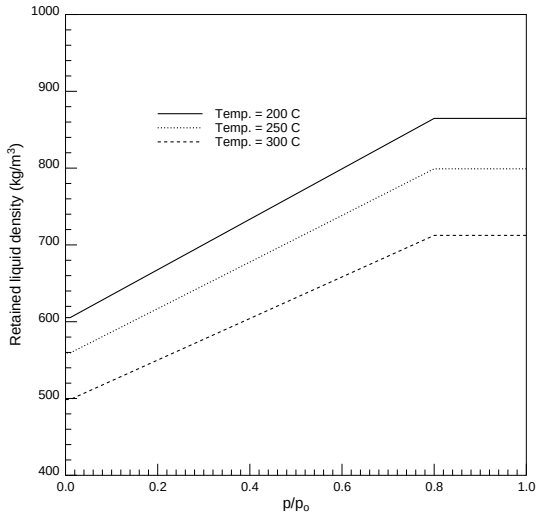

Figure 2.8: Retained liquid density as a function of pressure (Geysers sample)

Figure 2.9 shows liquid saturation inferred for the Geysers rock sample as computed with Eqn. 2.10 with the varying liquid density shown in Figure 2.8. On the same figure are water saturation values computed under the assumption of constant water density. As may be observed, only very small differences are obtained by using varying retained liquid densities.

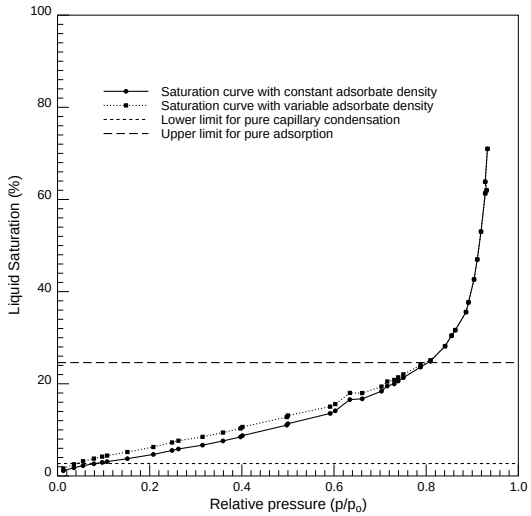

Figure 2.9: Geysers liquid saturation with variable liquid density.

2.3.3 Thermal Properties of the Retained Liquid Phases

To model heat effects of a retained liquid phase, accurate modeling of the internal energy and the heat of vaporization/desorption of the phase is necessary. Defay and Prigogine [19] showed that the heat of vaporization/desorption in a porous medium may be expressed by:

$$h_{T,p_v} \;=\; \Delta_e h_0 \;+\; \frac{2v_l}{r}\left[\sigma - T\frac{d\sigma}{dT}\right] \;-\; \frac{2\sigma T}{r}\frac{dv_l}{dT} \;+\; \frac{2\sigma v_l T}{r^2}\left(\frac{\partial r}{\partial T}\right)_{\xi} \tag{2.11}$$

Eqn. 2.11 does not distinguish between capillary condensed fluid and adsorbed fluid. Instead, it includes all heat effects generated by the phase transition of liquid to vapor in an initially liquid filled pore. Distinguishing between thermal characteristics of condensed and adsorbed fluids is achieved by use of pore size distribution

information. The first term in Eqn. 2.11 represents the heat of evaporation of water with no liquid curvature effects included and may be expressed as:

$$\Delta_e h_o \;=\; RT^2 \frac{\partial \ln p^o}{\partial T} \tag{2.12}$$

The second term in Eqn. 2.11 expresses the added heat due to the extension of the liquid surface by capillary curvature. The third term includes the heat of compression of the water due to capillary condensation. The fourth term expresses the the added heat due to an increase in the solid surface area as the pore is emptied. The fourth term is not straightforward to evaluate since it depends on the pore distribution in the solid matrix and the corresponding amount of adsorbed liquid associated with that range of pore sizes. The pore-dependent term is defined as:

$$\left(\frac{\partial r}{\partial T}\right)_{\xi} \;=\; \frac{dr}{dV_l} \cdot \frac{\partial v_l}{\partial T} \cdot n_l \tag{2.13}$$

where, dr/dV_l is obtained from pore size measurements and, n_l is a measure of the amount adsorbed or condensed.

In this research, a pore size distribution measured from a Geysers rock sample was used as a basis for determining the effects of pore drying on the heat of vaporization. Nitrogen adsorption was used for determining pore size distributions and adsorbed mass in. All measurements were carried out by Micromeritics [37] on a sample taken from well NEGU-17 at the Geysers. In the sample studied, porosity was determined to be 0.6 % which is consistent with matrix porosity reported by Gunderson [32]. Pore volume as a function of pore radius is shown in Figure 2.3. The rate of change of radius with respect to pore volume as a function of radius (needed in Eqn. 2.11) is shown in Figure 2.10. Worth noting from Figure 2.3 is the fact that pores of radius less than 50 $\mathring{A}$ contribute very little to the total pore volume.

Figure 2.11 shows the magnitude of heat effects due to the extension of the liquid interface as surface curvature occurs. As liquid is evaporated from a curved interface, more energy is required than in evaporation of an uncurved interface due to an increased stretching of the curved interface. As is shown in Figure 2.11, heat effects due

to surface stretching are quite small. The maximum addition to the heat of vaporization due to surface stretching is about 2 %. Heat effects due to surface stretching are assumed to terminate when pore filling adsorption dominates ($r_e \approx 35$ $\mathring{A}$) since adsorbate is assumed to exist as a separate phase.

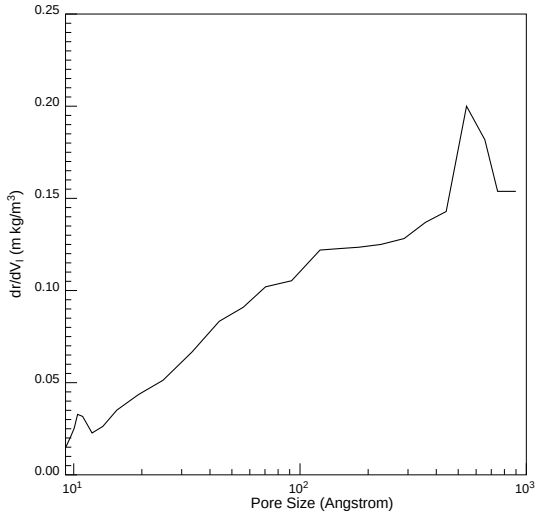

Figure 2.10: Rate of change of radius with respect of volume (Geysers sample)

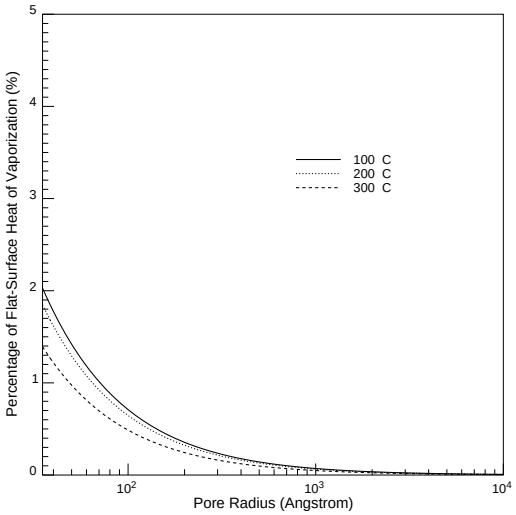

Figure 2.11: Surface extension effects on the heat of vaporization

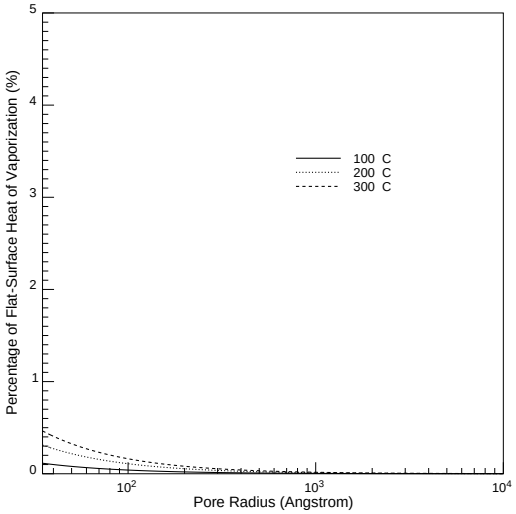

Figure 2.12: Liquid compression effects on the heat of vaporization

Figure 2.12 shows the magnitude of heat effects due to the capillary compression of condensed liquid. Figure 2.12 shows that more heat is required to evaporate capillary condensed liquid than flat-surface condensed liquid since attractive forces between fluid particles have been increased. The increase in evaporation energy is shown, however, to be small. The maximum effects of capillary compression on heat of vaporization are shown to be a 0.5 % increase. Heat effects due to capillary compression are assumed to terminate when pore filling adsorption dominates ($r_e \approx 35\ \mathring{A}$) since adsorbate is assumed to exist as a separate phase with no capillary compression effects.

Figure 2.13 shows the magnitude of heat effects due to an increase in the solid surface area as the pore is emptied. In other words, this figure shows the added energy needed to dry a pore as liquid recedes. Figure 2.13 shows that more heat is required to evaporate liquid retained in pores since liquid/solid attractive forces must be overcome. The magnitude of this term will vary with material tested but it is shown to be large for Geysers core material in very small pores. Heat effects due to pore drying influence the heat of vaporization for the entire range of pore sizes and, therefore, include the effects of both evaporation and desorption. The curves shown in Figure 2.13 are not smooth due to data used in calculating the curves. The rate

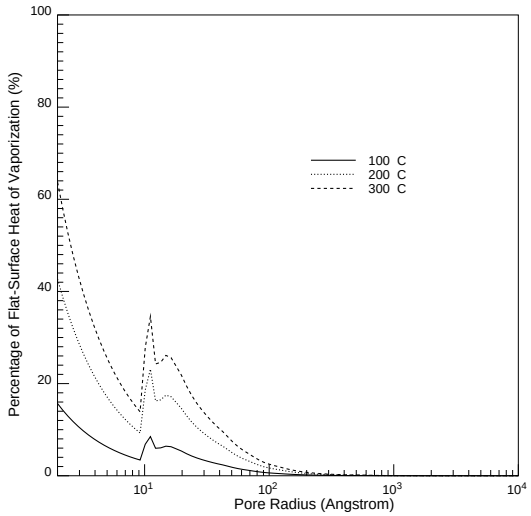

Figure 2.13: Pore drying effects on the heat of vaporization

of change of radius with respect to pore volume, shown in Figure 2.10, was used to compute pore drying effects and the roughness in the curve translated to roughness in the heat of pore drying curve shown in Figure 2.13.

Figure 2.14 shows the heat of vaporization for water as a function of pore radius for a range of temperatures. A notation is included in the figure to denote the 100 $\mathring{A}$ pore radius. About 90 % of Geysers liquid resides in pores of radius larger than 100 %. It is clear from Figure 2.14 that most of the liquid in the Geysers reservoir may be considered saturated liquid from a heat balance standpoint. For very small pores, the heat of vaporization effects can become large, but for a large range of pore sizes, heat of vaporization effects are not significant. Comparison of heat of vaporization effects with pore size distribution data at the Geysers shows that the heat of vaporization for about 80 % of the liquid stored varies from flat surface values by only about 3 %. Further, less than 1 % of the stored liquid has heat of vaporization values varying from flat surface values by more than 15 %. These results lead to the conclusion that, for most of the liquid stored at the Geysers, heat of vaporization does not vary significantly from saturated liquid values at a given temperature. Therefore, it is reasonable to use heat of vaporization values based on flat surface thermodynamics.

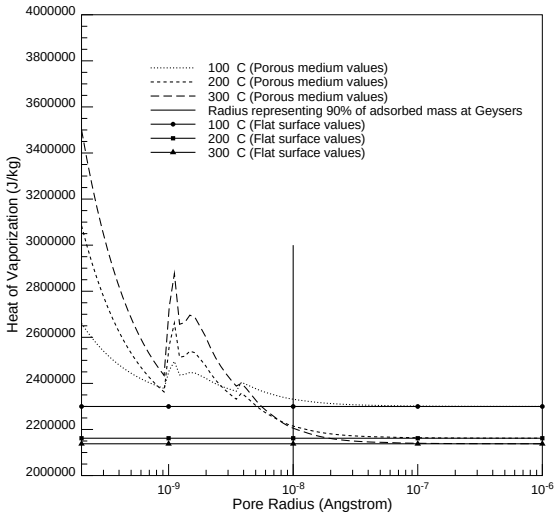

Figure 2.14: Effects of pore size and temperature on the heat of vaporization

Finally, Eqn. 2.11 shows that the increase in heat of vaporization is a surface phenomenon. In other words, the properties of the bulk retained liquid do not change significantly as liquid condenses, only the surface forces change. This observation, combined with the result that the vast majority of the liquid stored at the Geysers has thermal properties within a few percent of saturated water leads us to the conclusion that it may be assumed that the internal energy of the retained liquid phase is the same as the internal energy of the bulk liquid phase. So, from a heat balance standpoint, adsorbed and capillary condensed liquid may be considered identical to liquid water at saturated conditions.

2.3.4 Summary of Thermodynamic Properties

Analysis of the thermodynamics of retained liquids in geothermal reservoirs indicates that the properties may vary significantly from the properties of saturated liquid. It is shown that for pore sizes present in geothermal reservoirs, both density and heat of vaporization may be significantly altered.

Density of the capillary condensed phase varies from saturated density in large pores ($r_e \approx 10^4 \mathring{A}$ at 300 °C) to slightly less than saturated density in extremely small pores ($r_e \approx 50 \mathring{A}$ at 300 °C). Table 2.1 shows that the maximum density difference

is 2.26%. Even without any knowledge of the pore size distribution in a geothermal reservoir, density differences for the capillary condensed liquid were shown to be negligible.

Pore-filling adsorbate density was shown to be significantly less than saturated liquid density at a given temperature but, for the Geysers reservoir, was shown to account for a very small fraction of the total mass. Based on a simple linear relation, a relationship between retained liquid density and relative pressure was derived for the Geysers geothermal reservoir.

Heat of vaporization of the adsorbed phase varies from the heat of vaporization of liquid water in large pores ($r_e \geq 10^4 \mathring{A}$) to a maximum of about 1.5 times that value in the smallest pores that may be occupied by a water molecule ($r_e \approx 2\mathring{A}$). Internal energy effects were shown to be small since heat of vaporization effects are shown to be surface, rather than bulk liquid, dependent (Eqn. 2.11). Also, since internal energy of the vapor phase is shown to be virtually identical to the internal energy of vapor in the absence of a porous medium and heat of vaporization effects are shown to be small in the Geysers geothermal reservoir, it is inferred that the internal energy of the liquid phase must also be similar to the internal energy of a liquid phase in the absence of a porous medium.

Thus, thermal properties of retained liquid at the Geysers were shown to be nearly identical to the properties of liquid water at saturated conditions.

Chapter 3

Analysis of the Energy Balance

In computing the heat balance in geothermal reservoirs, a number of assumptions are commonly made. First, the assumption of thermal equilibrium is made whether an adsorbed phase is present or not. No calculations have been presented to determine if this is a good assumption for a range of conditions. Second, assumptions about the sizes of various terms in the energy balance on flow through porous media are often made without justification. A systematic analysis of the sizes of terms in the energy balance is needed to determine which terms may be neglected under a range of conditions. Third, the influence of an adsorbed phase on the fate of injected water must be studied to determine if the presence of an adsorbed phase significantly effects the rate of boiling of injected water.

The assumption of thermal equilibrium was tested, the relative importance of each term in the overall energy balance was determined, and the fate of injected water was studied for a range of conditions.

3.1 Validity of Thermal Equilibrium Assumption

In most studies of flow in geothermal reservoirs, the assumption of instantaneous thermal equilibrium is made. In other words, the time for the diffusion of heat from the matrix to the liquid is assumed to be much less than the residence time of the fluid. To test the validity of this common assumption, a comparison of fluid

velocity with heat diffusion velocity was carried out for a range of reservoir conditions. Computations were made for the flow of single phase liquid and for the flow of liquid in the presence of an adsorbed phase.

Single-phase fluid flow may be modeled by Darcy's law:

$$v = \frac{k}{\mu}\frac{dp}{dx} \tag{3.1}$$

Since most geothermal reservoirs are characterized by fracture porosity, pores may be approximated by a slit. For simplicity, heat conduction in a slit was modeled by heat conduction across a space spanned by two parallel planes as given by Carslaw and Jaeger [15]:

$$T(y,z) = \frac{4T_o}{\pi}\sum_{n=0}^{\infty}\left(\frac{1}{2n+1}\right)\exp\left(-\kappa(2n+1)^2\pi^2 t/l^2\right)\sin\left[\frac{(2n+1)\pi y}{l}\right] \tag{3.2}$$

where; T_o is the initial temperature, and l is the separation between the parallel planes (i.e. the fracture width), y is the distance measured from one of the planes, and κ, the thermal diffusivity, is defined as the ratio of thermal conductivity, k_t, and the heat capacity per unit volume, ρC_p.

$$\kappa = \frac{k_t}{\rho C_p} \tag{3.3}$$

To compare fluid residence time to characteristic heat diffusion time, reservoir rock and fluid characteristics must be assumed. Data for this analysis was taken from the range of properties at the Geysers geothermal field. From pressure data at the Geysers collected by Barker et. al. [7], a maximum pressure gradient of about 450 Pa/m was obtained. At 230 °C, fluid viscosity is 0.116×10^{-3} Pa·s and permeability can range from about 1×10^{-12} m^2 in large pores and fractures to about 1×10^{-16} m^2 in the matrix. Based on these ranges of values, a range in fluid velocity may be calculated and used to determine fluid residence time before the onset of boiling. The range of liquid velocity was computed from 4×10^{-6} m/s in large pores and fractures to 4×10^{-10} m/s in the reservoir matrix.

When cool injectate is heated by contact with hot rock, the thermal diffusivity of the liquid changes. Computation of the thermal diffusivity of water over a range of temperatures was carried out to determine the magnitude of this variation and to determine if one value of thermal diffusivity could be used in thermal diffusion computations. Table 3.1 shows the tabulated values of the thermal diffusivity of water. The thermal diffusivity is shown to reach a maximum at about 150 °C and it may also be observed that the diffusivity does not vary much for a wide range of temperatures. In fact, diffusivity values do not vary by more than 11% from the diffusivity value calculated at 50 °C. Therefore, the thermal diffusivity of liquid water at 50 °C, (1.563×10^{-7}) was used in thermal calculations.

A dimensionless temperature was defined as:

$$\bar{T} = \frac{T}{T_o} \tag{3.4}$$

where, T_o is the initial temperature of the rock matrix. Eqn. 3.2 was solved for dimensionless temperature at the pore center as a function of time for a series of pore sizes. Figure 3.1 shows the time required to heat injected fluid to the temperature of the rock matrix assuming constant thermal diffusivity. In other words, Figure 3.1 shows the time required to reach thermal equilibrium for a range of pore sizes.

Thermal equilibrium in pores of radius less than 10 μm is essentially instantaneous. In very large pores and fractures (1 cm) equilbrium may take on the order of 100 s. Thus, even for large fractures, the time required for injected liquid to reach the temperature of the rock matrix is small.

Based on these calculations, it was concluded that the assumption of instantaneous thermal equilibrium is valid.

3.2 Effects of Adsorbed Phase on The Heat Transfer Mechanism

In the previous section, the thermal equilibrium assumption was tested and shown to be valid for a simple solid/liquid system. In geothermal reservoirs, the process of

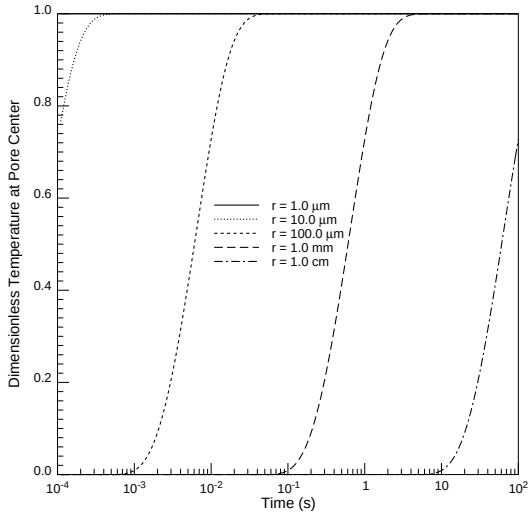

Figure 3.1: Time required for thermal equilibration of injected fluid

boiling injected liquid is a complicated process which may be affected by the presence of an adsorbed phase. In this section, the influence of the adsorbed phase on the heat transfer mechanism was studied and conclusions were drawn about the effects of an adsorbed phase on the boiling of injected fluids.

An expression for the heat transfer coefficient in a porous material was derived by Navruzov [51]:

$$h = \frac{k_f}{\delta_f} \tag{3.5}$$

where, k_f is the thermal conductivity of the liquid in the pore and δ_f is the thin liquid layer near the solid surface over which most of the thermal resistance is concentrated. In porous systems with no adsorbed phase present, the thermal conductivity is that of water at a given temperature and pressure. When an adsorbed phase is present, heat transfer will be altered by a thin film of adsorbed water at a temperature different than that of injected water. Table 3.1 presents the thermal conductivity of saturated water for a range of temperatures. The maximum variation in thermal conductivity over a range of temperatures likely in geothermal reservoirs is always less that 15

%. Therefore, assuming that the thickness is constant over which heating resistance occurs, the maximum variation in heat transfer is also 15 %. When an adsorbed phase is present, the temperature and, therefore, the thermal conductivity of the adsorbed phase must be larger than the thermal conductivity of the injected water. This means that the effect of an adsorbed phase on the heat transfer to injected water is an increase in the transfer rate resulting in more rapid boiling than without adsorption, thus enhancing the validity of the thermal equilibrium assumption. This increase in heat transfer is small, however, limited to a 15 % increase over the transfer rate without an adsorbed phase present.

3.3 The Energy Balance

A detailed analysis of the energy balance is necessary to determine the effects of an adsorbed phase on the storage and transfer of energy in geothermal reservoirs. The purpose of this section is to study the heat balance to determine the size of each term and the range of conditions for which each term is important. Information on the importance of each term may then be used in modeling the flow of geothermal fluids.

Garg and Pritchett [27] performed an analysis of an energy balance for geothermal reservoirs in the absence of an adsorbed phase. Their work was used as a basis from which to study the heat balance with an adsorbed phase present.

In deriving the energy balance it was assumed that the rock matrix is incompressible (i.e. porosity is constant). The incompressible matrix assumption is a good one in most geothermal reservoirs which are usually characterized by very small fracture porosity. It was also assumed that the fluids and the rock matrix are in local thermal equilibrium. The assumptions of local thermal equilibrium was shown to be valid earlier in this chapter where it was proven that equilibrium between the rock matrix and the flowing fluids occurs rapidly in low porosity systems. The complete energy balance for flow in a geothermal reservoir is:

$$\frac{\partial}{\partial t}\left[(1-\phi)\rho_r E_r \;+\; \phi S_w \rho_w E_w \;+\; \phi S_v \rho_v E_v \;+\; \phi S_a \rho_a E_a\right]$$

$$
\begin{aligned}
&+ \nabla \cdot [\phi S_w \rho_w E_w u_w \; + \phi S_v \rho_v E_v u_v] \; + \; \frac{\dot{m}}{2} \left[|u_w|^2 \; - \; |u_v|^2 \right] \\
&= \; \nabla \cdot (\kappa_m \nabla T) \; - \; p_w \nabla \cdot [\phi S_w u_w] - \; p_v \nabla \cdot [\phi S_v u_v] \\
&+ \; \left[\frac{S_w^2 \phi^2 \mu_w}{k k_{rw}} \right] |u_w|^2 + \; \left[\frac{S_v^2 \phi^2 \mu_v}{k k_{rv}} \right] |u_v|^2 + Q_e
\end{aligned} \tag{3.6}
$$

Many of the symbols used in Eqn. 3.6 have been defined previously, but those as yet undefined are explained as follows: the internal energy of a phase, p, is denoted by E_p; mass flux from one phase to another is defined denoted by $\dot{m}$; and the thermal diffusivity of the entire system including both solid and fluid components is κ_m.

Garg and Pritchett [27] showed that many of the terms in Eqn. 3.6 may be neglected under certain conditions. They showed that the phase transition term, $[\dot{m}/2(|u_w|^2 \; - \; |u_v|^2)]$, is always small. They also showed that the pressure work terms, $p_f \nabla \cdot [\phi(S_f) u_f]$, and the viscous dissipation terms, $[S^2 \phi^2 \mu_f / k k_{rf}] |u_f|^2$ may be neglected under certain conditions. Specifically, for liquid-dominated systems both terms are small and may be neglected. For vapor-dominated systems, both terms are too large to ignore independently but they tend to cancel each other so neglecting both terms is valid. Therefore, in this research, the phase transition term and all pressure work and viscous dissipation terms were neglected. The resulting energy balance is:

$$
\begin{aligned}
\frac{\partial}{\partial t} &\left[(1-\phi) \rho_r E_r \; + \; \phi S_w \rho_w E_w \; + \; \phi S_v \rho_v E_v \; + \; \phi S_a \rho_a E_a \right] \\
&+ \nabla \cdot [\phi S_w \rho_w E_w u_w \; + \phi S_v \rho_v E_v u_v] \\
&= \; \nabla \cdot (\kappa_m \nabla T) \; + \; Q_e
\end{aligned} \tag{3.7}
$$

In the analytical and numerical models used in this research, it was assumed that injected liquid water boils rapidly upon injection into geothermal reservoirs. Due to the large heat capacity of the rock matrix at the Geysers and the rapid thermal equilibration rate show earlier in this chapter, the assumption of rapid boiling is probably a good one. Upon removing the liquid water terms from Eqn. 3.7, the heat balance becomes:

$$\frac{\partial}{\partial t}\left[(1-\phi)\rho_r E_r \;+\; \phi S_v \rho_v E_v \;+\; \phi S_a \rho_a E_a\right] \;+\; \nabla\cdot\left[\phi S_v \rho_v E_v u_v\right] = \;\nabla\cdot(\kappa_m \nabla T) \;+\; Q_e \tag{3.8}$$

The internal energy of the rock matrix is given by:

$$E_r \;=\; C_r T_r \tag{3.9}$$

The thermal conductivity of mixture of solid, liquid, and vapor is given by an averaging technique which accurately determines the thermal conductivities of several fluids in a porous medium (from Garg [28]):

$$(1-\phi)\left[\frac{2}{3} \;+\; \frac{1}{3}\left(\frac{\kappa_r}{\kappa_m}\right)\right]^{-1} \;+\; \phi(1-S_v)\left[\frac{2}{3} \;+\frac{1}{3}\left(\frac{\kappa_a}{\kappa_m}\right)\right]^{-1} + \phi S_v\left[\frac{2}{3} \;+\; \frac{1}{3}\left(\frac{\kappa_v}{\kappa_m}\right)\right]^{-1} \;=\; 1 \tag{3.10}$$

In low porosity systems, the rock conductivity term dominates, so thermal conductivity of the mixture κ_m was assumed to be the rock thermal conductivity.

The energy sink term, Q_e, accounts for energy lost from the system by production of liquid. Since it was assumed that the only free-flowing phase is vapor, the energy sink term is expressed on a volume basis by:

$$Q_e \;=\; u_v h_v \tag{3.11}$$

Finally, it was assumed that the internal energy of the adsorbed phase, E_a, is equivalent to the internal energy of the saturated water phase, E_w. This assumption is based on the thermodynamic analysis in Chapter 2 in which it was shown that the internal energy of adsorbed liquid is not significantly different than that of saturated water in a typical vapor dominated geothermal reservoir.

The final form of the energy balance used in this research is written as:

$$\frac{\partial}{\partial t}\left[(1-\phi)\rho_r C_r T \;+\; \phi S_v \rho_v E_v \;+\; \phi S_a \rho_a E_w\right] \;+\; \nabla\cdot\left[\phi S_v \rho_v E_v u_v\right] = \;\nabla\cdot(\kappa_m \nabla T) \;+\; Q_e \tag{3.12}$$

Table 3.1: Thermal Diffusivity of Water

Temp (∘C)	C_p (J/kg·K)	ρ (kg/m^3)	K (W/m·K)	κ (m^2/s)
20.0	4170.9	1000.0	0.60023	1.439×10^{-7}
50.0	4172.7	989.73	0.64537	1.563×10^{-7}
70.0	4170.9	979.50	0.66503	1.635×10^{-7}
100.0	4170.9	960.22	0.68125	1.686×10^{-7}
120.0	4239.0	945.05	0.68547	1.711×10^{-7}
150.0	4170.9	919.05	0.68446	1.732×10^{-7}
200.0	4170.9	866.60	0.66553	1.716×10^{-7}
250.0	4170.9	799.10	0.62140	1.601×10^{-7}

Chapter 4

Semi-Analytical Model

In analyzing the effects of adsorption on flow through porous media, it is important to isolate, as clearly as possible, the effects of adsorption so the physics of adsorption-influenced flow may be fully understood. Derivation of the conservation equation for fluid flow with adsorption leads to a highly nonlinear equation which may be solved either numerically or by analytical methods. While there are benefits to solving the equation in either way, an analytical solution is preferred because adsorption effects are more clearly isolated and the effects of adsorption may be studied without the use of costly and complicated numerical simulation.

In this case, due to the highly nonlinear nature of the equation to be solved, a purely analytical solution was found to be impossible without oversimplification of the problem. Therefore, a semi-analytical procedure was used which couples the method of similarity analysis with finite difference solution of an ordinary differential equation. Similarity analysis was used because it allows the partial differential equation for vapor flow with adsorption to be solved in a general manner and allows for separation of adsorption effects.

4.1 Derivation of Analytical Solution

The conservation of mass for isothermal vapor flow with an adsorption phase present is expressed as:

$$\phi\frac{\partial\rho_v(1-S_a)}{\partial t} \;+\; \phi\rho_a\frac{\partial S_a}{\partial t} \;+\; \nabla\cdot(u_v\rho_v) \;=\; 0 \tag{4.1}$$

The first two terms in the above equation describe the time rate of change of vapor and adsorbate mass, respectively. Since adsorbate does not flow freely, the third term involves only free vapor. Rearranging Eqn. 4.1 and imposing the restriction of one dimensional flow:

$$\phi\frac{\partial(\rho_v-\rho_v S_a)}{\partial t} \;+\; \phi\rho_a\frac{\partial S_a}{\partial t} \;+\; \frac{\partial}{\partial x}(u_v\rho_v) \;=\; 0 \tag{4.2}$$

The adsorbate saturation, S_a is pressure dependent and is described by an adsorption isotherm, X(p):

$$S_a \;=\; \frac{1-\phi}{\phi}\frac{\rho_r}{\rho_a}X(p) \tag{4.3}$$

Upon substitution of Eqn. 4.3 into Eqn. 4.2 and simplifying:

$$\left[1-\left(\frac{1-\phi}{\phi}\right)\frac{\rho_r}{\rho_a}X\right]\frac{\partial\rho_v}{\partial t} \;+\; \left[\left(\frac{1-\phi}{\phi}\right)\frac{\rho_r}{\rho_a}(\rho_a-\rho_v)\right]\frac{\partial X}{\partial t} \;+\; \frac{1}{\phi}\frac{\partial}{\partial x}(u_v\rho_v) \;=\; 0 \tag{4.4}$$

Eqn. 4.4 may be simplified further by observing:

$$\frac{\partial X}{\partial t} \;=\; \frac{\partial\rho_v}{\partial t}\frac{\partial X}{\partial\rho_v} \tag{4.5}$$

Substitution of Eqn. 4.5 into Eqn. 4.4 yields:

$$\left[\{1-\left(\frac{1-\phi}{\phi}\right)\frac{\rho_r}{\rho_a}X\} \;+\; \{\frac{\partial X}{\partial\rho_v}\left(\frac{1-\phi}{\phi}\right)\frac{\rho_r}{\rho_a}(\rho_a-\rho_v)\}\right]\frac{\partial\rho_v}{\partial t} \;+\; \frac{1}{\phi}\frac{\partial}{\partial x}(u_v\rho_v) \;=\; 0 \tag{4.6}$$

Vapor velocity is obtained from Darcy's law:

$$u_v \;=\; -\frac{k}{\mu_v}\frac{\partial p}{\partial x} \tag{4.7}$$

Upon substitution of Eqn. 4.7 into Eqn. 4.6:

$$\phi A(p)\frac{\partial \rho_v}{\partial t} \;=\; \frac{\partial}{\partial x}\left(\frac{k\rho_v}{\mu_v}\frac{\partial p}{\partial x}\right) \;=\; 0 \tag{4.8}$$

where the nonlinear adsorption term, *A(p)*, is given by:

$$A(p) \;=\; \{1-\left(\frac{1-\phi}{\phi}\right)\frac{\rho_r}{\rho_a}X\} \;+\; \{\frac{\partial X}{\partial \rho_v}\left(\left(\frac{1-\phi}{\phi}\right)\rho_r \;-\; \left(\frac{1-\phi}{\phi}\right)\frac{\rho_r\rho_v}{\rho_a}\right)\} \tag{4.9}$$

Pressure and density of the vapor are related by the real gas law:

$$pV \;=\; znR_vT \tag{4.10}$$

$$\rho_v \;=\; \frac{Mp}{zR_vT} \tag{4.11}$$

The continuity equation, Eqn. 4.8, may be written in terms of pressure by using the real gas law. Substituting the expression for vapor density, Eqn. 4.11 into Eqn. 4.8, the continuity equation becomes:

$$\frac{\partial}{\partial x}\left[\frac{1}{\mu z}\frac{\partial p^2}{\partial x}\right] \;=\; \frac{\phi A(p)c_v}{kz}\frac{\partial p^2}{\partial t} \tag{4.12}$$

It is important to understand the form of the compressibility term, c_v. First, since vapor compressibility is much larger that rock compressibility, the total system compressibility in a vapor dominated system is approximated by the vapor compressibility. Second, the form of the vapor compressibility is determined by analysis over a range of temperature and pressure. The expression for vapor compressibility is:

$$c_v \;=\; \frac{-1}{V}\left(\frac{\partial V}{\partial p}\right)_T \;=\; \frac{1}{\rho_v}\left(\frac{\partial \rho_v}{\partial p}\right)_T \tag{4.13}$$

Combining Eqns. 4.13 and 4.11 leads to the following general expression for compressibility:

$$c_v \;=\; \frac{1}{p} \;-\; \frac{1}{z}\frac{dz}{dp} \tag{4.14}$$

For the range of pressure encountered in geothermal reservoirs, compressibility may be closely approximated by:

$$c_v = \frac{1}{p} \tag{4.15}$$

Figures 4.1 and 4.2 compare NIST [26] tabulated steam viscosity and viscosity approximated by *1/p* for a range of pressures at 200 and 300 °C, respectively. The figures confirm the assumption that for the temperatures and pressures found in most geothermal reservoirs, compressibility may be approximated by *1/p*. This approximation may be used in Eqn. 4.12.

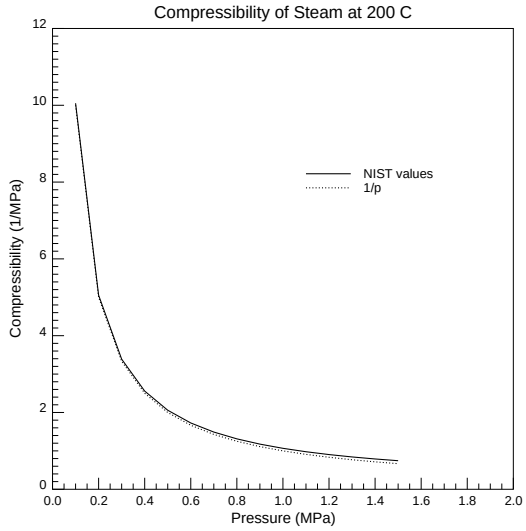

Figure 4.1: Compressibility of steam at 200 C

Eqn. 4.12 is quite nonlinear in its current form. Viscosity (μ), compressibility (c), the adsorptive nonlinear term ($A(p)$), and the gas deviation factor (z) are all functions of pressure. To eliminate some of the nonlinearities and to simplify the expression somewhat, the real gas pseudopressure derived by Al-Hussainy, Ramey, and Crawford [3] was introduced:

$$m(p) = \int_{pb}^{p} \frac{2p}{\mu z} dp \tag{4.16}$$

Use of Eqn. 4.16 in Eqn. 4.12 leads to the continuity equation in terms of pseudopressure:

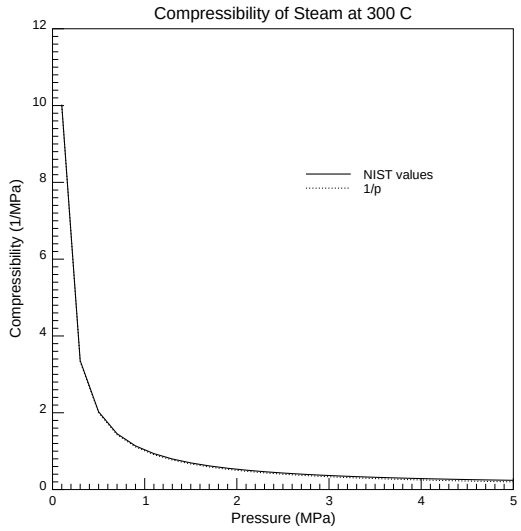

Figure 4.2: Compressibility of steam at 300 C

$$\frac{\partial^2 m(p)}{\partial x^2} = \frac{\phi A(p) c_v \mu}{k} \frac{\partial m(p)}{\partial t} \tag{4.17}$$

Eqn. 4.17 is still highly nonlinear. By introduction of Agarwal pseudotime [2], the remaining pressure dependent terms (except for the adsorptive nonlinear term) are eliminated. The Agarwal pseudotime [2] has been altered to include the constant porosity and permeability terms.

$$t_a(p) = \int_{pb}^{p} \frac{k \left[\frac{dt}{dp}\right]}{\phi \mu c_t} dp \tag{4.18}$$

Substitution of Eqn. 4.18 into 4.17 leads to:

$$\frac{\partial^2 m(p)}{\partial x^2} = A(p) \frac{\partial m(p)}{\partial t_a(p)} \tag{4.19}$$

Now, the only nonlinear effects are those due to adsorptive effects and are completely isolated in the nonlinear term, *A(p)*.

For a semi-infinite linear reservoir producing at a constant pressure well, the boundary conditions for Eqn. 4.19 may be written:

$$\text{Inner Boundary}: m(p)(x = 0, t) \;=\; m(p_w) \tag{4.20}$$

$$\text{Outer Boundary}: m(p)(x \to \infty, t) \;=\; m(p_i) \tag{4.21}$$

$$\text{Initial Condition}: m(p)(x, t = 0) \;=\; m(p_i) \tag{4.22}$$

4.1.1 Analysis of Adsorption Pressure Effects.

By studying the relative sizes of components of the nonlinear term, *A(p)* given in Eqn. 4.9, it is possible to determine the importance of various adsorption effects. The nonlinear adsorptive term is influenced by both the amount of fluid adsorbed (the second term on the right in Eqn. 4.9) and by the rate at which this fluid either adsorbs or desorbs (the third term on the right in Eqn. 4.9).

A range of adsorption isotherms were used to compute *A(p)* over a range of reservoir temperatures. Langmuir isotherms with widely varying shapes and magnitudes were used to determine adsorption effects. An analysis follows on the relative sizes of the terms in the adsorptive nonlinear function, *A(p)*.

Adsorption Isotherms

A Langmuir model was chosen to represent adsorption isotherms. This model was used because a large range of isotherm shapes are easily modeled. Langmuir isotherms usually described by the following relationship:

$$X(p/p_s) \;=\; \frac{p/p_s}{a \;+\; bp/p_s} \tag{4.23}$$

Correa and Ramey [16] showed that the Langmuir equation, Eqn. 4.23 can be rewritten in a different form:

$$X(p/p_s) \;=\; d\left[\frac{cp/p_s}{1 \;+\; (c-1)p/p_s}\right] \tag{4.24}$$

where: d is the amplification factor for the isotherm defining the maximum adsorbed amount, c is the shape factor. Isotherms are concave up for $c < 1$ and concave down for $c > 1$. The amplification factor, d, and the shape factor, c, are related to the original Langmuir equation model parameters, a and b, by the following relationships:

$$c \;=\; 1 \;+\; b/a \tag{4.25}$$

$$d \;=\; (a \;+\; b)^{-1} \tag{4.26}$$

The form of the Langmuir isotherm shown in Eqn. 4.24 was chosen because it represents a simple model for matching a wide range of isotherm shapes. In this research, the isotherm model is simply used to generate a range of isotherm shapes and is not meant to imply anything about the physics of the adsorptive process.

A range of normalized adsorption isotherm shapes are shown in Figure 4.3. Adsorption values are normalized to the maximum adsorbed amount and the shape factor, c, is varied from 0.01 to 100. The range of isotherms shown in Figure 4.3 is felt to be more than adequate to include any adsorption effects likely to occur in a porous medium.

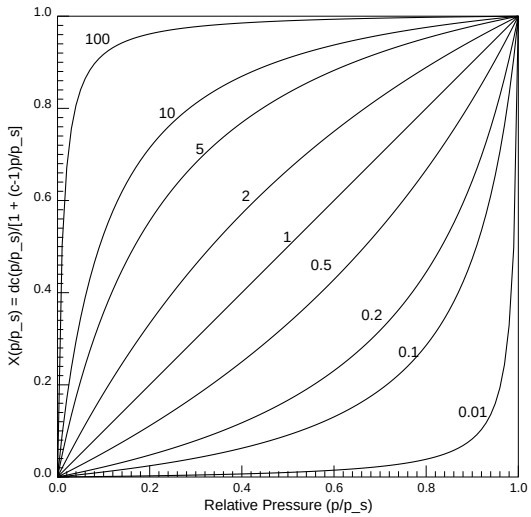

Figure 4.3: Langmuir isotherms for a range of shape factors, c

Figures 4.3 and 4.4 show the sizes of the adsorbed mass term and the rate of change of adsorbed mass term in Eqn. 4.9, respectively. Clearly, for most isotherms, and for most reservoir conditions, the rate of change of the adsorbed mass is much more significant than the mass present. Values of the adsorbed mass term in Eqn. 4.9 range from 0 to 1. The mass rate of change term in Eqn. 4.9, on the other hand, has a large range and dominates the adsorption nonlinear term for all adsorption isotherms.

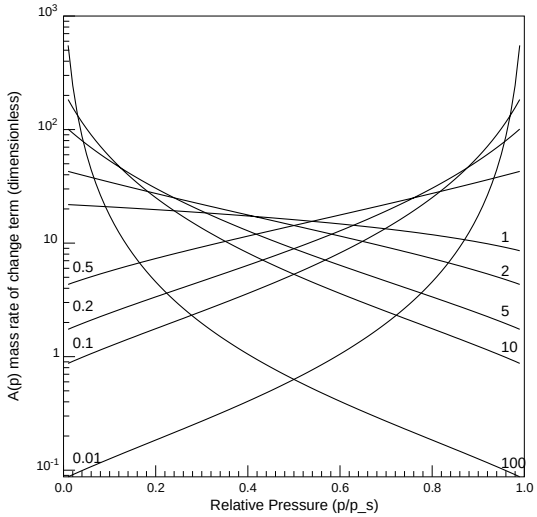

Figure 4.4: Size of the mass rate of change term in the nonlinear term

4.1.2 Similarity Analysis

Eqns. 4.19 - 4.22 may be solved semi-analytically by use of similarity analysis. Eqn. 4.19 may be non-dimensionalized by use of the following dimensionless variables:

$$\bar{m} = \frac{m(p)}{m(p_i)} \tag{4.27}$$

$$\bar{x} = \frac{x}{L} \tag{4.28}$$

$$\bar{t} \;=\; \frac{t(p)}{L^2} \tag{4.29}$$

Upon substitution of Eqns. 4.27 - 4.29 into Eqn. 4.19 a dimensionless equation is obtained:

$$\frac{\partial^2 \bar{m}}{\partial \bar{x}^2} \;=\; A(\bar{m})\frac{\partial \bar{m}}{\partial \bar{t}} \tag{4.30}$$

with dimensionless boundary conditions:

$$\text{Inner Boundary}: \bar{m}(\bar{x}=0,\bar{t}) \;=\; \frac{m(p_w)}{m(p_i)} \;=\; \bar{m}_o \tag{4.31}$$

$$\text{Outer Boundary}: \bar{m}(\bar{x}\rightarrow\infty,\bar{t}) \;=\; 1 \tag{4.32}$$

$$\text{Initial Condition}: \bar{m}(\bar{x},\bar{t}=0) \;=\; 1 \tag{4.33}$$

The partial differential equation, Eqn. 4.30, may be converted to an ordinary differential equation by assuming the the dimensionless pseudopressure may be expressed as:

$$\bar{m} \;=\; \Theta(\bar{t})f(\eta) \tag{4.34}$$

where η is the similarity expression:

$$\eta \;=\; \frac{\bar{x}}{2\sqrt{\bar{t}}} \tag{4.35}$$

The constant inner boundary condition (Eqn. 4.20) specifies the value of $\Theta(\bar{t})$:

$$\Theta(\bar{t}) \;=\; \bar{m}_o \tag{4.36}$$

Upon substitution of Eqns. 4.34 - 4.36 into Eqn. 4.30 an ordinary differential equation is obtained:

$$\frac{d^2 f}{d\eta^2} \;+\; 2\eta A(f)\frac{df}{d\eta} \;=\; 0 \tag{4.37}$$

with boundary conditions:

$$\text{Inner Boundary}: f(\eta \to 0) \;=\; 1 \tag{4.38}$$

$$\text{Outer Boundary}: f(\eta \to \infty) \;=\; \frac{1}{\bar{m}_o} \tag{4.39}$$

Eqn. 4.37 must be solved by numerical methods for two reasons. First, the boundary conditions represent values of $f(\eta)$ at two different boundaries so numerical methods must be employed to determine the shape of the function between endpoints. Second, the nonlinear term, *A(f)* is not solved analytically, but, rather, is solved by means of table lookup so a numerical scheme is necessary to introduce accurate values of *A(f)*. A finite difference solution was chosen for this purpose since the solution, *f*, is a simple function of η.

In discretized form Eqn. 4.37 becomes:

$$\left[\frac{f_{i+1} - 2f_i + f_{i-1}}{h^2}\right] \;+\; \eta A(f)\left[\frac{f_{i+1} - f_{i-1}}{h}\right] \;=\; 0 \tag{4.40}$$

where, h represents a discrete step in η. Eqn. 4.40 may be written in matrix form and solved numerically:

$$\begin{bmatrix} \beta_1 & \alpha_1 & & & & & & \\ \gamma_1 & \beta_2 & \alpha_2 & & & & & \\ & \gamma_3 & \beta_3 & \alpha_3 & & & & \\ & & \cdot & \cdot & \cdot & & & \\ & & & \cdot & \cdot & \cdot & & \\ & & & & \gamma_{N-2} & \beta_{N-2} & \alpha_{N-2} & \\ & & & & & \gamma_{N-1} & \beta_{N-1} & \end{bmatrix} \begin{bmatrix} f_1 \\ f_2 \\ f_3 \\ \cdot \\ \cdot \\ f_{N-2} \\ f_{N-1} \end{bmatrix} = \begin{bmatrix} -\gamma_1 f_0 \\ 0 \\ 0 \\ \cdot \\ \cdot \\ 0 \\ -\alpha_{N-1} f_{N-1} \end{bmatrix} \tag{4.41}$$

Entries in the matrix are:

$$\alpha_i \;=\; \left[\frac{1}{h^2} \;+\; \frac{\eta A(f)}{h}\right] \tag{4.42}$$

$$\beta_i = \left[-\frac{2}{h^2}\right] \tag{4.43}$$

$$\gamma_i = \left[\frac{1}{h^2} - \frac{\eta A(f)}{h}\right] \tag{4.44}$$

Solution of Eqn. 4.41 for several adsorption isotherm shapes yields a range of curves for $f(\eta)$ vs. η as a function of the shape factor describing the adsorbed phase. The computed similarity functions are shown in Figure 4.5. The shape factors used correspond to those shown in Figure 4.3.

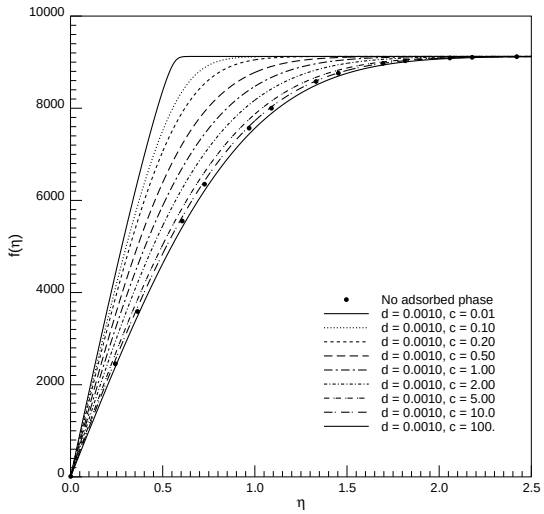

Figure 4.5: Similarity function for a range of adsorption isotherms

4.1.3 Solution Procedure

The matrix problem that was solved is shown in Eqns. 4.41 through 4.44. The tridiagonal matrix problem was solved by use of the Thomas algorithm. Since the problem is nonlinear, an iterative procedure was used.

1. Initial guesses of $f(\eta)$ vs. η are made. The lower boundary of $f(\eta) = 1$ is fixed at $\eta = 0$. The upper boundary of $f(\eta) = 1/\bar{m}_0$ is fixed at an arbitrary η

sufficiently large that errors are not introduced (selection of the upper boundary of η is discussed more fully later in this section).

2. The initial guesses for *f(η)* are distributed in a linear fashion between the fixed endpoints. The initial guesses for the *f(η)* are saved as old values.

3. The nonlinear adsorption function, *A(f)*, is determined each *f(η)*. In order to simplify the computation of *A(f)*, a table lookup procedure is employed. Most terms in the nonlinear adsorption term are easily obtained in terms of pressure, so a table lookup procedure allows simple evaluation of the nonlinear term.

   - Since *f(η)* is a unique function of pressure, p, a table lookup method was employed to determine pressure for each value of *f(η)*.
   - Based upon the pressure obtained by table lookup, the density and gas compressibility factor are obtained by table lookup based on pressure.
   - By using the data obtained from table lookup, the nonlinear adsorption term is computed for each *f(η)*.

4. Using the computed values for the nonlinear adsorption term the matrix problem is solved for *f(η)* at each node. These computed values are are saved as a new array of *f(η)*.

5. For each node, the new values of *f(η)* are compared to the old values of *f(η)*. If agreement is within some arbitrarily small tolerance, the iteration procedure is stopped. If agreement is not within that tolerance, new values of *f(η)* are saved as old values, nonlinear adsorption term values are updated and the computation procedure is continued.

6. The process of computing *f(η)* continues until old and new values are arbitrarily close. A tolerance in $f(\eta)$ of 10^{-3} was used in this research which corresponds to a tolerance of about 8×10^{-3} MPa in pressure.

Discretization of the solution domain (η) and setting the outer boundary are arbitrary. For this research, a fine grid was used to ensure accuracy of the solution.

Since the analytical solution was to be used as a check for the numerical solution, the grid size was set at 10^{-3} m·s$^{-0.5}$.

The outer boundary, which approximates an infinite outer boundary, must be sufficiently large that the solution is not influenced artificially. In order to ensure that the outer boundary does not affect the solution procedure, a sensitivity analysis on the effects of the outer boundary was performed. By increasing the placement of the outer boundary (increasing the largest η) and comparing the solutions, it was found that past a sufficiently large outer boundary, further perturbations in the boundary resulted in immeasurably small changes in the solution. Based on the sensitivity analysis, an outer boundary location of $\eta = 10.0$ was found to be sufficiently large for the range of cases studied here.

4.2 Pressure Depletion Effects of an Adsorbed Phase

Figure 4.6 shows the effects of adsorption on early time pressure depletion. Initial pressure depletion time may either be delayed or enhanced by the presence of an adsorbed phase depending on the shape of the adsorption isotherm. Concave down shaped isotherms ($c < 1$) tend to increase the rate of early time pressure depletion while concave up shaped isotherms ($c > 1$) decrease the rate of early time pressure depletion. Figure 4.6 shows that initial depletion delays due to concave up isotherm shapes may be an order of magnitude or greater. Initial depletion accelerations in pressure due to concave down isotherm shapes, on the other hand, are small.

Figure 4.6 also shows that strongly concave down isotherms ($c = 100$) may cause drawdown to occur more quickly than in an identical system with no adsorbed phase present.

At late times, the same general trends are noted. Figure 4.7 shows that the presence of an adsorbed phase can significantly decrease the pressure decline in a geothermal reservoir. Late time pressure data show that the slope of pressure decline is also decreased by the presence of an adsorbed phase. As shown in Figure 4.7 the time to reach a given pressure level increases when an adsorbed phase is present and the magnitude of this difference increases with time. This implies that the rate of

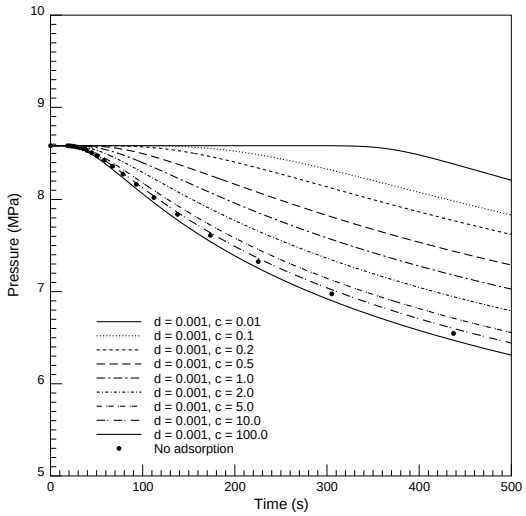

Figure 4.6: Early time depletion effects of adsorption

depletion is reduced by the presence of an adsorbed phase.

An adsorption isotherm typical of the Geysers geothermal reservoir (Section 2.3.1, Figure 2.5) was used to determine the semi-analytical solution and was compared to solutions generated with Langmuir isotherms. This comparison was carried out to determine the validity of using the Langmuir isotherm to model adsorption isotherms in the Geysers. Figure 4.8 shows pressure histories for a system influenced by adsorption which follows a range of adsorption isotherms. In three of the cases, the Langmuir model is used while in one of the cases, a measured Geysers isotherm is used. It is shown that, except for errors at high pressures where the shape of the Geysers isotherm was assumed, the Langmuir model creates pressure depletion effects almost identical to those created by measured Geysers isotherms. Early time pressure response is highlighted in Figure 4.9 and late time data is presented in Figure 4.10.

4.2.1 Effects of Adsorbate Density on Pressure Depletion

In Chapter 2 it was shown that the density of the adsorbed phase may be significantly different than the density of saturated liquid water at a given temperature. In this

section, the effects of this density variation on pressure depletion were investigated. It was found that over the entire depletion history, no noticeable difference in pressure was obtained by using a variable density for the adsorbed phase as opposed to assuming the adsorbate density is constant over the range of depletion pressures. Therefore, the assumption that adsorbate density is the same as saturated water density is valid from a modeling standpoint.

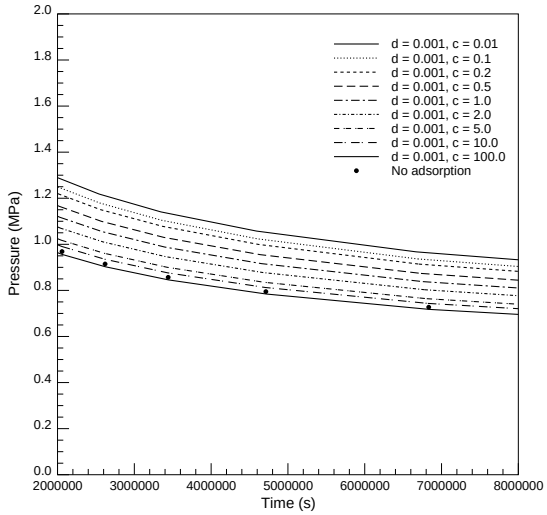

Figure 4.7: Late time depletion effects of adsorption

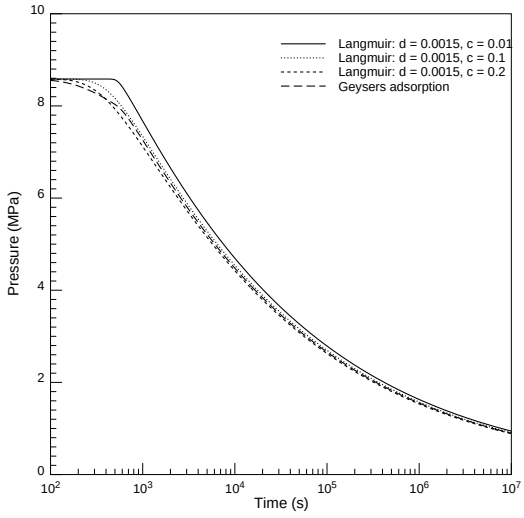

Figure 4.8: Comparison with Geysers isotherm

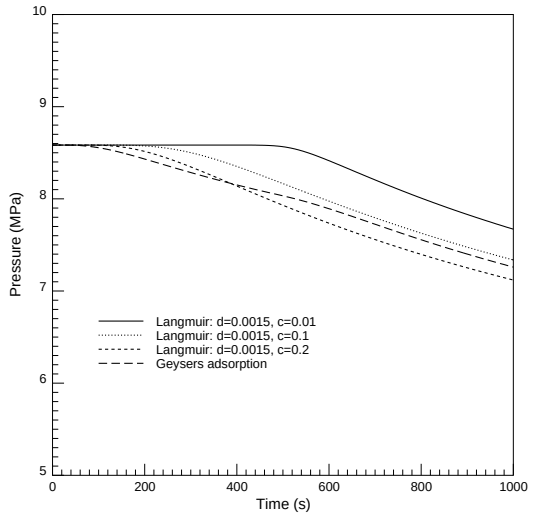

Figure 4.9: Comparison with Geysers isotherm (early time)

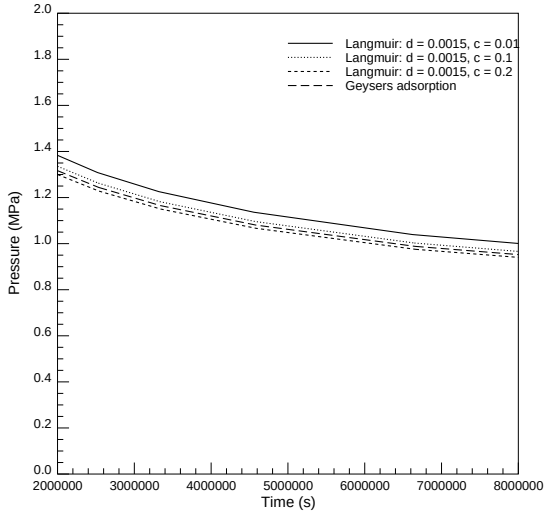

Figure 4.10: Comparison with Geysers isotherm (late time)

Chapter 5

Numerical Model

A numerical solution for flow through porous media was used to study the more complex thermal effects, which are not easily studied by analytical means, and also as a means to keep track of the fate of injected tracer. A three stage verification process was followed in the numerical investigation. First, an isothermal material balance was used to verify the numerical model for a fluid of constant compressibility without adsorption. This constant compressibility model was checked against existing analytical solutions. Second, the more complicated vapor flow without adsorption effects was simulated under both non-isothermal and isothermal conditions. Results were compared to determine the validity of the isothermal assumption in the analytical derivation. Third, numerical results for a wide range of adsorption isotherms were compared to the analytical results discussed in Chapter 4 to verify accuracy of the model for a range of reservoir conditions.

Analysis of tracer propagation for a range of reservoir adsorption conditions was used to determine general effects of an adsorbed phase on the propagation of injected tracer.

Numerical analysis was carried out on an example represented by a core with the following properties:

1. Length = 4.0 m.
2. Width = 0.1 m.

3. Height = 0.1 m.
4. Porosity = 0.05.
5. Permeability = 1.0×10^{-16} m^2 to 1.0×10^{-12} m^2.
6. Rock Compressibility = 0.0.
7. Rock Density = 2720.0 kg/m^3.
8. Initial Temperature = 300 °C.
9. Initial Pressure = 0.101 MPa to 7.0 MPa.
10. Production Boundary = Constant Pressure or Constant Flow Rate.
11. Outer Boundary = No Flow, Constant Pressure, or Constant Flow Rate.

Fluid properties were calculated from the National Institute for Standards and Technology (NIST) thermophysical database for steam [26].

Numerical Solution Technique

All simulations performed in this chapter were carried out in a linear model 4 m in length, and used grid blocks of constant height and width with the number of grid blocks varying depending on the problem solved. The time step size also varied depending on the size of the grid block and the maximum fluid velocity in the problem modeled. The time step size was selected at the beginning of each simulation based on the grid block size and the maximum velocity such that the Courant number never exceeded 1. The Courant number is defined as:

$$C = \frac{u_f \Delta t}{\Delta x} \tag{5.1}$$

Thus, the constraint on time step size was based on the relationship:

$$C \leq 1.0 \tag{5.2}$$

In each of the following sections, the discretizations in both space and time are provided for the particular problem discussed.

Solution of the linear flow problem requires solution of a tridiagonal matrix for pressure at each iteration level. The Thomas algorithm was employed for matrix solution in this research. Saturation is calculated explicitly based on pressure in each block so matrix solution for saturation was not necessary.

5.1 Single-Phase Liquid Flow Without Adsorption Effects

The conservation equation for single-phase fluid flow through porous media is:

$$\phi \frac{\partial \rho_f S_f}{\partial t} \; + \; \nabla \cdot (\rho_f u_f) \; = \; 0 \tag{5.3}$$

Eqn. 5.3 was discretized and solved with water compressibility and viscosity assumed constant. Darcy's law was assumed to model the flux of fluid in a porous media.

$$u_f \; = \; \frac{k k_{rf}}{\mu_f} \nabla p \tag{5.4}$$

The discretized flow equation for a one dimensional single-phase, single component system with constant grid block size may be written as follows for a fully implicit formulation:

$$\left[T_{fi+1/2}(p_{fi+1} - p_{fi}) \; - \; T_{fi-1/2}(p_{fi} - p_{fi-1})\right]^{\nu+1} \; - \; \frac{\Delta x}{\Delta t} \left[\Delta_t(\phi_{fi} \rho_{fi} S_{fi})\right] - q_{fi}^{\nu+1} \; = \; 0 \tag{5.5}$$

where, fluid transmissibility, T_f, is defined as:

$$T_{fi} \; = \; \frac{k_i k_{rfi} \rho_{fi}}{\mu_{fi} \Delta x} \tag{5.6}$$

and the time operator, Δ_t, operates as follows:

$$\Delta_t(\phi_{fi}\rho_{fi}S_{fi}) \;=\; \left[(\phi_{fi}\rho_{fi}S_{fi})^{\nu+1} \;-\; (\phi_{fi}\rho_{fi}S_{fi})^{\nu}\right] \tag{5.7}$$

Numerical results were compared with the analytical solution for constant compressibility flow in a semi-infinite porous medium with a constant pressure production boundary. Modeling of a semi-infinite analytical solution with a finite grid numerical model is possible as long as pressure effects in the numerical solution have not been felt at the outer boundary. In the following comparisons of numerical solutions with analytical solutions, the point at which outer boundary effects are felt in the numerical model corresponds to deviations in the numerical solution from analytical results. The analytical solution in dimensionless form is:

$$\bar{p} \;=\; \text{erfc}\left[\frac{\bar{x}}{2\sqrt{\bar{t}}}\right] \tag{5.8}$$

Where dimensionless variables are defined as:

$$\bar{x} \;=\; \frac{x}{L} \tag{5.9}$$

$$\bar{t} \;=\; \frac{kt}{\phi\mu c_t L^2} \tag{5.10}$$

$$\bar{p} \;=\; \frac{(p \;-\; p_i)}{(p_w \;-\; p_i)} \tag{5.11}$$

Figure 5.1 compares pressure histories at 0.5 m from the production boundary of the core. Initial pressure was 4.0 MPa and the constant pressure boundary was fixed at 0.101 MPa. The length was broken into 256 blocks of thickness (Δx) 0.015625 m each. Based on a permeability of 10^{-12} m^2 and a maximum pressure drop of 3.9 MPa over Δx, discretization in (Δt) time was computed to be 5×10^{-3} s. The comparison point was chosen to be near the production boundary since large pressure gradients near the boundary make the pressure effects difficult to model. It was felt that accurate modeling near the boundary implies accurate modeling over the entire domain. The pressure histories were compared for times below that at which the no flow boundary was felt in the core. The match is exact which indicates that the numerical solution is correct.

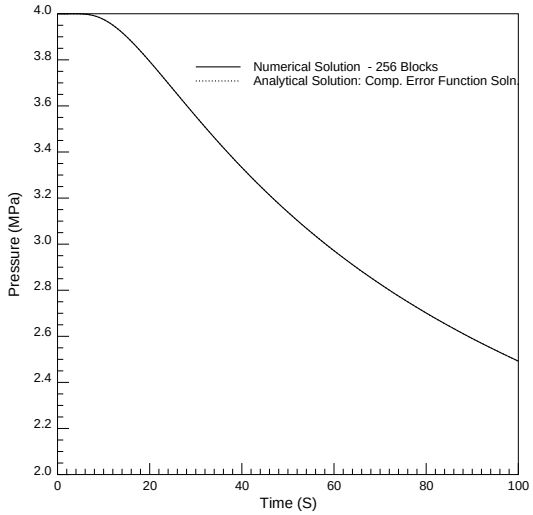

Figure 5.1: Pressure histories for constant compressibility flow.

5.2 Single-Phase Vapor Flow

Single-phase vapor flow was studied under isothermal and non-isothermal conditions and both with and without adsorption effects included. The material balance for vapor flow with adsorption is similar to Eqn. 5.3 with an added adsorption accumulation term.

$$\phi\frac{\partial\rho_v S_v}{\partial t} \;+\; \phi\frac{\partial\rho_a S_a}{\partial t} \;+\; \nabla(\rho_v u_v) \;=\; 0 \tag{5.12}$$

The discretized form of Eqn. 5.12 may be expressed as:

$$\Big[T_{vi+1/2}(p_{vi+1}-p_{vi}) \;-\; T_{vi-1/2}(p_{vi}-p_{vi-1})\Big]^{\nu+1} \;-\; \frac{\Delta x}{\Delta t}\left[\Delta_t(\phi_{vi}\rho_{vi}S_{vi})\right] - \frac{\Delta x}{\Delta t}\left[\Delta_t(\phi_{ai}\rho_{ai}S_{ai})\right] \;-\; q_{fi}^{\nu+1} \;=\; 0 \tag{5.13}$$

where the adsorbate saturation may be written in terms of an adsorption isotherm, *X(p)*, which relates mass adsorbed to pressure:

$$S_{ai} \;=\; \frac{1-\phi}{\phi}\frac{\rho_{ai}}{\rho_r}X(p_i) \tag{5.14}$$

Eqn. 5.13 was solved for pressure by use of an implicit finite difference scheme. Adsorbate saturation was updated based on the iteration level pressure and was allowed to change until the solution converged.

In all vapor flow numerical computations described in this chapter, (Δx) was chosen to be 0.015625 m. Based on a permeability of 10^{-12} m^2 and a maximum pressure drop of 3.9 MPa over Δx, discretization in (Δt) was computed to be 1×10^{-3} s. The relationship between Δx and Δt was based on the Courant number constraint shown in Eqn. 5.2. Vapor viscosity at 2.0 MPa was used to calculate velocity used in determining the Courant number.

A heat balance was used to calculate temperature changes in the system under single-phase flow conditions. Temperature changes were computed explicitly and at each iteration level. Convergence of the heat balance was required before pressure convergence was allowed. The heat balance used (as explained in Chapter 4) was:

$$\frac{\partial}{\partial t}\left[(1-\phi)\rho_r E_r \;+\; \phi S_v \rho_v E_v \;+\; \phi S_a \rho_a E_a\right] \;+\; \frac{\partial}{\partial x}\left[\phi S_v \rho_v E_v u_v\right] \;=\; \nabla\cdot(\kappa_m \nabla T) \;+\; Q_e \tag{5.15}$$

Eqn. 5.15 neglects a number of terms which are included in the complete heat balance (Chapter 4). Since only adsorbate and vapor phases were present, the water/vapor phase change term was neglected but heat effects of the adsorbed phase were included. Also, pressure work and viscous dissipation terms were neglected since they have been shown to be small and to counteract each other [27].

5.2.1 Validity of Isothermal Flow Assumption

To simplify the the analytical description of adsorption effects as described in the previous chapter, flow was assumed to be isothermal. In this section, numerical solutions including thermal effects for a wide range of flow conditions were used to determine the validity of the isothermal assumption.

First, vapor flow without adsorption was modeled under both isothermal and nonisothermal conditions. Results were compared to determine temperature effects on the single-phase flow of vapor. Flow was modeled in a simulated core with production from one end only. Figure 5.2 compares the pressure histories for vapor at 0.0625 m from the production end of the core under both isothermal and nonisothermal conditions. Due to the large heat capacity of the rock matrix, heat effects tend to diminish with distance from the production port, so measurement of heat effects were considered near the production port to show maximum adsorption heat effects. The isothermal pressure never deviated by more than 1 percent from nonisothermal pressure so the isothermal assumption, without adsorption, is a good one.

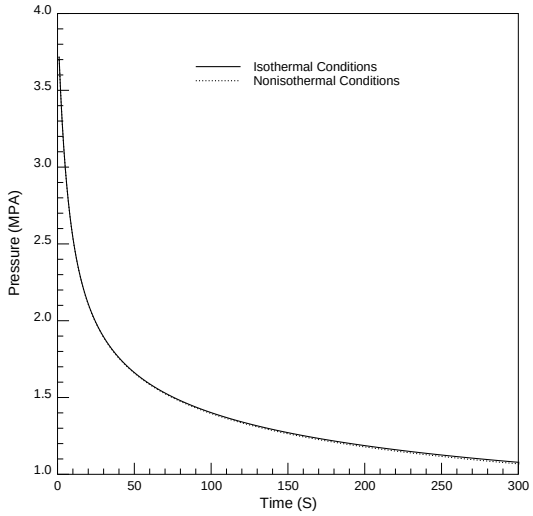

Figure 5.2: Vapor pressure histories under different thermal conditions.

When adsorbate is present, thermal effects become more significant. Desorption, like evaporation, is an endothermic process, so heat is drawn from the system as sorbed fluid is released to the vapor phase. As a result, temperature decline with adsorption effects is more significant than without them. These increased thermal effects cause an increased pressure effect. Table 5.1 shows the maximum deviations from isothermal pressure computations at 0.0625 m from the production end of a

core with an adsorbing phase present. Thermal simulations were carried out in a core initially near a relative pressure of 1.0. Results shown in Table 5.1 were obtained using a range of adsorption isotherms which encompass all magnitudes and shapes considered in this research. It is felt that the adsorption temperature effects considered here include a sufficient range of isotherms that they may be considered general. Thermal effects were shown to influence pressure depletion from a simulated core. Pressure variations from the isothermal case were shown to range from about 4 % to a maximum of about 10 %. In general, thermal pressure effects were shown to be large when the slope of the isotherm is large and small when the slope of the isotherm is small. Large isotherm slopes indicate a high rate of desorption as pressure is decreased which means a high rate of vaporization and a subsequent large heat loss due to the endothermic nature of adsorption. Since thermal effects never translated to pressure changes from isothermal conditions of more than 10 %, even when adsorbate saturation is very large, the isothermal assumption was assumed to be valid. Although pressure is affected by thermal effects which are not included in the analytical solution, these effects have been shown to be very small and do not impact the validity of the analytical results.

Results shown Table 5.1 indicate that when large amounts of adsorbed phase are initially present, thermal effects may strongly influence the pressure depletion in a core. For low initial adsorbed phase saturations, thermal effects on pressure depletion are small.

In Chapter 4, the isothermal assumption was made in deriving the analytical solution. Results shown in Table 5.1 indicate that the isothermal assumption is a good one.

5.2.2 Comparison with Analytical Solution - Adsorbed Phase Absent

In this section, analytical results were compared with numerical calculations for single-phase vapor flow in the absence of a desorbing liquid phase.

Figure 5.3 shows pressure histories at 0.5 m from the production end of a test

Table 5.1: Thermal Effects of Adsorbed Phase

Maximum adsorbate saturation (%)	Langmuir Shape factor	Maximum pressure effect (%)
33.0	0.01	7.0
33.0	1.0	5.0
33.0	100	3.5
67.0	100	10.0
67.0	100	6.5
67.0	100	5.0

core computed analytically and numerically. Vapor was produced from the production boundary under the constraint of constant pressure (0.101 MPa). The outer boundary was no flow for the numerical solution and infinite for the analytical solution. Initial pressure was 8 MPa and temperature of the system was held at 300 °C. Permeability was assumed to be 10^{-12} m^2. The agreement between analytical and numerical results is excellent. Slight disagreement at late times is due to outer boundary effects in the numerical solution.

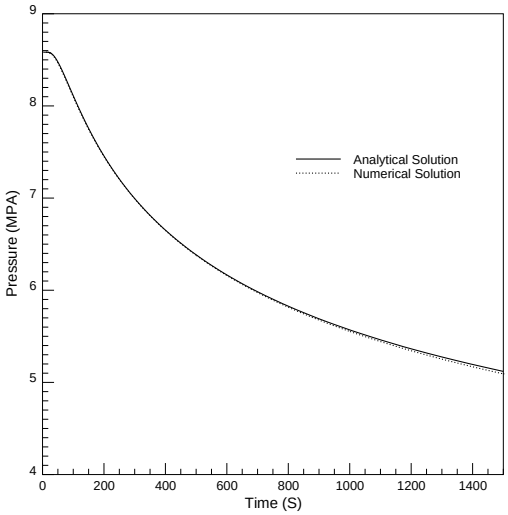

Figure 5.3: Analytical and numerical solutions with no adsorption

5.2.3 Comparison with Analytical Solution - Adsorbed Phase Present

The adsorbed phase is included by using an adsorption isotherm which defines adsorbed mass as a function of pressure for a given temperature. Adamson [1] showed that adsorption isotherms may take many shapes depending on the matrix material and pore configuration and a method of generalizing the effects is needed. Comparison of the numerical and analytical solutions is used to verify the numerical treatment of adsorption effects.

Constant Adsorbed Saturation

Pressure effects of constant adsorbed saturation corresponding to chemically sorbed liquid were computed both analytically and numerically to determine whether the effects of the presence of adsorbate without mass transfer are accurately modeled. Figure 5.4 shows pressure histories calculated numerically and analytically. Boundary and initial conditions and core properties are identical to those used in the previous section.

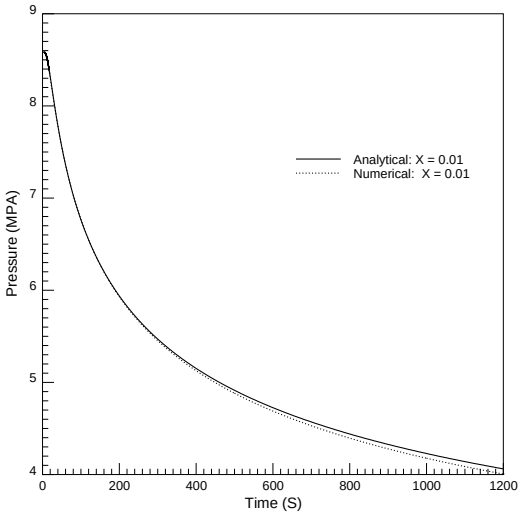

Figure 5.4: Analytical and numerical solutions with constant adsorption

Numerical and analytical computations shown in Figure 5.4 show excellent agreement except at late times when boundary effects are felt in the numerical solution. These results indicate that effects of the adsorbed mass without mass transfer are modeled accurately by numerical methods.

Variable Adsorbed Saturation

The mass transfer between adsorbate and vapor also must be modeled in order to fully quantify adsorption effects. Numerical and analytical computations were made for pressure decline in a simulated core with an adsorbed phase present for a range of adsorption isotherm shapes. Numerical and analytical results were compared. Figure 5.5 shows pressure histories computed analytically and numerically for vapor flow in the presence of an adsorbed phase described by a Langmuir isotherm ($d = 0.001$, $c = 0.01$). The numerical solution matches the analytical solution almost exactly.

The series of comparisons between analytical and numerical solutions described above indicates that the numerical scheme used accurately calculates the pressure response in a geothermal reservoir for all conditions of relevance.

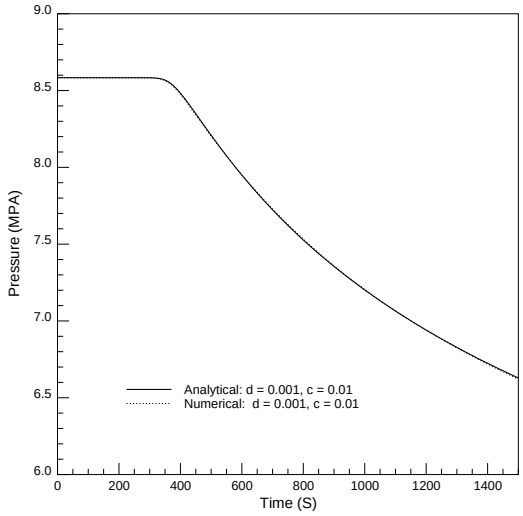

Figure 5.5: Analytical and numerical solutions with Langmuir adsorption

This check on the numerical results justifies the use of the numerical scheme in determining the fate of tracer introduced into a geothermal reservoir to track tracer flowing in the vapor phase.

5.3 Modeling Tracer Response

Modeling of the propagation of tracer is important because it highlights the different mechanisms that control the rate at which tracer is transported by vapor in a porous medium. The three mechanisms considered in this research were adsorption, diffusion partitioning, and preferential partitioning. Adsorption may effect the transport of tracer in two ways. First, if the adsorbed phase is not desorbing rapidly, it may cause an increase in propagation rate of the vapor and of the tracer due to a reduction in the area available for flow. Second, if the vapor carrying tracer adsorbs, the propagation of tracer may be slowed and the concentration of tracer in the vapor phase reduced. Thus, adsorption affects tracer propagation by affecting the transport of the fluid in which it resides (in this research, the vapor phase).

Diffusion partitioning may occur when a tracer is introduced into a porous medium in which one or more fluids reside. Diffusion of the tracer into the resident fluid may delay the tracer even though vapor flow rate may be unaffected or even enhanced. Thus, diffusion partitioning may occur whether adsorption occurs or not.

Preferential partitioning occurs when the tracer properties are such that it preferentially resides in one phase over another. In this research, preferential partitioning would occur if it was shown that tritiated water (HTO) has different boiling characteristics than pure water. In this chapter, the properties of T_2O, HTO, and water are studied to determine the likelihood of preferential partitioning of tritiated water into either the liquid or vapor phase.

Each of the mechanisms for tracer delay were investigated to determine the likely effects of each on tracer tests. To determine the effects of an adsorbed phase on tracer production characteristics, the capability for keeping track of an injected tracer was introduced into the numerical model.

5.3.1 Effects of Adsorption on Tracer Propagation

Since the tracer considered in this research is tritiated water which behaves very much like water, the propagation of tracer may be modeled identically to the propagation of a water component:

$$\begin{aligned} y_i^{n+1} T_{i+1/2}(p_{i+1} - p_i)^{n+1} - y_{i-1}^{n+1} T_{i-1/2}(p_i - p_{i-1})^{n+1} - \\ \frac{\Delta x}{\Delta t}\left[(y_{vi}\phi_{vi}\rho_{vi}S_{vi})^{n+1} + (y_{vi}\phi_{vi}\rho_{vi}S_{vi})^{n}\right] - \\ \frac{\Delta x}{\Delta t}\left[(y_{ai}\phi_{ai}\rho_{ai}S_{ai})^{n+1} + (y_{ai}\phi_{ai}\rho_{ai}S_{ai})^{n}\right] + \\ y_{inj}Q_{inj} - y_{prod}Q_{prod} = 0 \end{aligned} \tag{5.16}$$

In Eqn. 5.16 pressures, saturations, and fluid properties determined at the end of each time step in the computation of mass transport of vapor are used to compute the mass fraction of injected mass in the vapor phase, y_v in each block. To calculate mass fraction in the vapor phase explicitly, a relation is needed between the mass fraction in the adsorbed phase and in the vapor phase.

It was assumed that the mass fraction of injected tracer in the adsorbed phase is a weighted average of the fraction adsorbed at the old time step and the change in adsorbed mass over the time step. In equation form, the mass fraction in the adsorbed phase is given by:

$$y_a^{n+1} \;=\; \frac{y_v^{n+1}\Delta_t S_a \;+\; y_a^n S_a^n}{S_a^{n+1}} \tag{5.17}$$

The weighted mass average for tracer concentration is important because it allows numerical experiments to determine how adsorption of injected tracer affects the propagation and eventual recovery of the tracer. The adsorption process is commonly described as being a layering process in which layers of molecules of adsorbed liquid are laid down, one on top of the other, until adsorptive forces become too weak to hold more layers. In this static model, each layer is assumed to be stationary in the adsorbed phase. If this model were used, it would be necessary to release the adsorbed tracer in a layer-by-layer fashion in the reverse order of deposition. However, adsorption is not a stationary layering process even though it may be considered as such from a mass standpoint. In reality, adsorbed molecules are mobile in the adsorbed phase [1], so mixing within the adsorbed phase is constantly occurring. Thus, while adsorption of an injected tracer occurs at the concentration of tracer in the vapor phase, desorption of tracer occurs at a diluted concentration due to the presence of previously adsorbed liquid which mixes with adsorbed tracer. In this section, then, the effects of tracer propagation due solely to the adsorption phenomena are investigated. Later, the effects of diffusion and preferential partitioning will be investigated.

Loss of injected tracer by radioactive decay was also considered in tracer computations. At the end of each time level, the total amount of injected tracer was reduced by means of an exponential decay term:

$$y_f^n \;=\; y_f^n e^{-kt} \tag{5.18}$$

For tritium, the decay constant, k, is $1.83 \times 10^{-9} s^{-1}$ which gives rise to a half-life of about 12 years. Since tritium is a long-lived conservative tracer, and most tracer

tests are of short duration, decay of tritium tracer is usually negligible. In the cases considered here, radioactive decay was immeasurably small.

A series of numerical experiments were carried out to determine the effects of the presence of an adsorbed phase on tracer transport. These experiments were designed to investigate all aspects of tracer transport in porous media. The effects of initial distributions of tracer were studied. Tracer propagation under steady-state and transient conditions were compared and the reservoir pressure at initiation of tracer injection was varied to determine the effects of initial conditions on tracer propagation. Finally, the effects of preferential partitioning of tracer on the propagation of injected tritiated water were investigated.

Effects of Initial Tracer Distributions

A series of numerical experiments were carried out on a representation of one-dimensional flow in a core at an initial pressure of 8.58 MPa and initial temperature of 300 °C. These initial values of pressure and temperature correspond, approximately, to saturated conditions. One end of the 4 m long core was closed and the other end was produced at a constant pressure of 0.101 MPa. Thus, simple depletion of the core was modeled. The core was broken into 32 blocks of length 0.125 m. In the first series of tests, the vapor in the first block (closed end) was assumed to be tracer and the production of this tracer from the output end of the core was computed. These numerical tests correspond to a physical situation in which injected tracer stays entirely in the vapor phase with no tracer adsorbing. A schematic of the numerical core with assumed fluid saturations is shown in Figure 5.6. Figure 5.7 shows production histories for a series of adsorption isotherms as compared to the production history for tracer with no adsorbed phase present. For the numerical experiments illustrated in Figure 5.7, the maximum adsorbed amount was assumed to be 0.001 grams of adsorbed liquid per gram of rock.

Figure 5.8 compares the production histories for a range of isotherms with the maximum adsorbed amount assumed to be 0.01 grams of adsorbed liquid per gram of rock. Figures 5.7 and 5.8 both show that, in general, tracer in the vapor phase is produced more quickly when an adsorbed phase is present. Both magnitude of adsorption

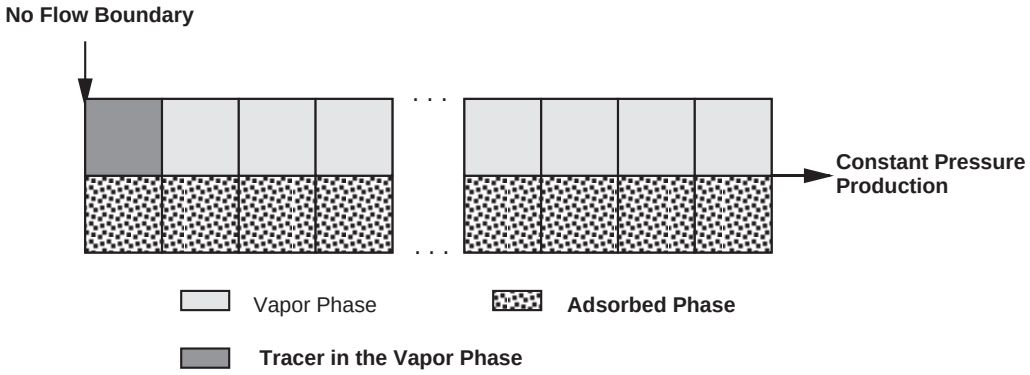

Figure 5.6: Schematic of numerical core with tracer in vapor phase.

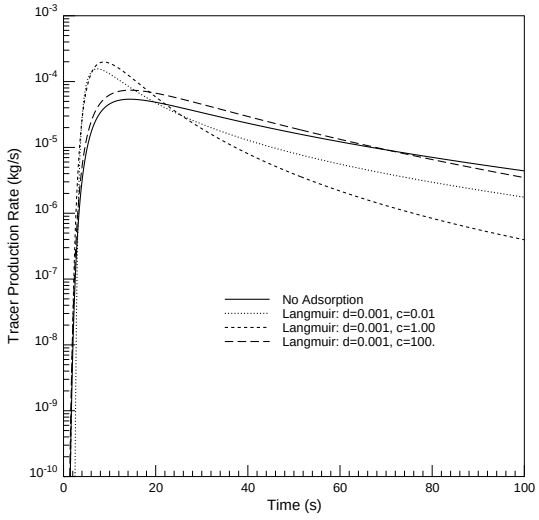

Figure 5.7: Tracer production histories with tracer in vapor phase.

and the shape of the controlling isotherm are shown to affect tracer propagation.

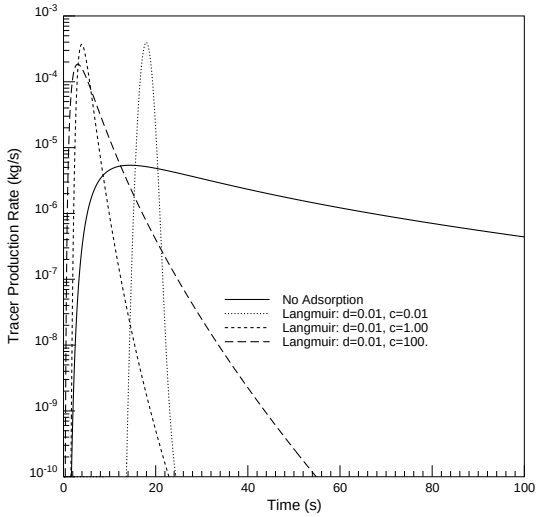

Figure 5.8: Tracer production histories with tracer in vapor phase.

Figure 5.7 shows accelerated tracer breakthrough for concave down (c = 100) isotherms and a delay in tracer breakthrough for concave up (c = 0.01) and linear (c = 1) isotherms. As pressure is depleted from the far end of the core, desorption occurs to replace the produced mass and, simultaneously, vapor from the closed end of the core begins to flow toward the pressure sink. When an immobile adsorbed phase is present, vapor is forced to flow through a smaller area and, therefore, vapor flow velocity is increased for a given pressure drop. For concave down isotherms, the mass replacement due to desorption is not rapid enough to overcome the increased flow rate of vapor due to a decreased flow path, and tracer propagation is increased. For linear isotherms, the two effects almost cancel and breakthrough times are not strongly altered. For concave up isotherms desorption mass replacement becomes dominant so pressure depletion in the vapor phase is slowed and tracer propagation is slowed as well.

Figure 5.8 shows the same general effects as described above in Figure 5.7. However, since adsorption mass is greater in the system shown in Figure 5.8, the mass

effects of adsorption are magnified.

In a second series of numerical experiments, tracer was assumed to exist, initially, only in the adsorbed phase in the block nearest the no flow boundary (Figure 5.9). Fluid was produced from the other end of the core at a constant pressure of 0.101 MPa. Figure 5.10 shows production rate histories for a series of isotherms when tracer was assumed to initially reside in the adsorbed phase. Both mass adsorbed and the shape of the adsorption isotherms were shown to alter the production history of tracer. For comparison purposes, since mass adsorbed varies with the Langmuir magnitude factor, d, the concentration was altered so initial mass in place was equal. As when tracer was confined to the vapor phase, concave up isotherms ($c < 1$) cause delays in tracer breakthrough for a given adsorbed mass. Comparison of tracer production controlled by isotherms having the same shape but with different magnitudes of adsorbed mass show that increased adsorbed mass also contributes to the production delay, but does not have a strong influence on the shape of the tracer production.

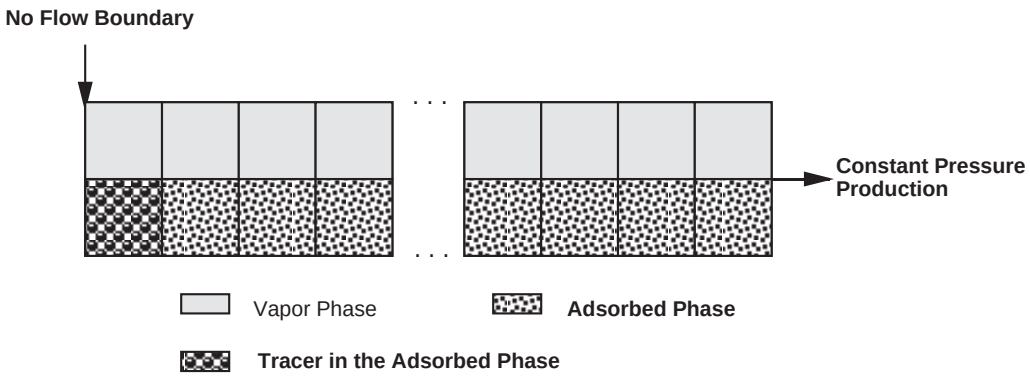

Figure 5.9: Schematic of numerical core with tracer in adsorbed phase.

Preliminary investigations indicate that the presence of an adsorbed phase can have a number of effects on propagation of tracers through porous media. Depending on the shape of the controlling isotherm, the pressure of the system, preferential phase

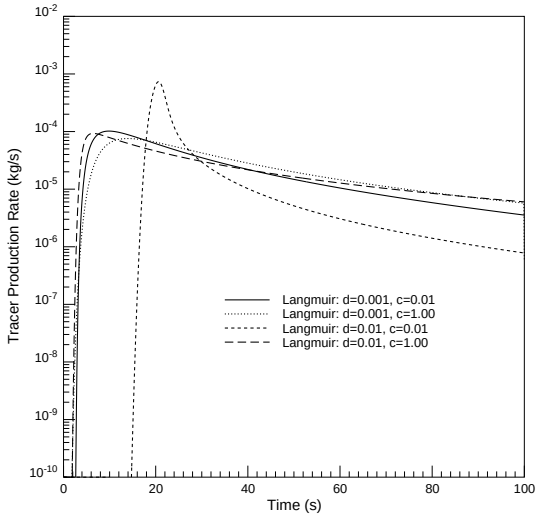

Figure 5.10: Tracer production histories with tracer in adsorbed phase.

residence of the tracer, the production characteristics of tracer can be significantly altered. To determine the likely effects of an adsorbed phase on propagation of injected tracer, a series of numerical experiments were carried out in which a slug of tracer was injected into a core and transport of the tracer was calculated. A range of initial conditions, controlling isotherms, and injection and production rates were used.

Steady-State Flow

In the following series of numerical representations of slug tests, both injection and production rates were held constant at 0.01 kg/s. Injection and production were allowed to continue without introduction of tracer until steady state conditions were obtained. When steady state flow was reached, a 0.001 kg slug of tracer was injected. The tracer propagation is shown in Figure 5.11 as a series of tracer concentration profiles in the vapor phase. Numerical runs were carried out for a series of adsorption isotherms and were compared. Results show that for steady state conditions, diffusion of the tracer is not strongly affected by the presence of an adsorbed phase, but convection of the tracer can be significantly increased by an adsorbed phase relative

to convection in the absence of an adsorbed phase. Diffusion is not strongly influenced because, under steady state conditions, neither adsorption nor desorption is occurring, so no fluid retardation is taking place. Only linear isotherms are highlighted in Figure 5.11 because, since no adsorption nor desorption is taking place, the shape factor of the isotherm does not influence the propagation of tracer. The magnitude factor of the isotherm, however, does affect tracer propagation, although these effects are not large. Comparison of tracer profiles at 21 seconds for isotherms with d = 0.001 and d = 0.01 indicate that a ten-fold increase in adsorbed mass causes a two-fold increase in vapor phase velocity. Therefore, while adsorbed mass does affect steady-state propagation of tracer, these effects are considered small.

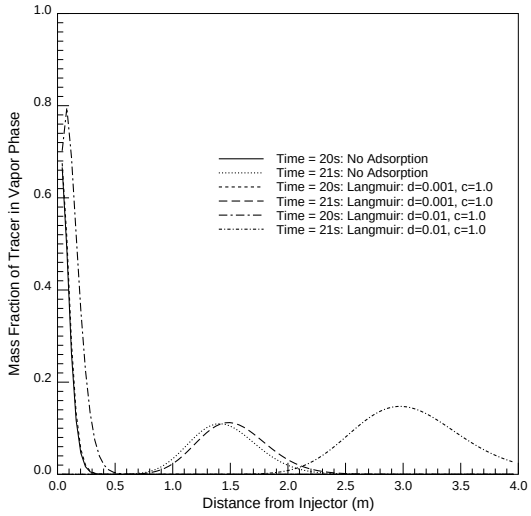

Figure 5.11: Tracer profiles for steady state conditions.

Transient Flow

In the next series of slug tests, the core initial pressure was set at 5.0 MPa and a 0.001 kg slug of tracer was injected upon initiation of injection so transient adsorption effects could be studied. Injection and production rates were both 0.01 kg/s. Figure 5.12 shows tracer propagation in the core under these transient conditions.

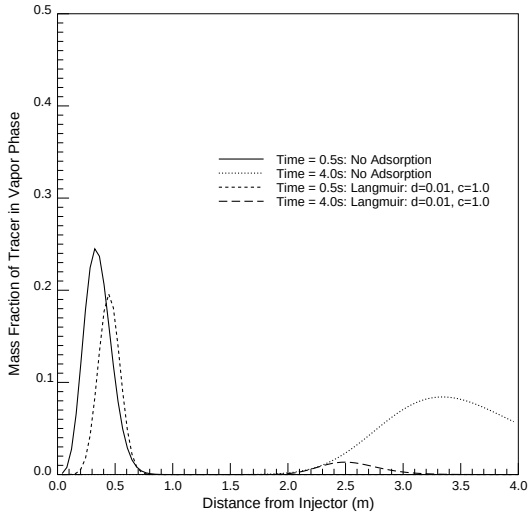

Figure 5.12: Tracer profiles for transient conditions.

In contrast to the results for steady-state flow, tracer propagation under transient conditions is shown to be slowed by the sorption process. Figure 5.12 shows that, at early times, before a large amount of the injected tracer has adsorbed onto the rock matrix, injected tracer propagates faster with an adsorbed phase present than without, as in steady-state conditions. Delays in tracer propagation eventually occur as the effects of adsorbed tracer overcome the increases in vapor velocity due to a smaller flow path. As tracer adsorbs and disappears from the vapor phase, the concentration spike of propagating tracer is decreased and the diffusion of the spike is decreased. Thus, when injected tracer adsorbs, the initial spike of produced tracer should be smaller and should be delayed as compared to a tracer that does not adsorb. Since the initial spike is decreased by the loss of mass to the adsorbed phase, further pressure depletion should continue production of adsorbed tracer. Thus, tracer testing in the presence of adsorption should be characterized by a longer production time than tracer testing in the absence of adsorption. For the test shown graphically in Figure 5.12, tracer delay is not large. Delays in tracer propagation are about 30 % even though maximum adsorbed saturation is increased from 0 to 75 %. In the next

series of tests, the magnitude of this production delay is studied for a wide range of adsorption isotherms and initial conditions.

Effects of Initial Condition

A series of slug tests was designed to investigate the influence of initial conditions on the transient effects of tracer sorption. These tests were used to illustrate the magnitude of tracer delay by adsorption, the amount of dispersion associated with tracer propagation, and the combined effects of initial pressure and adsorption isotherm on propagation of tracer. For all runs in this section, isotherms used were described by a Langmuir model with d = 0.01. The Langmuir shape factor, c, was varied from 0.01 to 100.0. Initial conditions in the core were then varied. Injection was described by a constant pressure boundary set to a maximum of 2 MPa greater than initial pressure and production was described by a constant pressure boundary of 0.101 MPa (atmospheric conditions). In all runs described in this section, the injection well was switched to production after tracer breakthrough at the production well. By comparing the the tracer production histories for the producer and the converted injector, conclusions are reached about the propagation of injected tracer for a range of initial conditions.

In the first test, the initial pressure was set at 7.0 MPa. This condition corresponds to initiation of tracer injection very early in the production life of a reservoir. Figure 5.13 shows the tracer rate histories at the production well for a series of isotherms. Clearly, both the adsorbed mass and the shape of the describing isotherm affect tracer propagation. When the isotherm is concave down (c = 100.0) nearly maximum adsorbate saturation is reached before initiation of injection. Therefore, the injected tracer is forced to flow through a smaller effective channel and, as a result breakthrough occurs more quickly and the concentration of produced tracer is higher. For concave up isotherms (c = 0.01) most of the adsorption occurs at pressures higher than 7 MPa for a reservoir at 300 °C so the breakthrough time is not strongly affected. However, subsequent adsorption of injected tracer reduces the concentration of tracer in the production stream.

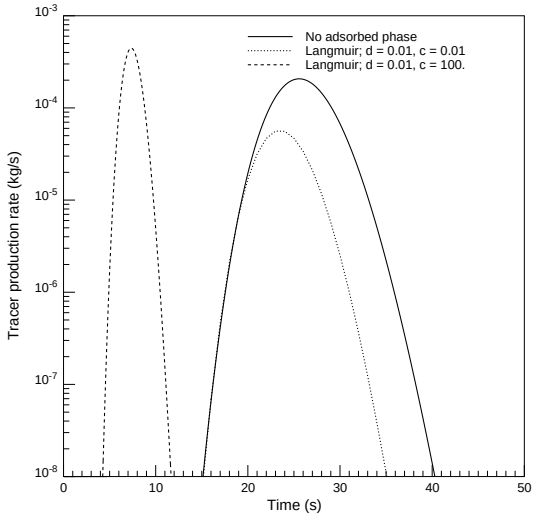

Figure 5.13: Tracer production for early initiation of injector.

In the second test, the initial pressure was set at 4.0 MPa. This condition corresponds to initiation of injection half way through the production life of a reservoir which starts at saturated conditions. Figure 5.14 shows the tracer rate histories at the production well for a range of conditions. For concave down (c = 100) isotherms, the breakthrough of tracer is accelerated compared to a no adsorption case since adsorbate saturation reduces the flow path area available for vapor flow. Initiation of injection at 4 MPa does not allow significant adsorption which might increase the diffusion of the produced tracer spike. Similarly, breakthrough of tracer for concave up (c = 0.01) isotherms is also accelerated relative to a no adsorption case for the reasons described above. In neither case is the magnitude of the adsorption spike significantly affected since very little adsorption or desorption takes place.

In the third test, the initial pressure was set at 0.101 MPa. This condition corresponds to initiation of tracer injection very late in the productive life of a reservoir which starts at saturated conditions. Figure 5.15 shows the tracer rate histories at the production well for a range of isotherms when injection is carried out at a constant pressure of 2.101 MPa. For strongly concave down isotherms (c = 100), no tracer

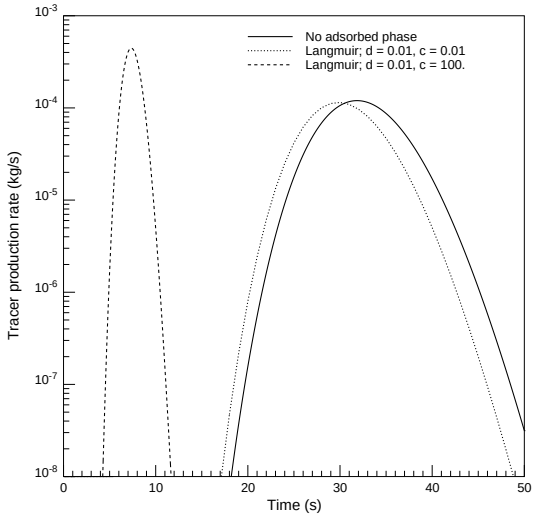

Figure 5.14: Tracer production for midlife injection initiation.

breaks through at the production well due to the large rate of adsorption of injectate at low pressures. For concave up isotherms (c = 0.01), the tracer production response is almost identical in shape to the no adsorption case but the magnitude is reduced slightly and the breakthrough is slightly retarded due to the adsorption of a small amount of injectate.

For the tracer production runs shown in Figures 5.13 through 5.15, tracer effects are shown to depend on the conditions at which injection of tracer is initiated. Only for cases of injection initiation very late in the life of the reservoir are adsorption delay effects shown to occur.

For the initial conditions described above, a second set of runs were made in which the injector was switched to a producer upon breakthrough of tracer at the production well. Figures 5.16, 5.17, and 5.18 show the subsequent production of tracer from the converted injection well for initial reservoir pressures of 8 MPa, 4 MPa, and 0.101 MPa, respectively.

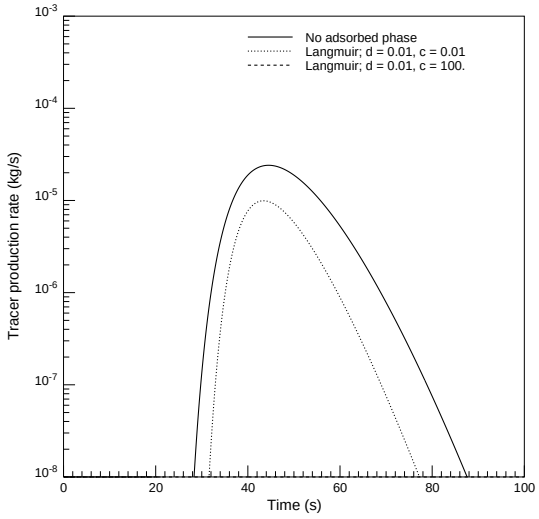

Figure 5.15: Tracer production for late initiation of injector.

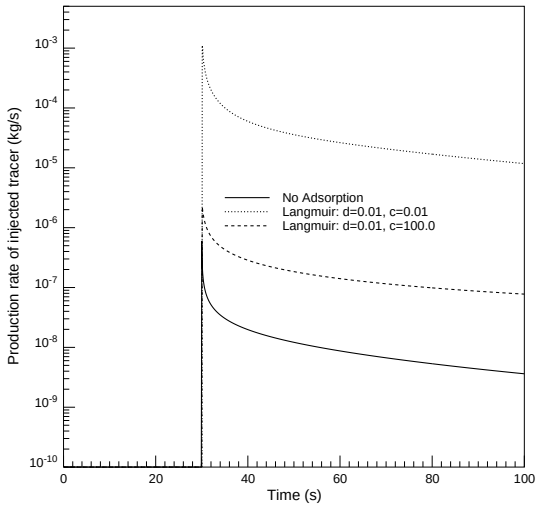

Figure 5.16: Tracer production from injector ($p_i = 8$ MPa).

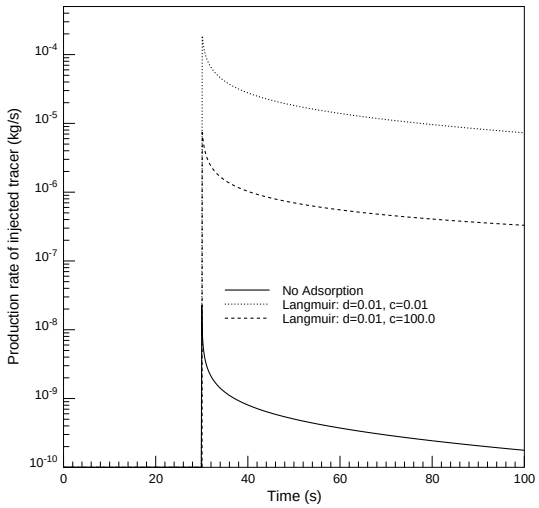

Figure 5.17: Tracer production from injector ($p_i = 4$ MPa).

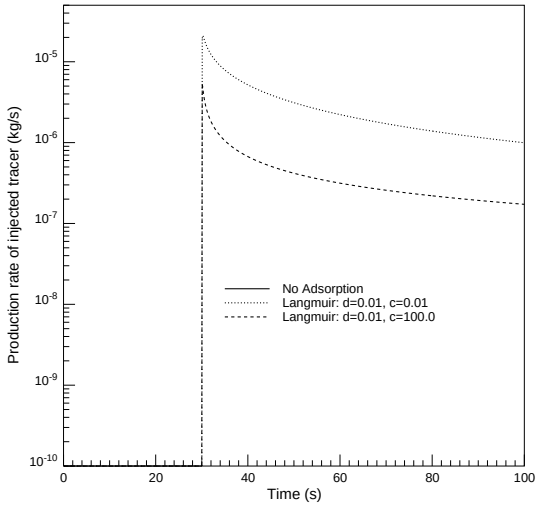

Figure 5.18: Tracer production from injector ($p_i = 0.101$ MPa).

5.3.2 Effects of Diffusion Partitioning on Tracer Propagation

To determine the likelihood of diffusion partitioning of tracer, investigations must be carried out about the sizes of the diffusive flux and the convective flux of the tracer in a given porous medium. In many reservoirs, the diffusive flux of a tracer in one dimension is described by the following form of Fick's Law:

$$v_{diff} = -D_{mol}\frac{\partial C}{\partial x} \tag{5.19}$$

In Eqn. 5.19, v_{diff} represents the diffusional flux of tracer, D_{mol} is the molecular diffusivity of the tracer, and the gradient of tracer concentration is expressed by $\partial C/\partial x$. Fick's law is written for diffusion in a bulk liquid and molecular diffusivities are generally expressed in terms of bulk liquid in the absence of a porous medium. When a porous medium is present, the diffusivity is decreased due to tortuosity of the porous medium. The diffusivity of tritiated water through water is reported by Leap [40] to be about 2.3 $\times 10^{-5} cm^2/s$. However, in a porous medium, the diffusivity is expected to be much lower. In a porous medium, both the porosity and the tortuosity of the medium cause a reduction in the diffusivity. In very small pores for which the pore radius approaches the mean free path of the liquid molecule, the diffusivity is reduced even further. Geankoplis [29] reports that the diffusivity coefficient in porous medium is related to the bulk phase diffusivity by the following relationship:

$$D_{pore} = D_{bulk}\left[\frac{\phi}{a^2}\right] \tag{5.20}$$

where, a is the actual pore length per distance in the direction of diffusion.

Eqn. 5.20 shows that the porous media diffusivity is a function of the porosity, ϕ, and the tortuosity (denoted by a) of the porous media. In many geothermal reservoirs, especially the Geysers, there are two types of porosity, fracture and bulk. It is usually assumed that flow occurs in the fractures and storage in the form of condensed and adsorbed liquid occurs in the bulk porosity matrix. Figure 5.19 shows a schematic of the porosity in a geothermal reservoir.

Porosities reported by Gunderson [32] show that porosity for a large region of reservoir in the Geysers is around 5 %. However, much of the total porosity is from

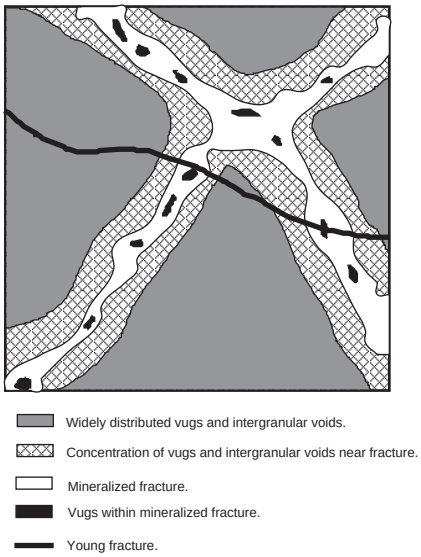

Figure 5.19: Schematic of porosity in a geothermal reservoir.

fracture porosity and a very small portion comes from the interparticle porosity of the system. Gunderson [32] also points out that fractures are usually separated by several centimeters. Therefore, when tracer is injected into a geothermal reservoir, it preferentially flows in the vapor phase in the fractures, but diffuses into the interparticle porosity along the fractures (Figure 5.19). Based on the description of Geysers porosity provided by Gunderson [32] and the diffusion model in Eqn. 5.20 an estimate of the diffusivity of tritiated water into the matrix surrounding fractures was computed. Making the conservative assumptions that interparticle porosity is 1 %, and that the measure of pore tortuosity, a, is 2, the diffusivity of tritiated water is estimated to be 5.8 $\times 10^{-10}$ m^2/s.

The diffusivity of tritiated water into the porous matrix and the permeability of the porous medium were then used to evaluate the relative sizes of the convective and diffusive terms to determine whether diffusion partitioning is significant at the Geysers.

Assuming that bulk flow occurs in fractures and adsorbed liquid is stored in smaller

pores surrounding the fracture (an assumption consistent with observed pore distributions in many geothermal reservoirs) diffusion into the porous matrix was compared with convection in the fracture. Eqn. 5.19 was used with the diffusivity of tritiated water computed as above to calculate the rate at which tritiated water diffuses into a 1 cm long pore with a maximum concentration gradient. In other words, the diffusive flux computed for the maximum concentration gradient was used so a maximum diffusive flux was computed. The maximum diffusion rate was found to be 5.8×10^{-8} m/s. If Darcy's law is assumed to approximate the flow rate in the fractures, convection rates ranging from 2.9×10^{-5} to 2.9×10^{-9} m/s were computed for the range of permeabilities measured at the Geysers. Thus, except in extremely low permeability regions, the convective flux is significantly greater than the diffusive flux. Furthermore, since only a maximum diffusive flux was used in the comparison, it is probable that the time to reach a concentration equilibrium between a tracer in flowing vapor and adsorbed liquid by diffusion alone is much too large for the assumption of instantaneous concentration equilibrium between vapor and adsorbed liquid to be valid for the range of permeability at the Geysers. However, for the lower permeable portions of the reservoir, the equilibrium assumption is probably valid, so investigation of the effects of diffusion partitioning is necessary. So, for permeabilities in the range 10^{-15} - 10^{-16} m^2, the assumption of instantaneous concentration equilibrium between the vapor and adsorbed liquid is probably true in the Geysers. An analytical solution for tracer convection, dispersion, and diffusion partitioning was derived based on a similar derivation by Antunez [5]. The purpose of deriving this analytical solution is to isolate the effects of diffusion partitioning of tracer into adsorbed liquid. Previously, the effects of adsorption were isolated from diffusion effects and were shown to be small. Here, the effects of diffusion are isolated from adsorption effects. The following assumptions were made for the derivation:

1. The adsorbed phase is immobile.

2. The vapor and adsorbed phase saturations are constant. This assumption separates the effects of diffusion from those of adsorption.

3. The tracer partitions instantly and equally between vapor and adsorbed liquid

phases by diffusion.

4. The formation is homogeneous and isotropic.

5. Flow is linear.

6. Dispersion is proportional to the local velocity: $K = |v|$

In a derivation analogous to that of Antunez [5], the mass conservation equation for tracer propagating in a porous medium was found to be:

$$\frac{\partial^2 C}{\partial x^2} - \frac{u_v}{K}\frac{\partial C}{\partial x} = \left(\frac{S_v\rho_v + S_a\rho_a}{K\rho_v S_v}\right)\frac{\partial C}{\partial t} \tag{5.21}$$

Eqn. 5.21 was solved with the following initial and boundary conditions:

$$C(x, t = 0) = 0 \tag{5.22}$$

$$C(x = 0, t) = C_o \tag{5.23}$$

$$C(x \to \infty, t) \to \infty \tag{5.24}$$

After manipulation, the final form of the equation may be written: (for detailed derivation, the reader is referred to Antunez [5])

$$\begin{aligned}\frac{C(x,t)}{C_o} = {} & \frac{1}{2}\exp\left[\frac{xu_v}{K}\right]\operatorname{erfc}\left[\frac{x\sqrt{\frac{S_v\rho_v+S_a\rho_a}{KS_v\rho_v}}}{2\sqrt{t}} - \frac{\frac{u_v}{K}\sqrt{t}}{2\sqrt{\frac{S_v\rho_v+S_a\rho_a}{KS_v\rho_v}}}\right] \\ & + \frac{1}{2}\exp\left[\frac{xu_v}{K}\right]\operatorname{erfc}\left[\frac{x\sqrt{\frac{S_v\rho_v+S_a\rho_a}{KS_v\rho_v}}}{2\sqrt{t}} + \frac{\frac{u_v}{K}\sqrt{t}}{2\sqrt{\frac{S_v\rho_v+S_a\rho_a}{KS_v\rho_v}}}\right]\end{aligned} \tag{5.25}$$

At late time, the second term in Eqn. 5.25 becomes negligible, so under these conditions, the solution for tracer concentration reduces to:

$$\frac{C(x,t)}{C_o} = \frac{1}{2}\exp\left[\frac{xu_v}{K}\right]\operatorname{erfc}\left[\frac{x\sqrt{\frac{S_v\rho_v+S_a\rho_a}{KS_v\rho_v}}}{2\sqrt{t}} - \frac{\frac{u_v}{K}\sqrt{t}}{2\sqrt{\frac{S_v\rho_v+S_a\rho_a}{KS_v\rho_v}}}\right] \tag{5.26}$$

In Eqns. 5.25 and 5.26, u_v refers to the steady state vapor velocity, C stands for the concentration of tracer, and K denotes the dispersion coefficient. In order to use the equations, their validity in geothermal reservoirs was tested. Volumetric flow rate was modeled by Darcy's law for single-phase flow.

$$q_{sc} = \frac{kAT_{sc}p}{\mu z T p_{sc}} \frac{dp}{dx} \tag{5.27}$$

For a pressure drop between the reservoir, p_e, and the well, p_w, Eqn. 5.27 may be written:

$$q_{sc} = \frac{kAT_{sc}}{\mu z T p_{sc}} \frac{p_e^2 - p_w^2}{2(x_e - x_w)} \tag{5.28}$$

which may be rearranged to the following form:

$$q_{sc} = \frac{kAT_{sc}}{\bar{\mu}\bar{z} T p_{sc}} \bar{p} \frac{p_e - p_w}{(x_e - x_w)} \tag{5.29}$$

In Eqn. 5.29, $\bar{p}$ is the arithmetic average reservoir pressure while $\bar{\mu}$ and $\bar{z}$ are calculated at the root mean square average pressure. These assumptions have been shown to be valid by Brigham [11] as long as there are not large variations in reservoir pressure or fluid properties.

The Geysers reservoir was chosen as a model for determining the effects of diffusion partitioning in tracer transport. Reservoir properties from sources cited throughout this report have been used in the following computations. An average pressure of 3.325 MPa was computed from a far-field pressure of 3.9 MPa and a well pressure of 2.75 MPa. Average values of viscosity and compressibility factor were found to be 1.76 $\times 10^{-5}$ Pa·s and 0.86, respectively. Over the pressure range considered, the viscosity varied by 1 % and the compressibility factor varied by 5% so the model assumed for the computation of vapor velocity is valid (Eqn. 5.29).

It was shown above that diffusion effects become large with respect to convection only for permeabilities on the order of 10^{-15} - 10^{-16} m^2. Therefore, this range was used in computing the volumetric flux of vapor. For the range in permeabilities used, the volumetric flux of vapor varies from 4 $\times 10^{-6}$ to 4 $\times 10^{-7}$ $m^3/m^2 \cdot s$

The velocity, computed as:

$$u_v = \frac{q_{sc}}{\phi S_v} \tag{5.30}$$

ranged from 8 $\times 10^{-5}$ to 8 $\times 10^{-6}$ m/s.

At the average reservoir pressure calculated above, the saturations of vapor and adsorbed liquid were computed. The vapor saturation was found to be 97% with the other 3% of the pore space occupied by adsorbed liquid. The densities of the phases at the reservoir conditions were computed to be 16.0 kg/m^3 for the vapor and 799 kg/m^3 for the adsorbed liquid. These values were used in computing tracer profiles for tracer propagation in a vapor dominated porous media both with and without an adsorbed phase present.

Figure 5.20 shows tracer profiles for vapor transport in a porous medium with permeability 10^{-16} m^2 and dispersion coefficient equal to 8.0 $\times 10^{-6} m^2/s$.

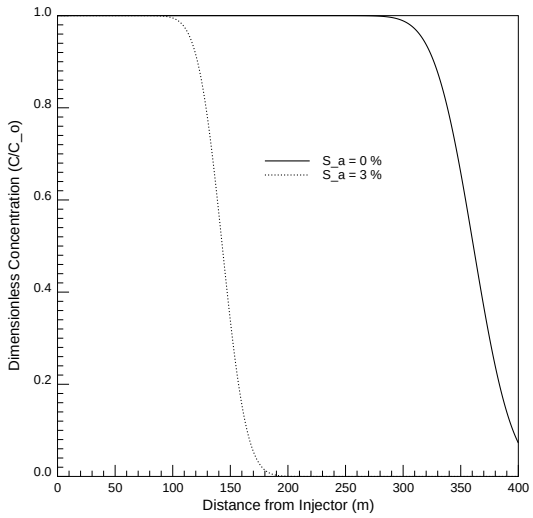

Figure 5.20: Pressure profiles for diffusion tracer delay.

Comparison of the generated concentration profiles in Figure 5.20 shows that the magnitude of delay due to diffusion partitioning of tracer from the vapor phase to the adsorbed phase is on the order of a 2 to 3-fold delay. Thus, the delay of tracer by diffusion alone is much more significant than delays due solely to adsorption effects.

5.3.3 Effects of Preferential Partitioning on Tracer Propagation

One of the main problems in using tracers to determine flow characteristics in porous media is that, often, tracers do not behave exactly like the fluid they are designed to track. In geothermal reservoirs, tritium is a commonly used tracer. It is used because, in the form in which it is carried through water (HTO), its characteristics are almost identical to those of water for a range of conditions [45]. However, even given the similarities between tritiated water and ordinary water, partitioning is often cited as a possible explanation for tracer diffusion during injection tests.

Greenkorn [30] and Deem, et. al. [18] showed that adsorption of tritiated water by sandstone is of the same order as would be expected for water. In determining the partitioning of tritiated water between the vapor and liquid phases, the controlling characteristics are the temperature-pressure relationship of the tracer and the density of the tracer. If the temperature-pressure characteristics of the tracer are significantly different than the liquid it is designed to track, the tracer will boil at different reservoir conditions and will, therefore partition differently between the liquid and vapor. If the densities of the tracer and tracked liquid are significantly different, the heavier liquid will preferentially tend to remain in the liquid phase even if boiling characteristics of the fluid are similar. Matsunaga and Nagashima [46] showed that, for a range of temperatures from 20 to 300 °C, the vapor pressure of T_2O varied by a maximum of 2.5 % from pure water values. Also, for temperatures below 180 °C, T_2O is actually more likely to partition into the vapor phase than the liquid phase based upon the temperature-pressure characteristics of the fluid. In vapor dominated reservoirs, temperatures are well above saturated conditions so boiling partitioning should not occur at all.

The density of gaseous T_2O was shown to be different than steam at temperatures likely in geothermal reservoirs. In the range of temperatures found in the Geysers (230 °C - 250 °C) the density of T_2O is 20 % greater than steam. It is sometimes assumed that the density differences between water and tritiated water will cause tritiated water to partition into the liquid phase. However, the saturation curve described

above clearly shows that the boiling characteristics of T_2O are almost identical to those of water. Thus, while the density of tritiated water in the liquid and vapor form may be up to 20 % larger than for water, the boiling characteristics are unaffected by the density differences of the liquids.

When using tritium as a tracer in geothermal reservoirs, it is introduced into the reservoir in the form of tritiated water, not as T_2O. Since there is only one tritium atom in a molecule of HTO, the boiling characteristics of tritiated water are even closer to water than are those of T_2O. So, since the boiling properties of tritiated water are almost identical to those of water, it may be concluded that tritiated water tracer does not tend to move into either the liquid or vapor phase in preference to water. Therefore, preferential partitioning does not influence the propagation of tracer.

Chapter 6

The Geysers Geothermal Reservoir

The Geysers geothermal field is the largest developed geothermal resource in the world. It is located in the Mayacmas range about 120 kilometers north of San Francisco near Santa Rosa, California (Figure 6.1). The Geysers field lies in dry, mountainous terrain and is characterized by several areas of surface thermal activity.

The Geysers field was discovered in 1847 and commercial use of the hot surface waters in spas began in the 1860's. Production of Geysers steam for generation of electricity began in the 1920's with the drilling of eight shallow wells between 1921 and 1925. The wells were drilled to depths of 60 to 190 m and steam pressures of 1.0 to 2.1 MPa were encountered. The development resulted in the generation of 35 kW of electrical power which was used by a local resort spa. The project had many problems and was abandoned in the early 1930's.

No further development of the Geysers took place until 1955 when modern development of the field began. Large scale development began in the 1960's and continued at an accelerated rate until the late 1980's when steep pressure decline in the field curtailed development. Geysers energy production peaked in the late 1980's at a gross capacity of about 2200 MW_e. Reddy and Goldemberg [62] estimate that the energy needs of an average American home are about 1 kW so energy production from the Geysers supports the equivalent of about 2.2 million homes. Therefore, the Geysers represents a significant energy resource.

Barker, et. al. [7] summarized the growth in generation capacity at the Geysers

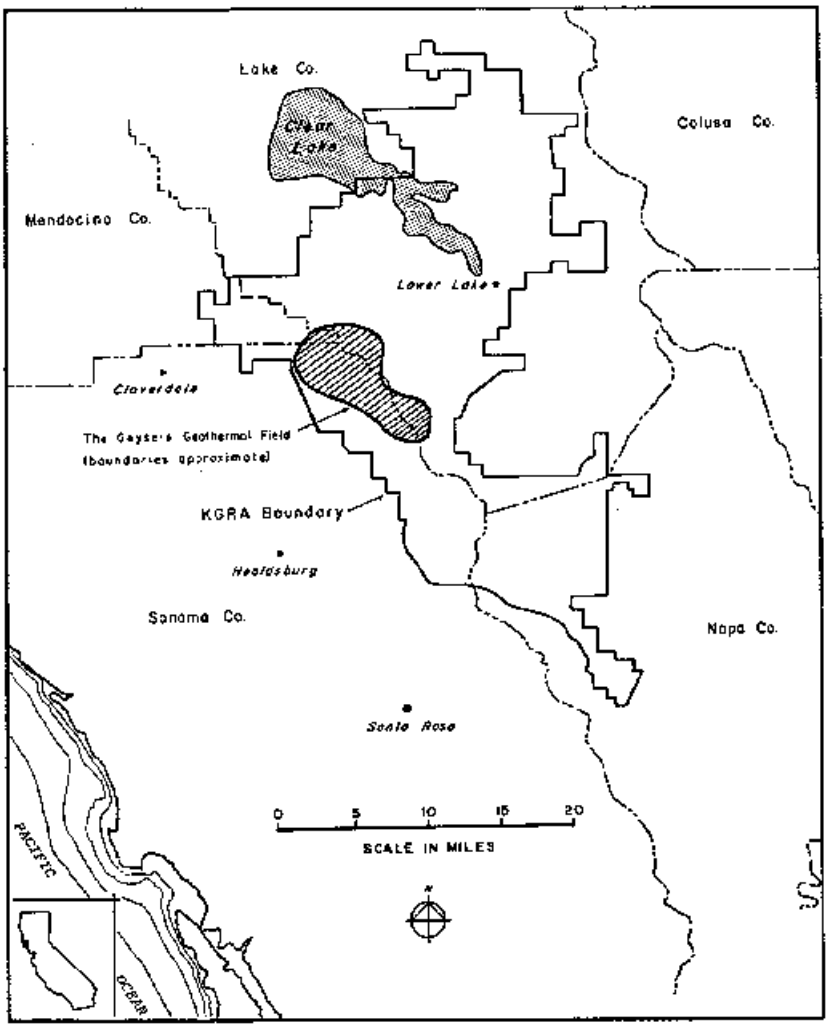

Figure 6.1: Location of the Geysers geothermal field (from Koenig [38])

as occurring in three phases:

1. **Phase I:** From 1960 to 1968, 82 MW of generation capacity was added at an average of 10 MW per year.

2. **Phase II:** From 1969 to 1981, 861 MW of generation capacity was added at an average of 67 MW per year.

3. **Phase III:** From 1982 to 1988, 861 MW of generation capacity was added at an average of 150 MW per year.

The accelerated rate at which the Geysers has been developed has had an effect on the production decline in the field. In approximately 1987, during Phase III development, listed above, well production decline rates began to steepen. Figure 6.2 (from Barker, et. al. [7]) shows mass production and net electrical generation for leases held by UNOCAL, Magma Power Co. and Thermal Power Co. (UMT). For the period shown in Figure 6.2, UMT leases accounted for almost all of the production at the Geysers. Field flow rate and electrical generation decline are shown to occur at 1987.

Figure 6.2: Geysers production (from Barker, et. al. [7])

The seemingly obvious reason for fieldwide production decline is that over production has resulted in an increase in decline rate. However, it is not clear that

extrapolation at decline rates currently experienced will yield accurate production forecasts. The proven existence of an adsorbed phase may significantly alter the production decline of the reservoir even if production is maintained at current levels. By characterizing the pressure effects of an adsorbed phase in geothermal reservoirs, the general depletion characteristics of a geothermal reservoir are determined. Then, by applying general results to known adsorptive characteristics at the Geysers, long-term effects of adsorption on depletion at the Geysers may be determined.

In Chapter 4, the general depletion effects of an adsorbed phase in a geothermal reservoir are shown. In Chapter 5, the general effects of an adsorbed phase on the injection and subsequent production of a tracer are highlighted. In this chapter, the effects of an adsorbed phase on depletion and the simultaneous injection and production at the Geysers geothermal reservoir are studied by making use of field data.

6.1 Geysers Reservoir Properties

The Geysers reservoir is heterogeneous and there is a large range in properties over the reservoir. A number of studies have attempted to determine Geysers reservoir properties and the range of values is shown in Table 6.1.

The reservoir properties listed in Table 6.1 include data sampled at widely separated portions of the field, and at widely varying times. These values, however, provide a framework within which adsorption effects at the Geysers can be analyzed. In numerical experiments carried out in this chapter, reservoir properties are varied within the ranges presented above to determine the likely fate of injected tracer.

Table 6.1: Geysers Reservoir Properties

Property	Range of Values
Pressure [7]	1.2 - 3.6 MPa
Temperature [72] [21]	230 - 250 °C
Porosity [32]	$0.6 - 5.8\%$
Permeability [7]	$5 \times 10^{-18} - 1.8 \times 10^{-13}$ m^2
Rock Density [21] [65]	2650 - 2720 kg/m^3
Rock Thermal Conductivity [69]	1.26 - 3.60 W/(m ° C)
Rock Heat Capacity [34]	1.30×10^3 kJ/(m^3 °C)

6.2 Injection at the Geysers

The method of cooling tower condensate disposal and mass replacement in the Geysers has been injection of surface water and condensed produced vapor. To assess the effectiveness of the injection program, knowledge of the fate of injected fluid is necessary. In particular, the information necessary for evaluation of an injection program includes knowledge of injector/producer connectivity and the potential for recharge of the Geysers adsorbed liquid.

Connectivity between an injector and producer determines the velocity with which injected fluid will travel between the injector and producer. As the fluid velocity increases and the distance between the injector and producer decrease, the residence time of the fluid decreases resulting in reduced heat transfer to the injected fluid and a reduced exploitation of heat reserves.

Recharge of the adsorbed liquid through injection is accomplished by increasing reservoir pressure and increasing the adsorbed mass as dictated by the porous medium's characteristic adsorption isotherm.

A method for keeping track of injected fluids is to inject a tracer along with the injectate; and, by recording subsequent production of tracer in surrounding wells, information on well connectivity and recharge potential may be inferred. Gulati, et. al., [31] pointed out five objectives in running a tracer survey:

1. To determine if any of the injected water is vaporizing.

2. To determine how much of the injected water is being produced as steam at the nearby production wells.

3. To determine the regional flow pattern of fluid in the reservoir.

4. To determine if the efficiency of water vaporization is declining or staying constant with time.

5. To determine if the regional flow pattern will undergo a substantial change when new units go on stream.

To these five objectives, a sixth may be added which may hold great significance for production from the Geysers and other geothermal reservoirs.

6. To determine the effects of vapor adsorption on the production delay of injected fluid.

Gulati, et. al., [31] go on to point out necessary characteristics of the tracer used to meet the six objectives listed above. The characteristics related to the physical properties of the tracer are:

1. It should not be adsorbed on the rocks.

2. Its phase should change only when the phase of the injected water changes.

3. When liquid with a certain concentration of tracer vaporizes, both vapor and liquid should have the same tracer concentration. [i.e. the tracer should not preferentially partition into either the vapor or liquid phase.]

4. The half life of tracer (if radioactive) should be more than one year because significant quantities might appear at production wells for a year or more.

In light of current evidence that liquid adsorption occurs to a fairly significant degree in Geysers reservoir rock, the first characteristic listed above should be altered to "It should not tend to adsorb to a greater degree than the phase in which it resides". In other words, an injected tracer should not selectively partition into any of the liquid phases present in the reservoir. An analysis carried out in Chapter 5 show that preferential partitioning effects are insignificant and may be ignored.

Finally, the half-life of tritium is about 12.5 years, thus it is a conservative tracer which does not decay appreciably over the life of most tracer tests.

The data summarized above indicates the following properties for tritiated water (HTO):

1. HTO does not adsorb on solid surfaces to a greater degree than water. Therefore, preferential adsorption of HTO will not occur in reservoir tracer tests.

2. Since the vapor pressure curve for HTO is nearly identical to that of water, the vaporization characteristics of HTO can be considered to be the same as those of water. Also, since phase partitioning is dependent upon the vaporization characteristics of a given fluid, partitioning is shown to be insignificant.

3. Most tracer tests last far less than 12.5 years, so the radioactive decay of tritium is usually negligible.

The characteristics of tritium tracer, therefore, are ideally suited to tracer analysis in geothermal reservoirs. An analysis of the effects of adsorption on propagation of an injected tracer was carried out within the context of the six objectives listed above. Results of tracer analysis were used to determine the effects of mass replacement due to injection.

6.2.1 History of Injection at the Geysers

In 1991, UNOCAL prepared a summary of injection projects carried out at the Geysers. The report is an excellent source for information about the history of injection at the Geysers and future plans for injection. For the remainder of this chapter, unless otherwise referenced, injection information is taken from the UNOCAL injection report [68]. A detailed map of the Geysers geothermal field showing operators of the field and the location of power generation plants (Figure 6.3) is provided by Barker, et. al. [7]. Unit locations roughly coincide with the location of power generation plants. Figure 6.3 is used as a reference for well locations throughout the rest of this chapter.

Reinjection of cooling tower condensate began at the Geysers in 1969 with an injection to production ratio of 5 %. At initiation of the injection program, all injectate was cooling tower condensate. In 1980, fresh water injection, extracted from Big Sulphur Creek, was initiated into the Units 1-6 area. A second fresh water facility began providing fresh water for injection in 1983. Fresh water injection peaked at 7 % in 1983 while total injection (including condensate) has stayed fairly constant at 20 - 25 % since the early 70's.

Figure 6.3: Unit location at the Geysers (from Barker, et. al. [7])

In general, two injection strategies have been used at the Geysers – deep injection and shallow injection. In deep injection, outlying wells with deep steam entries are used as injectors to minimize downward channeling of liquid water to nearby wells. Effects of deep injection are often difficult to quantify and while some short term benefits have been observed, it has been assumed that most of the benefits are long term [68]. The shallow injection strategy uses injection wells with steam entries higher than surrounding wells and relies on the vaporization of injected water as it channels toward surrounding production wells. Since breakthrough of shallow injectate is usually fairly rapid, benefits of shallow injection are generally short term. In the following sections, specific injection operations at the Geysers, for which data was collected, are described and the future of injection is discussed.

Unit 17 Injection

Injection into the Unit 17 area at the Geysers began in March, 1988, through well DX-72. Unit 17 injection was a deep injection project so effects were expected to be long term. In 1991, surrounding well rates were analyzed to determine the effects of injection. Wells DX-28 and DX-64 experience increased flow rates by 8 kilopounds per hour (kph) each and each well experienced a reduction in decline rate. Decline rate reduction in DX-28 was between 12.5% and 9.6% while decline rate reduction in DX-64 was about 12.5%. Wells DX-63 and DX-23 experienced temporary production increases, but decline rates were not altered on a long term basis.

Based on the production responses described above, effects of deep well injection were shown to have slight short-term effects (rate increase of 10 kph), and slightly greater long term flow rate effects (increases of 16 kph). Slight long term decline rate effects were also observed (decline rate reduction of 4%).

Unit 14 Injection

Another deep injection project was undertaken in the Unit 14 area of the Geysers field. The project was initiated in 1983 with injection of condensate and fresh water into GDCF 117A-19, GDC-18, and GDC-1. By 1987, production and thermal decline

in the reservoir indicated that injection should be curtailed. From 1987 through 1989, injection was limited to GDCF 117A-19 to allow the area to recover thermally. Following thermal recovery, low pressure, high heat conditions were evident in the Unit 14 area and injection was restarted in GDC-18. While high injection rates were maintained, a positive production response was noticed in offset wells but a lack of injection water reduced the effectiveness of the injection program. By 1992, only 10% of injectate had been recovered, but analysis of the injection program is continuing.

Unit 9-10 Injection

Injection at a rate of 500 gpm into LF-2 began on February 14, 1992. This injection program represented UNOCAL's first shallow injection project and was expected to produce short term results. Within two months of injection, seven offset production wells showed production increases totaling a 6% return of injected condensate. The nearest producer, LF-39, watered out very quickly after its early production increases and was shut-in. The Unit 9-10 injection program is currently being monitored for further injection effects.

Low Pressure Area Injection

Enedy, et. al. [22] described an injection project in the southeast Geysers. Data used in this section is from their report.

On September 20, 1989, a large scale injection program was initiated in the southeast Geysers with injection into C-11 [22] (Figure 6.4).

Although C-11 experienced several shut-in periods, production at about 800 gpm was maintained until June 4, 1990 when a five month shut-in period ensued. Injection was restarted for 8 days on August 8, 1990 and the test was concluded in November, 1990. Injection was directed at a Low Pressure Area (LPA) which was characterized by a low reservoir pressure (<1.5 MPa) and a high reservoir temperature (230 °C). Injection rate into C-11 is shown in Figure 6.5.

A total of 2 billion (9.1×10^8 kg) of condensate was injected into the LPA via C-11. The injection program had two major effects. First, reservoir pressure in the

LPA was increased. Figure 6.5 shows static pressure measured at observation well F-4, located 2400 ft (732 m) from C-11.

Figure 6.4: LPA well locations (from Enedy, et. al. [22])

Figure 6.5: F-4 observation well pressures (from Enedy, et. al. [22])

Second, the injection program resulted in increases in both mass and energy production rate. Figure 6.6 shows monthly production rates for wells owned by the three operators in the LPA. Wells owned by Calpine were declining at a 25 % rate before injection began but soon after injection, production rates began to incline at a 58 % rate. UNOCAL wells, declining at 5 % before injection, went on a 21 % incline after injection. And, NCPA wells switched from a 35 % decline to a 61 % incline due to the C-11 injection program.

Figure 6.6: LPA monthly flowrate (from Enedy, et. al. [22])

A 20 MW increase in steam production within 5 months of injection was noted by Enedy, et. al. [22]. Thus, heat extraction was increased due to injection into C-11.

The LPA injection program demonstrated that injection can be used as a means to increase production from the Geysers reservoir and increase the efficiency of heat extraction from the reservoir. An analysis of the LPA injection project in terms of adsorbed mass replacement is carried out later in this chapter.

The Future of Injection at the Geysers

Design of future injection projects at the Geysers will depend on the results of earlier injection projects and on results from research aimed at understanding the effects of injection on recharge.

Currently, operators at the Geysers are considering numerous injection options but uncertainty about the usefulness of injection makes decisions about these programs difficult. Under consideration are injection programs using ground water, surface water, treated waste water, and cooling tower condensate. Ground water extraction from the Cobb Mountain and Clear Lake volcanics is being considered as a possible water supplement for injection at the Geysers and extraction programs and costs are currently being evaluated.

Surface water is another possible source of injection water at the Geysers. Several water sources, Kelsey Creek, Putah Creek, and Big Sulphur Creek, are currently being considered for development as water sources. High costs and difficulties in obtaining water rights present obstacles to these sources.

UNOCAL, Lake County, Calpine, NCPA, and PG&E are currently considering construction of a pipeline to transport treated waste water to the Geysers from Lake County. As with ground water and surface water sources, costs of treated waste water are high and may prove to be too expensive for use at the Geysers.

Currently, most of the injected water at the Geysers comes from cooling tower condensation. Between 20% and 25% of produced water is collected and reinjected. Projects for increasing condensate recovery efficiency are costly and it is doubtful that it will be economically possible to increase injection of cooling tower condensate.

Uncertainty about development of injection programs is due, in large part, to uncertainties about the usefulness of water injection at the Geysers. While ongoing field studies are being used to further determine the observable short term effects of injection, the current research is aimed at determining the long term effects due to adsorption. During injection of water, pressure increases in the reservoir lead to an increase in the adsorbed mass. Determination of the magnitude of this added adsorbed mass is useful in determining the long term storage and production effects of an injection program. To quantify the recharge of adsorbed mass at the Geysers, field pressure data and tracer production data were used.

6.2.2 Effects of Injection on Adsorbate Recharge

Based on data gathered in the LPA injection test, estimates of the recharge of the adsorbed mass in the Geysers geothermal reservoir due to injection were prepared in this study. An overview of the LPA is shown in Section 6.2.1. Enedy, et. al. [22] analyzed test data to determine the potential for reinjection to increase reservoir pressure and increase steam production. However, they did not analyze the potential for recharge of adsorbed mass. In this section, data from the LPA injection test is used to estimate the recharge of adsorbed mass accomplished in a typical injection project.

In the LPA injection test, reservoir pressures, as measured at the wellhead in observation well F-4, increased from 1.03 MPa at the initiation of injection to 1.31 MPa at the end of the test. Assuming an average reservoir temperature of 230 °C, the relative pressure was increased from 0.3685 to 0.4687. Based on the Geysers adsorption isotherm shown in Section 2.3.1, Figure 2.5, this increase in pressure corresponds to an increase in adsorbed mass from 0.15 mg/g to 0.18 mg/g. Thus, the adsorbed mass was increased by 0.03 mg/g.

Enedy, et. al. [22] reported the area of the LPA as 790 acres or 3.2×10^6 m^2. Open well intervals were reported in three wells in the LPA. Open hole thickness in well 956A-2 was reported as 975 m, in well F-6 as 1036 m, and in well C-11 as 1933 m. Assuming a reservoir thickness of 2000 m and assuming that the entire thickness of the reseroir is available for flow, an effective LPA volume of 6.4×10^9 m^3 is obtained. Rock density was assumed to be 2.72×10^6 g/m^3. Based on the volume of rock and the rock density, the mass of rock in the LPA is 1.74×10^{16} g. It was shown above that the amount of increase of adsorbed mass based on the F-4 well pressure rise is 0.03 mg$_a$/g$_r$. Assuming the pressure rise was uniform in over the LPA, the increase in adsorbed mass is computed as 5.2×10^{11} g.

Total mass injected into the LPA through injector C-11 was reported by Enedy, et. al. [22] as about 2 billion pounds or 9.1×10^{11} g. Thus, using the mass adsorbed shown above, the estimated mass adsorbed is about 57 % of the total mass injected.

The above calculations, while approximate, indicate that the mass adsorbed in an injection project at the Geysers may be a large fraction of the injected mass.

6.3 Tracer Studies at the Geysers

Several tracer injection studies have been performed at the Geysers geothermal field with the intention of determining the fate of injected liquid. The two most complete tracer studies carried out to date are the Y-5 tracer study carried out by NCPA and the DX-8 tracer study carried out by UNOCAL. Due to limited availability of tracer data, only the DX-8 tracer study was analyzed. The purpose of analysis of the tracer response data is to determine if the recharge of the adsorbed phase is occurring in standard water injection programs. In previous sections, the short term effects were outlined based on field production during injection projects. In Section 6.2.2, the long term benefits of injection, i.e. recharge of the dense adsorbed phase, are shown to be small for the LPA injection project.

In the next section numerical tracer analyses were applied to data from a Geysers tracer test to determine if the presence of an adsorbed phase may be detected from tracer production data.

6.3.1 Effects of Adsorption on Geysers Tracer Tests

UNOCAL initiated a tritium tracer study, henceforth known as the DX-8 tracer study, on October 26, 1977 by injecting 100 curies of tritiated water into well DX-8 at a constant rate over a 24 hour period [67]. Surrounding production wells were sampled periodically until September, 1981, when low production concentration and the high cost of sampling promulgated an end to the tracer study.

Based on injection and production rates of wells involved in the DX-8 tracer study, a streamline model was developed to determine areas swept by each injection/production pair. In determining streamlines, the assumptions of constant injection and production rates and constant reservoir properties were made. While these assumptions are known to be in error, they were made to form a basis for computing the order of magnitude of permeability variation effects on propagation of tracer in the reservoir. It was observed that approximately 90 percent of all recovered tritiated water was produced in wells OS-1, OS-7, OS-23, OS-24, DX-2, DX-3, DX-21, and DX-29. Thus, only these wells were included in the streamline computations.

Streamline model

In developing the streamline model, the following assumptions were made:

1. Steady-state conditions prevail.
2. The line source approximation may be used to determine pressure at a point in the reservoir (i.e. flow is two-dimensional).
3. Total mass injected exactly balances total mass produced.
4. Fluid velocity may be calculated by Darcy's law.

While production and injection rates of the wells considered in this study varied over the period of interest, average rates were determined from early time data. Production rates of the 8 production wells were summed and the average injection rate was subtracted from this total. The remaining injection rate was assumed to come from outside the study area. In order to introduce fluids from the surrounding area, 12 imaginary wells were positioned around the study to provide the excess mass. Table 6.2 lists the rates used in computing streamlines and the percentage of tracer recovered from the production well.

Figure 6.7 shows a schematic of well locations used to develop the DX-8 streamlines.

Streamlines were computed in a stepwise fashion by use of the following procedure:

1. An injector is chosen as a basis for computing streamlines. In this case, DX-8 was chosen.
2. A series of flow vectors are assumed to leave the injector for a range of angles. These angles are chosen as a starting point for tracking injected fluid particles and are completely arbitrary. The length of the flow vector is small so the streamline is smooth.
3. Starting at the end of the initial arbitrary flow vector, the pressure gradients in the x and y directions are calculated from the derivative of the exponential

Table 6.2: Well Production Data

Well Name	Flow Rate (kg/s)	Tracer Recovered (% of total recovered)
DX-8	-43.4	0.0
OS-1	12.6	19.05
OS-7	13.5	3.52
OS-23	17.4	33.74
OS-24	20.0	10.79
DX-2	8.7	7.29
DX-3	5.6	7.64
DX-21	8.3	3.77
DX-29	13.5	2.38

integral solution. Pressure derivatives are calculated for the sum of all wells in the system.

4. The resulting pressure gradient at the point in the reservoir is used to calculate the velocity for the next flow vector.

5. Using the velocity and the predetermined vector length, a new small flow vector is drawn.

6. This process is repeated over small steps until the head of a vector coincides with the coordinates of a production well at which point the streamline is complete.

Figure 6.8 shows developed streamlines for the DX-8 tracer study.

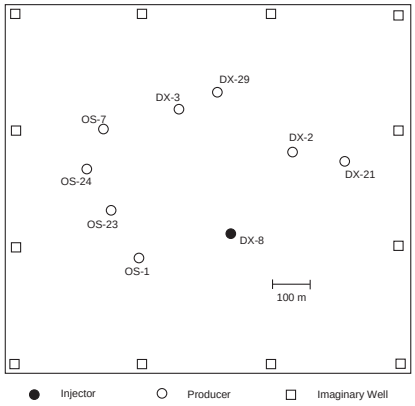

Figure 6.7: Schematic of well placement for streamline generation.

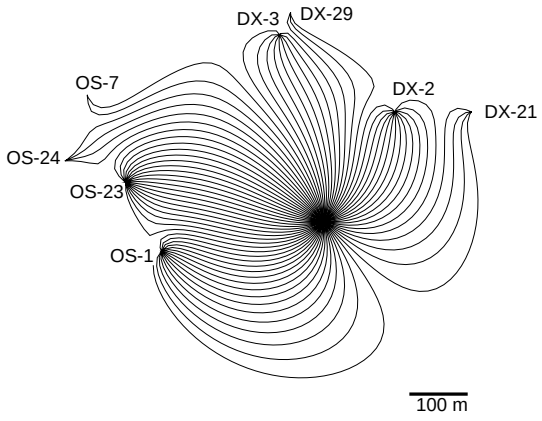

Figure 6.8: DX-8 tracer study streamlines.

Computation of Tracer Propagation

A numerical computation of tracer response for the DX-8/OS-23 well pair on computed stream tubes for that well pair was used to demonstrate the effects of adsorption on tracer response at the Geysers. Tracer production was simulated both with and without an adsorbed phase present. Simulations were carried out with the numerical model discussed in Chapter 5. Figure 6.9 shows computed stream tubes for the DX-8/OS-23 well pair. The stream tubes were computed as described in the previous section.

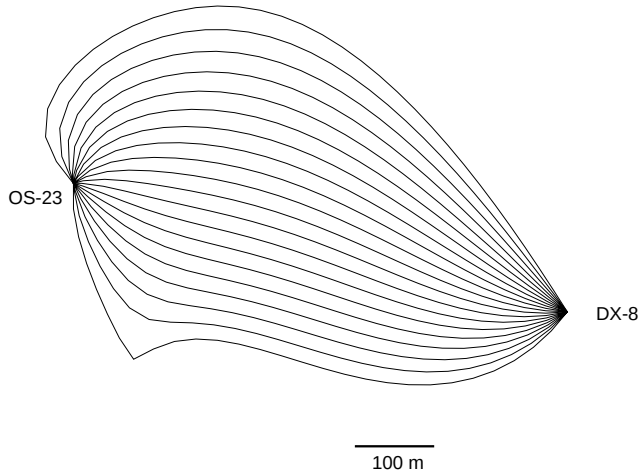

Figure 6.9: Streamlines for DX-8/OS-23 well pair.

Each stream tube shown in Figure 6.9 was approximated by a linear flow path. Each stream tube length was computed as the mid-tube length between injector and producer. The average width of each tube was computed by assuming unit thickness in each tube, computing the volume of the tube, and then constructing linear approximations of each tube with a constant width such that the volume of the tube remained constant. After linearizing each tube, individual tube data was computed as shown in Table 6.3. The height of the linearized stream tubes was computed by matching the initial breakthrough time of the tracer. By using a trial

method, it was found that using a height of 1 m, initial breakthrough time of the tracer was closely matched if a permeability of 5.8×10^{-15} m^2 was used in tube number 10 (Table 6.3). The breakthrough time can also be matched by simultaneously increasing the permeability and block height. However, since little information on the thickness of the permeable region is known and the permeability is within the reported permeability range in the Geysers (Table 6.1), a 1 m block height was used in all numerical simulations.

For all numerical calculations performed in this chapter, the space dimension was broken into 100 blocks. Thus, in the shortest tube, the block thickness (Δx) was about 3.5 m while in the longest tube, Δx was about 4.7 m. In order to ensure that the Courant number did not exceed 1, a maximum velocity was computed based on Geysers data. Using a maximum permeability of 10^{-12} m^2, a maximum pressure drop across a block of 1.15 MPa, and a minimum block thickness of 3.5 m, a maximum time step of about 200 s was computed. In all simulations carried out in this section, a time step of 100 s was used.

Production data and details about sampling were provided by UNOCAL [67]. Production rate and tracer production data for well OS-23 are summarized in Table A.1. Production rates and concentration of radioactive tracer were measured at the well-head. Steam samples were taken from a vent on the well, condensed, stored in a 6 ml bottle and sent in for analysis. A Hewlett-Packard Model 3375 Tricarb Liquid Scintillation Spectrometer was used to measure the amount of radioactivity in the sample. The rate of radioactivity produced from the well is computed by use of the following equation:

$$1 \text{ count}/(\min \cdot 6 \text{ ml}) \;=\; 3.4954 \times 10^{-8} \times G \; (\mu\text{Ci/s}) \tag{6.1}$$

where the production rate, G, is specified in units of lb/hr. Based upon Eqn. 6.1, the radioactivity production rate of from well OS-23 is shown in Figure 6.10.

The mass concentration of tritium in the OS-23 production stream was calculated by use of the following relationship between radioactivity of tritium and its concentration in water:

Table 6.3: OS-23 Stream tube data.

Tube Number	Mid-Tube Length (m)	Average Width (m)
1	405.1	7.1
2	385.6	6.6
3	374.3	6.5
4	365.9	6.4
5	359.7	5.9
6	355.2	6.1
7	352.4	6.0
8	351.1	5.9
9	351.4	6.1
10	353.1	5.6
11	356.4	6.2
12	361.4	6.5
13	368.3	6.5
14	377.1	6.3
15	388.2	7.0
16	401.8	7.3
17	418.5	7.1
18	439.3	8.1
19	465.8	8.6

$$\frac{3.2 \times 10^{-12} \text{ Ci}}{1.0 \text{ kg water}} = \frac{3 \text{ atoms T}}{10^{18} \text{ atoms H}} \tag{6.2}$$

Use of tabulated mass production rates, Q_m, and concentration production, Q_c, may be used to determine the radioactive concentration on a mass basis, R_c:

$$R_c \left[\frac{\text{Ci}}{\text{kg}}\right] = Q_c \left[\frac{\text{Ci}}{\text{s}}\right] / Q_m \left[\frac{\text{kg}}{\text{s}}\right] \tag{6.3}$$

Eqn. 6.2 may be used to determine the mass fraction of tritium tracer in the produced water at a given point in time. These data transformations were performed on radioactivity production data for well OS-23 and the results are shown in Figure 6.11. The figure represents tracer concentration at the production well without the influences of a variable production rate included. These concentration values may be used to model tracer transport in the reservoir.

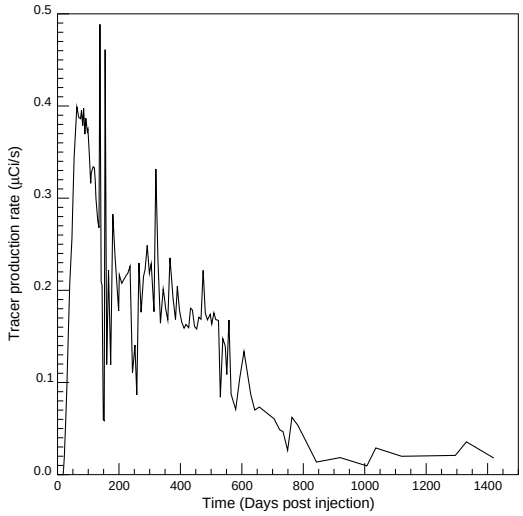

Figure 6.10: Tritium production from OS-23 (from UNOCAL [67])

A series of numerical runs were made to determine the propagation of tracer from the injection well, DX-8, to the production well, OS-23. Since it is known that permeability varies widely in the Geysers (see Table 6.1), a range of permeabilities were

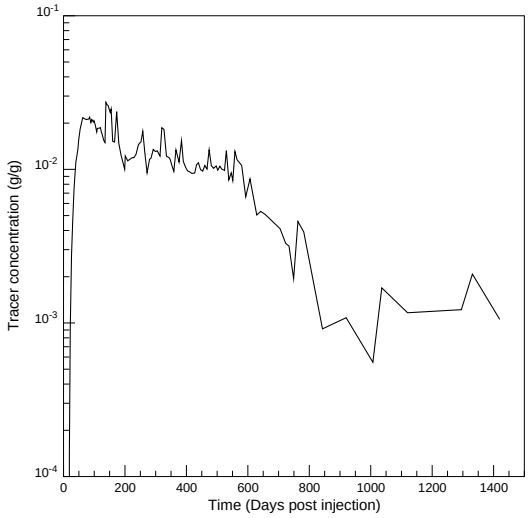

Figure 6.11: Mass concentration of produced tritium (from UNOCAL [67])

used in the generated stream tubes to determine if transmissibility effects can explain the long tail in tracer production response. Additionally, since variable permeability results in a variation in flow rates through the tubes, constant pressure boundary conditions were selected so tubes with high permeability would receive more injected fluid than tubes with lower permeability. Barker, et. al. [7] showed that reservoir pressure in the DX-8 area at initiation of the injection program ranged from about 2.0 MPa in the southwest section of the study area to just under 3.5 MPa in the northeast section. Based on this data, an average initial pressure of 2.75 MPa was assumed for the well pair studied. By 1981, at the completion of the tracer test, pressures ranged from 1.7 MPa in the southwest, to 3.1 MPa in the northeast. Injection pressure was assumed to be approximately the saturation pressure at 250 °C, 3.9 MPa, and the production pressure was assumed to remain constant at 1.0 MPa. Unfortunately, the injection rate was not closely monitored during the injection of tracer, so the injection concentration is unknown. The concentration was assumed, therefore to be 1.0 and breakthrough concentrations were then normalized to the initial breakthrough concentrations measured in the DX-8 study.

Based on the initial and boundary conditions described above and using the range of permeabilities shown in Table 6.1, a series of runs were made assuming the largest permeability in the center tube (tube 10) and decreasing permeability outward (toward tubes 1 and 19). Figure 6.12 shows the composite concentration of tritium at the production block for the stream tube model shown in Figure 6.9. Two sets of runs were made; one with adsorption effects and one without. Comparison of the two computed concentration curves shows that adsorption has very minor effects on tracer propagation. Figure 6.12 indicates that tracer velocity is slightly increased since very little adsorption of tracer occurs near the injector and very little pressure support from desorption occurs near the producer. Clearly, the delay in tracer transport shown in Figure 6.11 can be easily explained in terms of permeability an geometric variation.

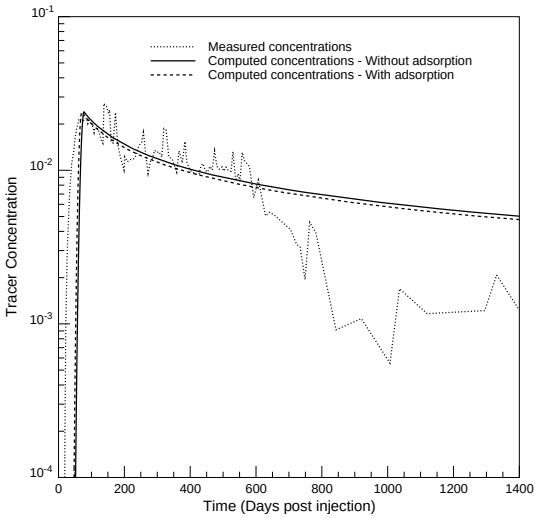

Figure 6.12: Mass concentration of producted tritium (stream tube model)

Based on the minor influences an adsorbed phase was shown to have on the propagation of tracer in Chapter 5, it is clear that the injected fluid delay can be affected much more strongly by permeability variations than by the presence of an adsorbed phase.

Chapter 7

Conclusions

Conclusions about the effects of an adsorbed phase in geothermal reservoirs in general and in the Geysers geothermal reservoir in particular are summarized below.

1. It has been shown that the density of adsorbed liquid residing in geothermal reservoirs may be significantly lower than the density of saturated liquid water at the same temperature. In pores filled with adsorbed liquid, density of the adsorbed liquid may be as small as 70 % of the density of saturated liquid. It has been shown that this pore filling adsorption phenomena almost certainly occurs in geothermal reservoirs.

2. Based upon pore size distributions in a geothermal reservoir, the saturations of capillary dominated and adsorption dominated liquid can be determined.

3. Using pore size distributions from the Geysers geothermal reservoir, it has been shown that, while adsorbed phase density may be significantly different from saturated liquid density, the volume occupied by adsorbed liquid is sufficiently small that no significant differences in liquid saturation estimates are caused.

4. Based on the pore size distribution and adsorption isotherm characterizing a porous medium, the density of the retained liquid phase may be determined as a function of pressure. This data may be used in modeling.

5. It was shown that the heat of vaporization in the Geysers geothermal reservoir can vary from the value at saturated conditions to about 1.5 times that value in very small pores.

6. Variations in heat of vaporization in the Geysers are shown to be largely due to the adsorption of liquid molecules and not due to surface stretching or liquid compression phenomena.

7. Due to low volumes represented by very small pores, it was concluded that at the Geysers, values of both the heat of vaporization of adsorbed liquid water and the internal energy may be assumed to be their values at saturated condition for modeling purposes with little loss of accuracy.

8. The assumption of instantaneous thermal equilibrium in a geothermal reservoir was shown to be valid in the presence of adsorption. For fracture-like pores of width up to 1 mm, thermal equilibrium is almost instantaneous.

9. The heat transfer rate between rock and injected liquid is shown to be affected slightly by the presence of an adsorbed phase. Heat transfer may be increased by 15 % by the presence of an adsorbed phase. Thus, with an adsorbed phase present, the validity of the thermal equilibrium assumption is enhanced.

10. By using a range of Langmuir isotherms, it was demonstrated that the nonlinear effects of an adsorbed phase on pressure depletion in a geothermal reservoir are due to the rate of change of mass stored and not on the value of the mass stored. Thus, pressure support is obtained when the slope of the controlling isotherm is large regardless of the mass adsorbed.

11. Real gas pseudopressure and the pseudotime may be used along with a similarity analysis to solve for adsorption pressure effects in a geothermal reservoir. The highly nonlinear partial differential equation describing such flow can be simplified to a nonlinear ordinary differential equation.

12. Initial pressure drawdown and the rate of pressure depletion have been shown to be significantly affected by the presence of an adsorbed phase. Time to initial

pressure drawdown may be delayed by an order of magnitude by an adsorbed phase.

13. By use of a measured adsorption isotherm from the Geysers, it has been shown that pressure depletion effects may be modeled closely using a Langmuir adsorption model.

14. The isothermal flow assumption used in deriving the analytical solution was shown to be valid for low porosity geothermal systems. A wide range of adsorbed masses and adsorption isotherm shapes were tested.

15. The effects of adsorption on tracer propagation were shown to be dependent on isotherm shape and initial conditions. A flat isotherm over the range of pressures experienced during injection of tracer results in very small influences on tracer propagation. Tracer transport may even be increased due to the presence of an adsorbed phase. At most, tracer delays due to adsorption were shown to be about 30 %.

16. Diffusion partitioning of tritated water tracer was shown to significantly delay the propagation of injected tracer. For a 3 % adsorbed phase saturation, tracer transport was shown to be 2 to 3 times slower than when no adsorbed phase was present.

17. Since the saturation curve for T_2O is nearly identical to that of ordinary water, it was concluded that preferential partitioning of tritium does not occur in vapor dominated reservoirs. Preferential partitioning refers to partitioning into either the vapor or liquid phases due to differences in boiling characteristics.

18. Estimates of recharge of the adsorbed phase during injection at the Geysers indicate that a large fraction of injected fluid becomes adsorbed liquid.

19. Permeability variations were shown to have much larger effects on tracer propagation than adsorption, diffusion partitioning of tracer, or preferential partitioning of tracer.

Nomenclature

English Variables

Variable	Description	Units
A	Nonlinear term	dimensionless
c	Compressibility	1/kPa
c	Langmuir shape factor	dimensionless
C	Heat capacity	kJ/kg $\cdot$ °C
d	Langmuir magnification factor	dimensionless
E	Internal energy	kJ/kg
h	Enthalpy	kJ/kg
k	Permeability	md
K	Thermal conductivity	kJ/s $\cdot$ m $\cdot$ °C
L	Characteristic length	m
n	Number of moles	dimensionless
p	Pressure	bar

English Variables (cont.)

Variable	Description	Units
q	Flow rate	kg/s or m^3/s
Q	Flow rate	kg/s or m^3/s
r	Radius	m
R	Universal gas constant	$kJ/kmol \cdot K$
S	Saturation	dimensionless
T	Temperature	°C
t	Time	s
u	Velocity	m/s
v	Specific volume	m^3/kg
V	Volume	m^3
X	Adsorbed mass	g_a/g_r
x	Distance	m
z	Real gas compressibility factor	dimensionless

Greek Variables

Variable	Description	Units
β	Partition weight factor	dimensionless
η	Similarity variable	dimensionless
μ	Viscosity	cp
ν	Iteration counter	dimensionless
ϕ	Porosity	dimensionless
ρ	Density	g/cc
σ	Surface tension	N/m

Subscripts

Subscript	Meaning
a	Adsorbate
d	Dimensionless
e	Energy
e	Effective
f	Final
g	Gas
i	Initial
l	Liquid
m	Matrix
n	Number of dimensions
o	Base value
p	Pressure or Constant pressure
prod	Amount produced
r	Rock
r	Relative
s	Saturated conditions
sc	Standard conditions
t	Total
v	Vapor
w	Water
∞	Infinity

Conversion Factors

Units		Conversion Multiplier		Units
g	×	2.205×10^{-3}	=	lb
g/cm^3	×	32.17	=	lb/ft^3
J	×	9.481×10^{-4}	=	Btu
m	×	3.281	=	ft
m^2	×	10^12	=	Darcy
m^3	×	35.31	=	Darcy
N	×	0.2248	=	lb
Pa	×	1.45×10^{-4}	=	psi
Pa	×	9.9931×10^{-6}	=	bar
Pa	×	9.869×10^{-6}	=	atm
Pa s	×	999.60	=	cp
W s	×	3.413	=	BTU/hr

Bibliography

[1] Adamson, A. W.: *Physical Chemistry of Surfaces*, fifth edition, John Wiley & Sons, Inc. (1990).

[2] Agarwal, R. G.: "Real Gas Pseudo-Time – A New Function for Pressure Buildup Analysis of MHF Gas Wells," paper SPE 8279 presented at the 1979 SPE Annual Meeting, Las Vegas, NV, Sept., 23-26.

[3] Al-Hussainy, R., Ramey, H. J., Jr., and Crawford, P. B.: "The Flow of Real Gases Through Porous Media," *J. Pet. Tech., Trans., AIME* (May 1966) No. 237, 637–642.

[4] Anbarci, K. and Ertekin, T.: "A Simplified Approach for In-Situ Characterization of Desorption Properties of Coal Seams," paper SPE 21808 presented at the 1991 Rocky Mountain Regional Meeting and Low-Permeability Reservoirs Symposium, Denver, April 15-17.

[5] Antunez, E. U.: *Semi-Analytic Approach to Analyze Single Well Tracer Tests*, PhD dissertation, Stanford University (1984).

[6] Aziz, K. and Settari, A.: *Petroleum Reservoir Simulation*, Applied Science (1979).

[7] Barker, B. J., Gulati, M. S., Bryan, M. A., and Riedel, K. L.: "Geysers Reservoir Performance," Geothermal Resources Council Transactions, Vol. 13 (1989) 349–367.

[8] Bhatia, S. K.: "Modeling the Pore Structure of Coal," *AIChE Journal* (1987) **33**, No. 10, 1707–1718.

[9] Blazek, C. F., Jasionowski, W. J., and Tiller, A. J.: "Charge/Discharge Characteristics of High-Capacity Methane Adsorption Storage Systems," Proceedings: 25th Intersociety Energy Conversion Engineering Conference – IECEC '90, IEEE, IEEE Service Center (Aug 1990) 306–314.

[10] Bojan, M. J., Vernov, A. V., and Steele, W. A.: "Simulation Studies of Adsorption in Rough-Walled Cylindrical Pores," *Langmuir* (1992) **8**, 901–908.

[11] Brigham, W. E.: "Reservoir Engineering Class Notes," Stanford Unversity (1989).

[12] Brigham, W. E. and Morrow, W. B.: "p/z Behavior for Geothermal Steam Reservoirs," *Society of Petroleum Engineers Journal* (Dec. 1977) 407–412.

[13] Calhoun, J. C., Jr. and Lewis, M., Jr.: "Experiments on the Capillary Properties of Porous Solids," *Trans. AIME* (1949) No. 2640, 931–937.

[14] Carlson, E. S. and Mercer, J. C.: "Devonian Shale Gas Production: Mechanisms and Simple Models," *Journal of Petroleum Technology* (April 1991) 476–482.

[15] Carslaw, H. S. and Jaeger, J. C.: *Conduction of Heat in Solids*, second edition, Clarendon Press, Oxford (1959).

[16] Correa, A. and Ramey, H. J., Jr.: "Quarterly Report, January - March 1993, Stanford Geothermal Program," Stanford Unversity (May 1993).

[17] Crank, J.: *The Mathematics of Diffusion*, Oxford, Clarendon Press (1964).

[18] Deem, R. L. and Farouq-Ali, S. M.: "Adsorption and Flow of Multiple Tracers in Porous Media," paper SPE CIM-9926 presented at the 1968 19th Annual Technical Meeting of Petroleum Society of CIM, Calgary, Canada, May 7-10.

[19] Defay, R. and Prigogine, I.: *Surface Tension and Adsorption*, second edition, J. W. Arrowsmith, Ltd. (1966).

[20] Doughty, C. and Pruess, K.: "A Similarity Solution for Two-Phase Water, Air, and Heat Flow Near a Linear Heat Source in a Porous Media," *Journal of Geophysical Research* (February 10 1992) **97**, No. B2, 1821–1838.

[21] Economides, M. J. and Miller, F. G.: "The Effects of Adsorption Phenomena in the Evaluation of Vapor Dominated Geothermal Reservoirs," *Geothermics* (1985) **14**, No. 1, 3–27.

[22] Enedy, S., Enedy, K., and Maney, J.: "Reservoir Response to Injection in the Southeast Geysers," *Monograph on the Geysers Geothermal Field*, C. Stone (ed.), Geothermal Resources Council (1992) 211–219.

[23] Evans, R., Marconi, U. M. B., and Tarazona, P.: "Capillary Condensation and Adsorption in Cylindrical and Slit-like Pores," *Journal of Chemical Society, Faraday Transactions II* (1986) **82**, 1763–1787.

[24] Fitzgerald, S. D. and Woods, S. D.: "The Injection of Water Into and Extraction of Vapour From a Geothermal Reservoir," Technical Report, Cambridge Unversity, England (July 1992).

[25] Fitzgerald, S. D. and Woods, S. D.: "Vapour Generation in Hot Permeable Rock Through Injection of Water," Proceedings: 17th Annual Workshop on Geothermal Reservoir Engineering, Stanford University (January 1992).

[26] Gallagher, J. and Haar, L.: *NIST Thermophysical Properties of Water (STEAM)*, National Institute of Standards and Technology (September 1988).

[27] Garg, S. K. and Pritchett, J.: "On Pressure-Work, Viscous Dissipation and the Energy Balance Relation for Geothermal Reservoirs," *Advances in Water Resources* (1977) **1**, No. 1, 41–47.

[28] Garg, S. K., Brownell, D. H., Jr., and Pritchett, J. W.: "Shock-Wave Propagation in Fluid-Saturated Porous Media," *Journal of Applied Physics* (1975) **46**, 702.

[29] Geankoplis, C.: *Mass Transfer Phenomena*, Holt, Rinehart and Winston, New York (1972).

[30] Greenkorn, R. A.: "Experimental Study of Waterflood Tracers," paper SPE 169 presented at the 1961 SPE Annual Meeting, Dallas, TX, Oct., 8-11.

[31] Gulati, M. S., Lipman, S. C., and Strobel, C. J.: "Tritium Tracer Survey at the Geysers," *Geothermal Resources Council, Transactions* (1978) **2**, 237–239.

[32] Gunderson, R. P.: "Porosity of Reservoir Graywacke at the Geysers," *Monograph on the Geysers Geothermal Field*, C. Stone (ed.), Geothermal Resources Council (1992) 89–93.

[33] Hawkins, J. M., Schraufnagel, R. A., and Olszewski, A. J.: "Estimating Coalbed Gas Content and Sorption Isotherm Using Well Log Data," paper SPE 24905 presented at the 1992 SPE Annual Technical Conference and Exhibition, Washington, Oct. 4-7.

[34] Herkelrath, W. N., Moench, A. F., and O'Neal, C. F.: "Laboratory Investigations of Steam Flow in a Porous Medium," *Water Resources Research* (1983) **19**, No. 4, 931–937.

[35] Hsieh, C. H. and Ramey, H. J., Jr.: "An Inspection of Experimental Data on Vapor Pressure Lowering in Porous Media," *Geothermal Resources Council, Transactions* (1978) **2**, 295–296.

[36] Hsieh, C. H and Ramey, H. J., Jr.: "Vapor-Pressure Lowering in Geothermal Systems," paper SPE 9926 presented at the 1981 SPE Annual Technical Conference and Exhibition, Bakersfield, Nov., 15.

[37] King, T.: *Pore Size Distribution Analysis*, Micromeritics Instrument Corporation (April 1993).

[38] Koenig, J. B.: "History and Development at The Geysers Geothermal Field," *Monograph on the Geysers Geothermal Field*, C. Stone (ed.), Geothermal Resources Council (1992) 7–18.

[39] Lane, H. S., Lancaster, D. E., and Watson, A. T.: "Characterizing the Role of Desorption in Gas Production from Devonian Shales," *Energy Sources* (1991) **13**, 337–359.

[40] Leap, D. I.: "Apparent Relative Retardation of Tritium and Bromide in Dolomite," *Ground Water* (1992) **30**, No. 4, 549–558.

[41] Leverett, M. C.: "Capillary Behavior in Porous Solids," *Petroleum Technology* (August 1940) No. 1223, 152–169.

[42] Lin, Y. and Ma, Y. H.: "A Comparative Chromatographic Study of Liquid Adsorption and Diffusion in Microporous and Macroporous Adsorbents," *Ind. Eng. Chem. Res.* (1989) **28**, 622–630.

[43] Matranga, K. R., Myers, A. L., and Glandt, E. D.: "Storage of Natural Gas by Adsorption on Activated Carbon," *Chemical Engineering Science* (1992) **47**, No. 7, 1569–1579.

[44] Matranga, K. R., Stella, A., Myers, A. L., and Glandt, E. D.: "Molecular Simulation of Adsorbed Natural Gas," *Separation Science and Technology* (1992) **27**, No. 14, 1825–1836.

[45] Matsunaga, N.: "Saturation Vapor Pressure and Critical Constants of H_20, D_20, and T_20," *International Journal of Thermophysics* (Nov. 1987) **8**, No. 6, 681–694.

[46] Matsunaga, N. and Nagashima, A.: "Estimation of the Thermodynamic Properties of Dense Gaseous D_2O and T_2O by a Modified Corresponding States Principle," *Ind. Eng. Chem. Res.* (June 1988) **27**, No. 6, 998–1003.

[47] McElhiney, J. E., Koenig, R. A., and Schraufnagel, R. A.: "Evaluation of Coalbed-Methane Reserves Involves Different Techniques," *Oil & Gas Journal* (Oct., 30 1989) **87**, No. 44, 63–72.

[48] McLarty, L. and Reed, M. J.: "The U.S. Geothermal Industry: Three Decades of Growth," *Energy Sources* (1992) **14**, No. 4, 443–455.

[49] Moench, A. F. and Atkinson, P. G.: "Transient-Pressure Analysis in Geothermal Steam Reservoirs with an Immobile Vaporizing Liquid Phase," *Geothermics* (1978) **7**, 253–264.

[50] Morrow, N. R., Cather, M. E., Buckley, J. S., and Dandge, V.: "Effects of Drying on Absolute and Relative Permeabilities of Low-Permeability Gas Sands," paper SPE 21880 presented at the 1991 Rocky Mountain Regional Meeting and Low-Permeability Reservoirs Symposium, Denver, April 15-17.

[51] Navruzov, Y. V.: "Heat Transfer to Liquids Boiling in Porous Structures," *Heat Transfer – Soviet Research* (1986) **18**, No. 2, 123–128.

[52] Nghiem, C. P. and Ramey, H. J., Jr.: "One-Dimensional Steam Flow in Porous Media under Desorption," Proceedings: 16th Annual Workshop on Geothermal Reservoir Engineering, Stanford University (Jan. 1991).

[53] Nguyen, V. U.: "A Fortran Program for Modeling Methane Gas Desorption from Coal," *Computers and Geosciences* (1989) **15**, No. 5, 695–707.

[54] Pogorelov, A. G. and Churmayev, O. M.: "Unsteady-State Models of Sorption Processes, as Exemplified by the Desulfurization of Natural Gas," *Fluid Mechanics – Soviet Research* (1990) **19**, No. 2, 54–62.

[55] Pruess, K.: "Heat Transfer in Fractured Geothermal Reservoirs with Boiling," *Water Resources Research* (1983) **19**, No. 1, 201–208.

[56] Pruess, K., Calore, C., Celati, R., and Wu, Y. S.: "An Analytical Solution for Heat Transfer at a Boiling Front Moving Through a Porous Medium," *Int. Journal of Heat Mass Transfer* (1987) **30**, No. 12, 2595–2602.

[57] Pruess, K. and Narasimhan, T. N.: "On Fluid Reserves and the Production of Superheated Steam From Fractured, Vapor-Dominated Geothermal Reservoirs," *Journal of Geophysical Research* (Nov. 1982) **87**, No. B11, 9329–9339.

[58] Pruess, K. and O'Sullivan, M.: "Effects of Capillarity and Vapor Adsorption in the Depletion of Vapor-Dominated Geothermal Reservoirs," Proceedings: 17th

Annual Workshop on Geothermal Reservoir Engineering, Stanford University (January 1992).

[59] Ramey, H. J., Jr.: "Adsorption in Vapor-Dominated Systems," Proceedings: Department of Energy Geothermal Program Review VIII (April 1990).

[60] Ramsay, J. D. and Booth, B. O.: "Determination of Structure in Oxide Sols and Gels from Neutron Scattering and Nitrogen Adsorption Measurements," *Journal of Chemical Society, Faraday Transactions I* (1983) **79**, 681–694.

[61] Ramsay, J. D. and Wing, G.: "Small Angle Neutron Scattering Investigations of Water Sorption in Porous Silica and Ceria Gels," *Journal of Colloid and Interface Science* (Feb. 1991) **141**, No. 2, 475–485.

[62] Reddy, A. K. N. and Goldemberg, J.: "Energy for the Developing World," *Energy for Planet Earth: Readings from Scientific American Magazine*, J. Piel (ed.), W. H. Freeman and Company, New York (1991) 59–72.

[63] Schettler, P., Parmely, C. R., and Lee, W. J.: "Gas Storage and Transport in Devonian Shales," *SPE Formation Evaluation* (Sept. 1989) **4**, No. 3, 371–376.

[64] Shang, S. and Horne, R. N.: "Quarterly Report, January - March 1993, Stanford Geothermal Program," Stanford Unversity (May 1993).

[65] Shang, S., Horne, R. N., and Ramey, H. J., Jr.: "Experimental Study of Water Vapor Adsorption on Geothermal Reservoir Rocks," Stanford Geothermal Program Technical Report, Stanford Unversity (December 1993).

[66] Udell, K. S.: "The Thermodynamics of Evaporation and Condensation in Porous Media," paper SPE 10779 presented at the 1982 California Regional Meeting of SPE, San Francisco, March, 24-26.

[67] UNOCAL: "DX-8 Tritium Study," DOE report (January 1991).

[68] UNOCAL: "Unocal Position Report on Injection," Draft report (1992).

[69] Walters, M. and Combs, J.: "Heat Flow in the Geysers-Clear Lake Geothermal Area of Northern California, U.S.A.," *Monograph on the Geysers Geothermal Field*, C. Stone (ed.), Geothermal Resources Council (1992) 43–53.

[70] *Geothermal Energy*, D. E. White (ed.), Stanford University Press (1973) Ch. 4, 69–94.

[71] Whiting, R. L. and Ramey, H. J., Jr.: "Application of Material and Energy Balances to Geothermal Steam Production," paper SPE 1949 presented at the 1967 SPE Annual Meeting, Houston, Oct. 1-4.

[72] Williamson, K. H.: "Reservoir Simulation of the Geysers Geothermal Field," Proceedings: 15th Annual Workshop on Geothermal Reservoir Engineering, Stanford University (Jan. 1990).

[73] Woods, A. W. and Fitzgerald, S. D.: "The Generation of Vapour in a Hot Rock through Injection of Cold Water," Technical Report, Cambridge Unversity, England (April 1992).

Appendix A

Computational Data

Numerical computations in this research used gas compressibility factors computed by the National Institute of Standards and Technology [26]. Figure A.1 shows gas compressibility factors for steam for a range of pressures and temperatures.

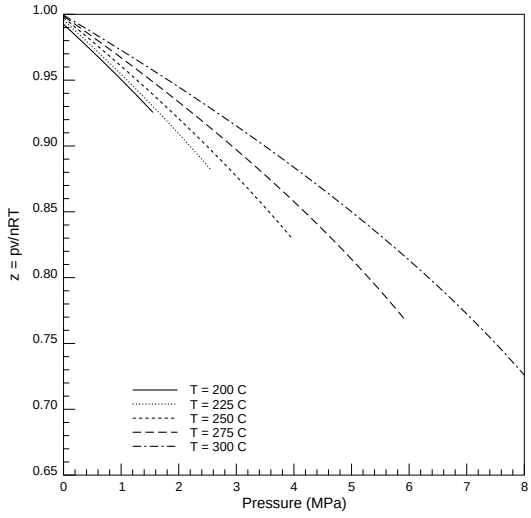

Figure A.1: Gas law deviation factors for steam.

Tracer production data used in Chapter 6 were provided by UNOCAL [67]. Table A.1 shows the mass production rate and measured radioactivity of produced water for well OS-23.

Table A.1: Well OS-23 Tracer Production Data

Day of Sample	Counts/min-6ml	Flowrate (lbs/hr)
0.	0.0	155700.
18.	0.0	155700.
19.	0.5	155700.
22.	3.4	154600.
26.	9.9	152100.
30.	16.9	153000.
34.	26.2	152100.
36.	30.6	152100.
40.	39.9	150000.
47.	49.1	149600.
49.	55.3	147000.
54.	65.8	149500.
62.	77.5	145500.
63.	78.3	145800.
69.	76.8	144400.
75.	76.0	145400.
78.	76.4	148000.
82.	76.7	141300.
85.	78.8	144300.
89.	72.7	145400.
92.	76.1	145400.
97.	73.3	145400.
99.	74.8	143350.
103.	70.5	142150.
108.	63.2	143100.
110.	66.6	140800.
116.	66.8	143100.
120.	67.4	141300.
123.	63.1	144000.

Day of Sample	Counts/min-6ml	Flowrate (lbs/hr)
125.	61.6	139400.
131.	55.6	141750.
135.	53.9	142200.
138.	98.3	142200.
142.	94.8	63100.
145.	94.1	62500.
149.	88.4	19300.
152.	84.7	19800.
155.	89.2	147900.
160.	54.9	62300.
166.	54.3	116800.
173.	85.6	39800.
180.	53.2	152000.
187.	44.8	152000.
199.	36.1	140700.
201.	44.1	140700.
209.	41.0	144900.
224.	43.0	144000.
229.	42.9	145800.
236.	45.2	143100.
244.	52.3	60400.
252.	54.4	73900.
258.	63.7	38900.
265.	45.5	144400.
272.	34.3	147000.
280.	41.9	146934.
285.	42.7	149131.

Day of Sample	Counts/min-6ml	Flowrate (lbs/hr)
292.	48.6	146418.
299.	47.1	132655.
305.	47.6	137570.
314.	44.0	115000.
320.	67.3	141000.
327.	65.6	101000.
335.	43.9	107100.
344.	42.9	134300.
348.	41.4	132700.
352.	38.6	133400.
359.	35.0	137100.
366.	48.2	139600.
376.	40.2	136200.
384.	55.5	86800.
390.	40.5	144300.
397.	37.3	136700.
404.	35.2	134700.
412.	34.6	131400.
418.	33.9	137500.
427.	34.1	133800.
433.	38.6	133800.
439.	39.8	128400.
446.	35.9	128100.
453.	35.1	128800.
460.	38.2	127900.
467.	36.2	133300.
474.	48.3	131300.

Day of Sample	Counts/min-6ml	Flowrate (lbs/hr)
481.	38.2	131300.
488.	36.6	131300.
497.	37.9	131300.
502.	35.6	131300.
509.	37.8	132900.
515.	36.2	133000.
524.	35.5	134800.
530.	47.7	50400.
538.	30.8	137100.
546.	34.2	116700.
551.	30.5	101900.
558.	47.1	101900.
565.	41.6	60000.
580.	38.2	53000.
593.	23.9	125000.
607.	31.2	122500.
629.	18.2	136800.
642.	19.2	104400.
657.	18.3	114668.
705.	14.8	117126.
723.	11.9	117126.
734.	11.4	117126.
749.	7.0	107700.
763.	16.5	107700.
782.	14.1	109040.
843.	3.3	118220.
920.	3.9	135690.

Day of Sample	Counts/min-6ml	Flowrate (lbs/hr)
1007.	2.0	135690.
1036.	6.1	135690.
1120.	4.2	135690.
1295.	4.4	135690.
1331.	7.5	135690.
1420.	3.8	135690.

Appendix B

Computer Programs

The following program was used for numerical computations in the semi-analytical model (Chapter 4).

```
************************************************************************
*  SOLVES NONLINEAR ODE.                                               *
*                                                                      *
*  JOHN W. HORNBROOK                                                   *
*  STANFORD UNIVERSITY                                                 *
************************************************************************
*
      Parameter (NX = 10000)
      Implicit Real*8 (A-H,O-Z)
      Real*8 F(NX), X(NX), DXDF(NX), ALPHA(NX), BETA(NX), GAMMA(NX),
     *    RHS(NX), A(NX), FNEW(NX), ETA(NX), FOLD(NX), DPDRO(NX),
     *    PRESS(NX), FTAB(NX), PRESSURE(NX), ROV(NX), ROPRESS(NX),
     *    DENSV(NX), ZPRESS(NX), ZTAB(NX)
      Open (Unit=7,File='INPUT',Status='OLD')
      Open (Unit=8,File='output',Status='UNKNOWN')
      Open (Unit=9,File='fetatable',Status='OLD')
      Open (Unit=10,File='rotable',Status='OLD')
      Open (Unit=11,File='ztable',Status='OLD')
*
```

```
************************************************************************
* NOMENCLATURE                                                         *
************************************************************************
*     C          LANGMUIR SHAPE FACTOR                                 *
*     D          LANGMUIR MAGNITUDE FACTOR                             *
*     H          GRID SIZE                                             *
*     PHI        POROSITY                                              *
*     PI         INITIAL PRESSURE (MPa)                                *
*     PTS        NUMBER OF COMPUTATION POINTS                          *
*     PW         WELL PRESSURE (MPa)                                   *
*     RHOW       WATER DENSITY                                         *
*     RHOR       ROCK DENSITY                                          *
*     RHOA       ADSORBED PHASE DENSITY                                *
*     AMOL       MOLECULAR WEIGHT OF WATER                             *
*     RGAS       REAL GAS CONSTANT                                     *
*     TEMP       TEMPERATURE                                           *
*     fetatable  EXTERNAL FILE OF SIMILARITY FUNCTION VS. PRESSURE     *
*     rotable    EXTERNAL FILE OF DENSITY VS. PRESSURE                 *
*     ztable     EXTERNAL FILE OF Z-FACTOR VS. PRESSURE                *
*     output     OUTPUT FILE                                           *
************************************************************************
* READ IN DATA                                                         *
************************************************************************
      Read (7,5000) PHI, RHOW, RHOR, AMOL, RGAS, TEMP, C, D, PTS, H
************************************************************************
      PI = 8.5837
      PW = 0.101
      AMOLTERM = (AMOL/(RGAS*TEMP)) * 1.0E3
      NPT = INT(PTS)
************************************************************************
*  READ IN TABLE OF P VS. F                                            *
************************************************************************
*
```

```
      NTAB = 0
      Do 10 I = 1, 5000
        Read (9,5100,End=20) PRESS(I), FTAB(I)
        NTAB = NTAB + 1
   10 Continue
*
   20 NTRO = 0
      Do 30 I = 1, 5000
        Read (10,5200,End=40) ROPRESS(I), ROV(I)
        NTRO = NTRO + 1
   30 Continue
*
   40 NZ = 0
      Do 50 I = 1, 5000
        Read (11,5100,End=60) ZPRESS(I), ZTAB(I)
        NZ = NZ + 1
   50 Continue
*************************************************************************
*  INITIALIZE VALUES OF F                                               *
*************************************************************************
   60 AMBAR0 = 1.09598472E-4
      F0 = 1.0
      FN = 1.0 / AMBAR0
      Do 70 I = 1, NPT
        F(I) = 1.0
   70 Continue
*************************************************************************
*  GENERATE MATRIX ENTRIES                                              *
*************************************************************************
   80 Do 90 I = 1, NPT
        ETA(I) = I * H
        Call TABBIN(FTAB,PRESS,NTAB,F(I),PRESSURE(I))
        Call TABBIN(ROPRESS,ROV,NTRO,PRESSURE(I),DENSV(I))
```

```
        Call TABBIN(ZPRESS,ZTAB,NZ,PRESSURE(I),Z)
        PP = PRESSURE(I) + 1.0E-6
        PM = PRESSURE(I) - 1.0E-6
        Call TABBIN(ZPRESS,ZTAB,NZ,PP,ZP)
        Call TABBIN(ZPRESS,ZTAB,NZ,PM,ZM)
        DZDP = (ZP-ZM) / 2.0E-6
        PREL = PRESSURE(I) / PI
*
        If (PREL.GT.0.83) Then
          RHOA = RHOW
        Else If (PREL.LT.0.10) Then
          RHOA = 0.7 * RHOW
        Else If (PREL.LT.0.83.AND.PREL.GT.0.1) Then
          RHOA = (PREL-0.1) * 292.771 + 498.686
        End If
*
        X(I) = D * (C*PREL) / (1.+(C-1.)*PREL)
        DXDF(I) = D * C * PI / ((-PRESSURE(I)+C*PRESSURE(I)+PI)**2.0)
        DPDRO(I) = 1. / (AMOLTERM/Z-(AMOLTERM/(Z*Z))*DZDP*PRESSURE(I))
        A1 = ((1.-PHI)/PHI) * (RHOR/RHOA)
        B = (((1.-PHI)/PHI)*(RHOR/RHOA)) * (RHOA-DENSV(I))
        A(I) = (1.-A1*X(I)+(B*DPDRO(I)*DXDF(I)))
        ALPHA(I) = (1./(H*H)) + (ETA(I)*A(I)/(H))
        BETA(I) = -(2./(H*H))
        GAMMA(I) = (1./(H*H)) - ((ETA(I)*A(I))/(H))
        RHS(I) = 0.00
        If (I.EQ.1) Then
          RHS(1) = RHS(1) - GAMMA(1) * F0
          GAMMA(1) = 0.0
        Else If (I.EQ.NPT) Then
          RHS(NPT-1) = RHS(NPT-1) - ALPHA(NPT-1) * FN
          ALPHA(NPT) = 0.0
          ALPHA(NPT-1) = 0.0
```

```
        End If
   90 Continue
*************************************************************************
*  SOLVE MATRIX PROBLEM                                                 *
*************************************************************************
      NPTM = NPT - 1
      Call THOMAS(BETA,ALPHA,GAMMA,RHS,FNEW,NPTM)
*************************************************************************
*  CHECK FOR CONVERGENCE                                                *
*************************************************************************
      DIFMAX = ABS(FNEW(1)-F(1))
      Do 100 I = 1, NPT
        If (FNEW(I).LT.0.0) Then
          FNEW(I) = 0.00000
        End If
        DIF = ABS(FNEW(I)-F(I))
        If (DIF.GT.DIFMAX) Then
          ID = I
          DIFMAX = DIF
        End If
  100 Continue
      DIFTOL = 0.001
      If (DIFMAX.GT.DIFTOL) Then
        Do 110 I = 1, NPT
          If (FNEW(I).LT.0.0) Then
            F(I) = 0.000000
          Else
            F(I) = FNEW(I)
          End If
  110   Continue
        Go To 80
      Else
        Go To 120
```

```
      End If
*************************************************************************
*  WRITE RESULTS                                                        *
*************************************************************************
  120 Do 130 I = 1, NPT
        FOLD(I) = FNEW(I)
  130 Continue
      Do 140 I = 1, NPT
        Write (8,5300) ETA(I), FNEW(I)
  140 Continue
      Stop
 5000 Format (///5F10.2///5F10.2///F10.2)
 5100 Format (E18.4,E18.4)
 5200 Format (T12,E13.4,E12.4)
 5300 Format (E15.8,5X,E10.4)
      End
```

The following program was used for the simulation of vapor flow in the presence of a sorbing phase (Chapter 5).

```
*************************************************************************
*  SIMULATES THE FLOW OF VAPOR IN A LINEAR SYSTEM                       *
*  WITH CONSTANT PRESSURE INNER BOUNDARY AND NO                         *
*  FLOW OUTER BOUNDARY.  THERMAL EFFECTS ARE INCLUDED.                  *
*                                                                       *
*  JOHN W. HORNBROOK                                                    *
*  STANFORD UNIVERSITY                                                  *
*************************************************************************
*
      Parameter (NX = 300)
      Implicit Real*8 (A-H,O-Z)
      Real*8 PV(NX), PVO(NX), RHOV(0:NX), VOL(NX), RHOVAV(NX),
     *    VISCV(NX), VISCVAV(NX), RKRV(NX), AVP(NX), BVP(NX), CVP(NX),
     *    PSAT(NX), ENINTAN(NX), UV(NX), ENT(NX,NX), B(NX,NX),
```

```
     *    C(NX,NX), RHOVN(NX), AREA(NX), DTVPDPVIP(NX), PSATN(NX),
     *    DPV(NX), QV(NX), RKRVUP(NX), PVN(NX), VISCVN(NX), RKRVN(NX),
     *    UVN(NX), DRHOVDPI(NX), DTVPDPVI(NX), DTVMDPVI(NX),
     *    DTVMDPVIM(NX), DACCNDP(NX), TV(NX), DRODP(NX), DSINKDPI(NX),
     *    DACCDP(NX), DFLOWDPI(NX), FLOWV(NX), SA(NX), SAN(NX),
     *    XOLD(NX), XNEW(NX), RHS(NX), RHSACC(NX), SV(NX), SVN(NX),
     *    DTVDP(NX), DADSDP(NX), RHOA(NX), RHOAN(NX), ENINTV(0:NX),
     *    TVTEMP(NX), RHSADS(NX), ENINTVN(NX), COND(0:NX), VW(0:NX),
     *    VV(0:NX), AV(NX), BV(NX), DQDP(NX), DKROMUDP(NX),
     *    PRESSURE(NX), CV(NX), ENTH(NX), DENSV(NX), VVISC(NX),
     *    ENTHV(NX), ENTHVN(NX), DXDP(NX), DSRODP(NX), TEMPV(NX),
     *    TEMPVN(NX), ENINTA(NX),
      Common /UNITS/ IT, ID, IP, IH, FT, FD, FP, FH, /UNITC/ NT, ND, NP,
     *    NH
      Common /PARAMS/ TS, DS, PS, Z0, ASS, SSS, RSS, ALPHA(4), BETA(4)
      Common /PROPS/ P, AD, GD, HD, UD, SD, CVD, CPD, DPDD, DPDT, DVDT,
     *    W, CJTT, CJTH
      Common /ACONST/ WM, GASCON, TZ, AA, Z, DZ, Y
      Open (Unit=7,File='INPUTADS',Status='OLD')
*
      Open (Unit=8,File='press.out',Status='UNKNOWN')
      Open (Unit=9,File='temp.out',Status='UNKNOWN')
      Open (Unit=10,File='sat.out',Status='UNKNOWN')
************************************************************************
* NOMENCLATURE                                                         *
************************************************************************
* A               SPECIFIES ADSORBED PHASE                             *
* AREA            BLOCK AREA                                           *
* COND            THERMAL CONDUCTIVITY                                 *
* DP              DELTA PRESSURE                                       *
* DT              TIME STEP SIZE                                       *
* DX              BLOCK THICKNESS                                      *
* ENINT           INTERNAL ENERGY                                      *
```

```
* ENTH            ENTHALPY                                              *
* N               DENOTES NEW TIME ITERATION VALUE                      *
* O               DENOTES OLD TIME ITERATION VALUE                      *
* P               PRESSURE                                              *
* PSAT            SATURATION PRESSURE                                   *
* Q               MASS FLUX                                             *
* RHO             DENSITY                                               *
* RKR             RELATIVE PERMEABILITY                                 *
* T               TRANSMISSIBILITY                                      *
* TEMP            TEMPERATURE                                           *
* U               VELOCITY                                              *
* V               SPECIFIES VAPOR PHASE                                 *
* VISC            VISCOSITY                                             *
* VOL             BLOCK VOLUME                                          *
* press.out       PRESSURE OUTPUT FILE                                  *
* temp.out        TEMPERATURE OUTPUT FILE                               *
* sat.out         SATURATION OUTPUT FILE                                *
************************************************************************
* READ IN DATA                                                          *
************************************************************************
      Read (7,5000) TMAX, DTMIN, RKRVMAX, SVP, IBCFLG, ALEN, HEIGHT,
     *    WID, DT, BLK, PERM, CR, PHI, VQ, TEMP, SVI, PVI, AVWO, AVW1,
     *    AVW2, AVW3, IOPT, IT, ID, IP, IH, DERIVDP, ITMAX, ALANG,
     *    BLANG, RHOR, ISOCHK, PWF, NB1, NB2, NB3, T1, T2, T3, XB,
     *    XSLOPE
************************************************************************
* INITIALIZE BLOCK VALUES                                               *
************************************************************************
      NBLK = INT(BLK)
      NBLKP = NBLK + 1
      DX = ALEN / BLK
*
      Do 10 I = 1, NBLK
```

```
        SV(I) = SVI
        PV(I) = PVI
        PVO(I) = PV(I)
        PVN(I) = PV(I)
        TEMPV(I) = TEMP
        TEMPVN(I) = TEMP
   10 Continue
*
      If (IBCFLG.EQ.1) Then
        PV(NBLK) = PWF
        PVN(NBLK) = PWF
      End If
*
*************************************************************************
* START OUTER LOOP                                                      *
*************************************************************************
      TIME = 0.0
   20 TIME = TIME + DT
      ITKOUNT = 0
   30 ITKOUNT = ITKOUNT + 1
*************************************************************************
* CALCULATE SATURATION PRESSURES IN EACH BLOCK                          *
*************************************************************************
      Do 40 I = 1, NBLK
   40 Continue
*************************************************************************
* CALCULATE ROCK AND FLUID PROPERTIES FOR EACH BLOCK                    *
*************************************************************************
      Do 50 I = 1, NBLK
        VOL(I) = DX * WID * HEIGHT
        AREA(I) = HEIGHT * WID
*  CALCULATE ADSORBATE PROPERTIES
*
```

```
        If (XSLOPE.GT.0.0) Then
          PDM = 0.0
          IDM = 7
          Call NIST(TEMPV(I),PDM,IDM,RHOA(I),PSAT(I),V,ENINTA(I),C)
          Call NIST(TEMPVN(I),PDM,IDM,RHOAN(I),PSATN(I),V,ENINTAN(I),C)
        End If
*
*  OLD TIME STEP PROPERTIES
*
        Call NIST(TEMPV(I),PV(I),IOPT,RHOV(I),ENINTV(I),VISCV(I),
     *      ENTHV(I),CVO)
        If (XSLOPE.GT.0.0) Then
          XOLD(I) = XSLOPE * (PV(I)/PSAT(I)) + XB
          SA(I) = ((1.-PHI)/PHI) * (RHOR/RHOA(I)) * XOLD(I)
        Else
          XOLD(I) = 0.0
          SA(I) = 0.0
        End If
        SV(I) = SVI - SA(I)
        RKRV(I) = 1.0
*
*  NEW TIME STEP PROPERTIES
*
        Call NIST(TEMPVN(I),PVN(I),IOPT,RHOVN(I),ENINTVN(I),VISCVN(I),
     *      ENTHVN(I),CVO)
        If (XSLOPE.GT.0.0) Then
          XNEW(I) = XSLOPE * (PVN(I)/PSATN(I)) + XB
          SAN(I) = ((1.-PHI)/PHI) * (RHOR/RHOAN(I)) * XNEW(I)
        Else
          XNEW(I) = 0.0
          SAN(I) = 0.0
        End If
        SVN(I) = SVI - SAN(I)
```

```
        RKRVN(I) = 1.0
   50 Continue
*************************************************************************
* CALCULATE AVERAGE DENSITY AND VISCOSITY AT BLOCK CONNECTION           *
*************************************************************************
      RHOVAV(1) = 0.0
      RHOVAV(NBLKP) = 0.0
      VISCVAV(1) = 0.0
      VISCVAV(NBLKP) = 0.0
      Do 60 I = 2, NBLK
        PVNAVG = (PVN(I-1)+PVN(I)) / 2.0
        Call NIST(TEMPVN(I),PVNAVG,IOPT,RHOVAV(I),EN,VISCVAV(I),ENT,CV)
   60 Continue
*************************************************************************
* CALCULATE TRANSMISSIBILITIES BETWEEN BLOCKS                           *
*************************************************************************
      TV(1) = 0.0
      TV(NBLKP) = 0.0
      Do 70 I = 2, NBLK
        RKRVUP(I) = 1.0
        TV(I) = (PERM*RKRVUP(I)*RHOVAV(I)) / (DX*VISCVAV(I))
        If (I.EQ.NBLK) Then
          TV(NBLK) = (PERM*RKRVUP(NBLK-1)*RHOVN(NBLK-1)) / (DX*
     *        VISCVN(NBLK-1))
        End If
   70 Continue
*************************************************************************
* CALCULATE DERIVATIVES IN TV(I+) WITH RESPECT TO PV(I)                 *
*************************************************************************
      DTVPDPVI(1) = 0.0
      DTVPDPVI(NBLKP) = 0.0
      Do 80 I = 2, NBLK
        IM = I - 1
```

```
        FRONT = PERM * RKRVUP(I) / DX
        PVIP = PVN(IM) + DERIVDP
        PVIM = PVN(IM) - DERIVDP
        Call NIST(TEMPVN(I),PVIM,IOPT,RHOVM,EN,VISCVM,ENT,CV)
        Call NIST(TEMPVN(I),PVIP,IOPT,RHOVP,EN,VISCVP,ENT,CV)
        TVP = FRONT * (RHOVN(I)+RHOVP) / (VISCVN(I)+VISCVP)
        TVM = FRONT * (RHOVN(I)+RHOVM) / (VISCVN(I)+VISCVM)
        DTV = TVP - TVM
        DPP = 2.0E6 * DERIVDP
        DTVPDPVI(I) = DTV / DPP
   80 Continue
*************************************************************************
* CALCULATE DERIVATIVES IN TV(I+) WITH RESPECT TO PV(I+1)               *
*************************************************************************
      DTVPDPVIP(1) = 0.0
      DTVPDPVIP(NBLKP) = 0.0
      Do 90 I = 2, NBLK
        IM = I - 1
        FRONT = PERM * RKRVUP(I) / DX
        PVIP = PVN(I) + DERIVDP
        PVIM = PVN(I) - DERIVDP
        Call NIST(TEMPVN(I),PVIM,IOPT,RHOVM,EN,VISCVM,ENT,CV)
        Call NIST(TEMPVN(I),PVIP,IOPT,RHOVP,EN,VISCVP,ENT,CV)
        TVP = FRONT * (RHOVP+RHOVN(IM)) / (VISCVP+VISCVN(IM))
        TVM = FRONT * (RHOVM+RHOVN(IM)) / (VISCVM+VISCVN(IM))
        DTV = TVP - TVM
        DPP = 2.0E6 * DERIVDP
        DTVPDPVIP(I) = DTV / DPP
   90 Continue
*************************************************************************
* CALCULATE DERIVATIVES IN TV(I-) WITH RESPECT TO PV(I)                 *
*************************************************************************
      DTVMDPVI(1) = 0.0
```

```
      DTVMDPVI(NBLKP) = 0.0
      Do 100 I = 2, NBLK
        IM = I - 1
        FRONT = PERM * RKRVUP(I) / DX
        PVIP = PVN(I) + DERIVDP
        PVIM = PVN(I) - DERIVDP
        Call NIST(TEMPVN(I),PVIM,IOPT,RHOVM,EN,VISCVM,ENT,CV)
        Call NIST(TEMPVN(I),PVIP,IOPT,RHOVP,EN,VISCVP,ENT,CV)
        TVP = FRONT * (RHOVN(IM)+RHOVP) / (VISCVN(IM)+VISCVP)
        TVM = FRONT * (RHOVN(IM)+RHOVM) / (VISCVN(IM)+VISCVM)
        DTV = TVP - TVM
        DPP = 2.0E6 * DERIVDP
        DTVMDPVI(I) = DTV / DPP
  100 Continue
*************************************************************************
* CALCULATE DERIVATIVES IN TV(I-) WITH RESPECT TO PV(I-1)               *
*************************************************************************
      DTVMDPVIM(1) = 0.0
      DTVMDPVIM(NBLKP) = 0.0
      Do 110 I = 2, NBLK
        IM = I - 1
        FRONT = PERM * RKRVUP(I) / DX
        PVIP = PVN(IM) + DERIVDP
        PVIM = PVN(IM) - DERIVDP
        Call NIST(TEMPVN(I),PVIM,IOPT,RHOVM,EN,VISCVM,ENT,CV)
        Call NIST(TEMPVN(I),PVIP,IOPT,RHOVP,EN,VISCVP,ENT,CV)
        TVP = FRONT * (RHOVP+RHOVN(I)) / (VISCVP+VISCVN(I))
        TVM = FRONT * (RHOVM+RHOVN(I)) / (VISCVM+VISCVN(I))
        DTV = TVP - TVM
        DPP = 2.0E6 * DERIVDP
        DTVMDPVIM(I) = DTV / DPP
  110 Continue
*************************************************************************
```

```
* CALCULATE DERIVATIVES OF DENSITY AND X IN BLOCK I W.R.T. PV(I)           *
*****************************************************************************
      Do 120 I = 1, NBLK
        PVP = PVN(I) + DERIVDP
        PVM = PVN(I) - DERIVDP
        Call NIST(TEMPVN(I),PVM,IOPT,RHOVNM,EN,VISCVM,ENT,CV)
        Call NIST(TEMPVN(I),PVP,IOPT,RHOVNP,EN,VISCVP,ENT,CV)
        DRO = RHOVNP - RHOVNM
        DPP = 2.0E6 * DERIVDP
        DRODP(I) = DRO / DPP
*
        If (XSLOPE.GT.0.0) Then
          XUP = XSLOPE * (PVP/PSAT(I)) + XB
          XDWN = XSLOPE * (PVM/PSAT(I)) + XB
          DELTAX = XUP - XDWN
          DXDP(I) = DELTAX / DPP
        Else
          XUP = 0.0
          XDWN = 0.0
          DELTAX = 0.0
          DXDP(I) = 0.0
        End If
*
        If (XSLOPE.GT.0.0) Then
          SAUP = ((1.-PHI)/PHI) * (RHOR/RHOA(I)) * XUP
          SADN = ((1.-PHI)/PHI) * (RHOR/RHOA(I)) * XDWN
          SVUP = SVI - SAUP
          SVDN = SVI - SADN
          DSRO = SVUP * RHOVNP - SVDN * RHOVNM
          DSRODP(I) = DSRO / DPP
        Else
          SAUP = 0.0
          SADN = 0.0
```

```
          SVUP = 0.0
          SVDN = 0.0
          DSRO = 1.0 * (RHOVNP-RHOVNM)
          DSRODP(I) = DSRO / DPP
        End If
  120 Continue
*************************************************************************
* CONSTRUCT AV(I) TERMS                                                 *
*************************************************************************
      DFLOWDPI(1) = DTVPDPVI(2) * (PVN(2)-PVN(1)) - TV(2)
      DFLOWDPI(NBLK) = 0.0
      Do 130 I = 2, NBLK - 1
        IUP = I + 1
        IM = I - 1
*
*  FLOW TERM
*
        DFLOWDPI(I) = DTVPDPVI(IUP) * (PVN(IUP)-PVN(I)) - DTVMDPVI(I) *
     *      (PVN(I)-PVN(IM)) - TV(IUP) - TV(I)
  130 Continue
*
*  ACCUMULATION TERM AND ADSORPTION TERMS
*
      Do 140 I = 1, NBLK
        DACCDP(I) = (PHI*DX/DT) * (DSRODP(I))
        DADSDP(I) = ((1.-PHI)*RHOR*DX/DT) * (DXDP(I))
  140 Continue
*
*  AV(I)
*
      Do 150 I = 1, NBLK
        AV(I) = DFLOWDPI(I) - DACCDP(I) - DADSDP(I)
  150 Continue
```

```
**************************************************************************
* CONSTRUCT BV(I) TERMS                                                  *
**************************************************************************
      BV(NBLK) = 0.0
      BV(NBLK-1) = 0.0
      Do 160 I = 1, NBLK - 2
        IUP = I + 1
        BV(I) = DTVPDPVIP(IUP) * (PVN(IUP)-PVN(I)) + TV(IUP)
  160 Continue
**************************************************************************
* CONSTRUCT CV(I) TERMS                                                  *
**************************************************************************
      CV(1) = 0.0
      Do 170 I = 2, NBLK - 1
        IM = I - 1
        CV(I) = (-1.) * (DTVMDPVIM(I)*(PVN(I)-PVN(IM))) + TV(I)
  170 Continue
**************************************************************************
* CONSTRUCT THE RIGHT HAND SIDE VECTOR                                   *
**************************************************************************
*
*  FLOW TERM
*
      FLOWV(1) = TV(2) * 1.0E6 * (PVN(2)-PVN(1))
      FLOWV(NBLK) = 0.0
      Do 180 I = 2, NBLK - 1
        IUP = I + 1
        IM = I - 1
        FLOWV(I) = TV(IUP) * 1.0E6 * (PVN(IUP)-PVN(I)) - TV(I) * 1.0E6 *
     *      (PVN(I)-PVN(IM))
  180 Continue
*
*  ACCUMULATION TERM AND ADSORPTION TERM
```

```
*
      Do 190 I = 1, NBLK - 1
        RHSACC(I) = (DX/DT) * PHI * (SVN(I)*RHOVN(I)-SV(I)*RHOV(I))
        RHSADS(I) = (DX/DT) * PHI * (SAN(I)*RHOAN(I)-SA(I)*RHOA(I))
  190 Continue
*
      Do 200 I = 1, NBLK - 1
        RHS(I) = FLOWV(I) - RHSACC(I) - RHSADS(I)
        RHS(I) = -RHS(I)
  200 Continue
*************************************************************************
* SOLVE MATRIX PROBLEM                                                  *
*************************************************************************
      NBMINUS = NBLK - 1
      Call THOMAS(AV,BV,CV,RHS,DPV,NBMINUS)
*************************************************************************
* CALCULATE VELOCITY IN EACH BLOCK AND MASSS FLOW RATE FROM LAST BLOCK  *
*************************************************************************
*
      QV(NBLK-1) = (PERM*RKRVUP(NBLK-1)*RHOVN(NBLK-1)*AREA(NBLK-1)) * ((
     *    PVN(NBLK-1)-PVN(NBLK))*1.0E6) / ((DX/2.)*VISCVN(NBLK-1))
      Do 210 I = 1, NBLK - 1
        VVTEMP = (PERM*RKRVUP(NBLK-1)/(VISCVN(NBLK-1)*DX)) * (PVN(I)-
     *      PVN(I+1)) * 1.0E6
        VV(I) = ABS(VVTEMP)
  210 Continue
*************************************************************************
* COMPUTE HEAT BALANCE                                                  *
*************************************************************************
      If (ISOCHK.EQ.1) Then
        Do 220 I = 1, NBLK
*
          SV(0) = 0.0
```

```
          RHOV(0) = 0.0
          ENINTV(0) = 0.0
          VV(0) = 0.0
*
          SV(NBLK+1) = 0.0
          RHOV(NBLK+1) = 0.0
          ENINTV(NBLK+1) = 0.0
          VV(NBLK+1) = 0.0
*
          TEMPV(NBLK+2) = 0.0
          TEMPV(NBLK+1) = 0.0
          TEMPV(0) = 0.0
          TEMPV(-1) = 0.0
*
          COND(0) = 0.0
          COND(NBLK+1) = 0.0
          IUP = I + 1
          IPP = I + 2
          IM = I - 1
          IMM = I - 2
          Call HEATBV(DX,DT,PHI,SV(I),SVN(I),RHOV(I),RHOVN(I),
     *         ENINTV(I),ENINTVN(I),RHOR,ENINTR,ENINTRN,PERM,RKRV(I),
     *         MDOT,VV(I),SV(IP),RHOV(IUP),ENINTV(IUP),VV(IUP),SV(IM),
     *         RHOV(IM),ENINTV(IM),VV(IM),PV(I),TEMPV(I),TEMPV(IPP),
     *         TEMPV(IMM),VISCV(I),COND(IM),COND(IUP),TRN,VOL(I),QV(I),
     *         ENTHVN(I),SA(I),SAN(I),RHOA(I),RHOAN(I),ENINTA(I),
     *         ENINTAN(I))
          TEMPVN(I) = TRN
  220   Continue
      End If
*************************************************************************
* CHECK FOR MAXIMUM DELTA PV                                            *
*************************************************************************
```

```
      DPVMAX = ABS(DPV(1))
      Do 230 I = 1, NBLK
        If (ABS(DPV(I)).GT.DPVMAX) Then
          DPVMAX = ABS(DPV(I))
        End If
  230 Continue
*************************************************************************
* CHECK FOR MAXIMUM RIGHT HAND SIDE                                     *
*************************************************************************
      RHSMAX = ABS(RHS(1))
      Do 240 I = 1, NBLK
        If (ABS(RHS(I)).GT.RHSMAX) Then
          RHSMAX = ABS(RHS(I))
        End If
  240 Continue
*************************************************************************
* CHECK TO SEE THAT DPV AND RHS VALUES ARE WITHIN TOLERANCES            *
*************************************************************************
      RHSTOL = 1.0E-8
      DPVTOL = 1.000
      If (RHSMAX.LE.RHSTOL.AND.DPVMAX.LE.DPVTOL) Then
        Do 250 I = 1, NBLK
          PVN(I) = PVN(I) + DPV(I) * 1.0E-6
          PV(I) = PVN(I)
          TEMPV(I) = TEMPVN(I)
  250   Continue
*************************************************************************
* WRITE OUTPUT                                                          *
*************************************************************************
*
*  HISTORIES
*
        Write (8,5100) TIME, PVN(1)
```

```
        Write (9,5100) TIME, TEMPVN(2)
        Write (10,5100) TIME, SAN(3)
*************************************************************************
        If (TIME.GE.TMAX) Then
          Go To 270
        Else
          Go To 20
        End If
      Else
        Do 260 I = 1, NBLK
          PVN(I) = PVN(I) + DPV(I) * 1.0E-6
  260   Continue
        If (ITKOUNT.GE.ITMAX) Then
          Print *, 'MAXIMUM ITERATION CONSTRAINT EXCEEDED'
        Else
          Go To 30
        End If
      End If
  270 Stop
 5000 Format (///4F10.2,I10///3F10.2,2E15.2///2E10.2,3F10.2///5F10.2///
     *    F10.2,4I10///I10,F10.2,I10,F10.2,F10.2///F10.2,I10,F10.2,2I10
     *    ///I10,4F10.2,///F10.2)
 5100 Format (E15.8,5X,E20.9)
 5200 Format (I10,5X,F15.4)
      End
```

The following subroutine was used to calculate the heat balance for the flow of vapor in the presence of a sorbing phase.

```
*****************************************************************
*                                                               *
*  CALCULATES HEAT BALANCE FOR VAPOR FLOW                       *
*                                                               *
*  JOHN W. HORNBROOK                                            *
```

```
*  STANFORD UNIVERSITY
*************************************************************************
      Subroutine HEATBV(DX,DT,PHI,SV,SVN,RHOV,RHOVN,ENINTV,ENINTVN,RHOR,
     *    ENINTR,ENINTRN,PERM,RKV,MDOT,VV,SVP,RHOVP,ENINTVP,VVP,SVM,
     *    RHOVM,ENINTVM,VVM,PV,TEMP,TEMPP,TEMPM,TEMPNI,TEMPNUP,TEMPNDN,
     *    VISCV,CONDM,CONDP,TRN,VOL,Q,ENTH,SA,SAN,RHOA,RHOAN,ENINTA,
     *    ENINTAN)
      Implicit Real*8 (A-H,O-Z)
      Real*8 NINE
      CPR = 1.017
      CONDR = 2.5
*************************************************************************
*  NOMENCLATURE                                                         *
*************************************************************************
*  CONDR     ROCK CONDUCTIVITY                                         *
*  CPR       ROCK SPECIFIC HEAT                                        *
*  DT        TIME STEP SIZE                                            *
*  DX        BLOCK THICKNESS                                           *
*  ENINTA    ADSORBATE INTERNAL ENERGY AT OLD TIME STEP                 *
*  ENINTAN   ADSORBATE INTERNAL ENERGY AT NEW TIME STEP                *
*  ENINTVM   VAPOR INTERNAL ENERGY IN DOWNSTREAM BLOCK                 *
*  ENINTVP   VAPOR INTERNAL ENERGY IN UPSTREAM BLOCK                   *
*  ENTH      ENTHALPY OF PROUCED FLUID                                 *
*  PERM      PERMEABILITY                                              *
*  PHI       POROSITY                                                  *
*  Q         MASS FLOW RATE OUT OF PRODUCTION BLOCK                    *
*  RHOR      ROCK DENSITY                                              *
*  RHOV      VAPOR DENSITY AT OLD TIME STEP                            *
*  RHOVM     VAPOR DENSITY AT DOWNSTREAM BLOCK                         *
*  RHOVP     VAPOR DENSITY AT UPSTREAM BLOCK                           *
*  SA        ADSORBED PHASE SATURATION AT OLD TIME STEP                *
*  SAN       ADSORBED PHASE SATURATION AT NEW TIME STEP                *
*  SVM       VAPOR PHASE SATURATION AT DOWNSTREAM BLOCK                *
```

```
*  SVP       VAPOR PHASE SATURATION AT UPSTREAM BLOCK              *
*  TEMP      TEMPERATURE AT OLD TIME STEP                          *
*  TRN       TEMPERATURE AT NEW TIME STEP                          *
*  VOL       BLOCK VOLUME                                          *
*  VVP       VAPOR VELOCITY IN UPSTREAM BLOCK                      *
*  VVM       VAPOR VELOCITY IN DOWNSTREAM BLOCK                    *
*****************************************************************
*
      ONE = (RHOR/DT) * (((1.-PHI)*CPR*TRN)-((1.-PHI)*CPR*TEMP))
*
      THREE = (1./DT) * ((SVN*PHI*RHOVN*ENINTVN)-(SV*PHI*RHOV*ENINTV))

*
      FOUR = (1./DT) * ((SAN*PHI*RHOAN*ENINTAN)-(SA*PHI*RHOA*ENINTA))
*
      FIVE = (CONDR/DX) * (TEMPNUP-2.*TEMPNI+TEMPNDN)
*
      SIX = (1./(2.*DX)) * ((PHI*SVP*RHOVP*ENINTVP*VVP)-(PHI*SVM*RHOVM*
     *    ENINTVM*VVM))
*
      NINE = 1.0E3 * (PV/(2.*DX)) * ((PHI*SVP*VVP)-(PHI*SVM*VVM))
*
      ELEVEN = 1.0E-3 * ((SV**2.)*(PHI**2.)*VISCV*(VV**2.)) / (PERM*RKV)
*
      FLUX = Q * (ENTH) / VOL
*
      RHS = (-THREE-FOUR+FIVE-SIX-NINE+ELEVEN-FLUX)
      RHSMOD1 = (DT/RHOR) * RHS
      RHSMOD2 = RHSMOD1 + ((1.-PHI)*CPR*TEMP)
      TRN = RHSMOD2 / ((1.-PHI)*CPR)
      Return
      End
```

A number of subroutines are not included in this text but can be found elsewhere. Subroutine NIST is available from the National Institute of Standards and Technology [26] and subroutines THOMAS and TABBIN which solve a tridiagonal matrix and perform linear interpolation, respectively, are available from Aziz and Settari [6].